FAST NEUTRON POLARIZATION STUDIES

by

REFAAT M.A. MAAYOUF, M.Sc.

Thesis submitted for the degree of
DOCTOR OF PHILOSOPHY
University of Edinburgh

October 1972

ABSTRACT OF THESIS

The present situation regarding polarization of neutrons from the $D(d,n)^3He$ reaction for deuteron energies $\leq$ 10 MeV is surveyed along with the experimental arrangements used to obtain the data. Out of the techniques used before for measuring the $D(d,n)^3He$ polarization, two main techniques, used for the measurements reported in this thesis, are emphasized. One of them is by scattering from helium which is discussed along with calculations performed in order to test the degree of agreement between the phase-shifts available for determining the ^4He analysing powers. The other is by using Mott-Schwinger scattering from heavy nuclei at small angles. This one is discussed in detail and the differential scattering cross-sections at small angles measured to date along with the models used to describe them are surveyed.

Measurements of the $D(d,n)^3He$ polarization using both types of polarimeter are described. First, two sets of measurements with the ^4He polarimeter are described. One of them was carried out at an incident deuteron energy of 0.5 MeV; the other one was performed at deuteron energies between 1 and 5 MeV. This is followed by a description of the Mott-Schwinger polarimeter along with two sets of measurements. The first of them was carried out with deuterons incident with energy 0.82 MeV and the polarization of neutrons emitted at 46° was detected using scattering from lead. The other one was mainly for comparison with the measurement carried out at 0.5 MeV with the helium polarimeter and employed scattering from Cu, Pb and U samples.

All the results obtained with both polarimeters are discussed
at the end of the thesis.   The resulting $D(d,n)^3He$ polarizations
at reaction laboratory angle 45 ± 5° are compared with values re-
ported in the literature for the mean deuteron energy range ≤ 10 MeV.
Two angular distributions of the reaction polarization reported in
this thesis are also compared with published values.   The measure-
ments with the Mott-Schwinger polarimeter also resulted in differ-
ential scattering cross-sections of Cu, Pb and U at small angles
which are compared with cross-sections based on optical model
calculations.   Finally both polarimeters are compared and the
possibility of improving the efficiency of the Mott-Schwinger
polarimeter is discussed.

CONTENTS

CHAPTER THREE

$D(d,n)^3He$ POLARIZATION MEASUREMENTS USING MOTT-SCHWINGER SCATTERING

CHAPTER ONE

INTRODUCTION

CHAPTER ONE

INTRODUCTION

1.1. Introduction

One of the main sources used to obtain neutrons of several MeV is the $D(d,n)^3He$ reaction. It was suggested that a strong spin-orbit force exists during the reaction, in order to interpret data about the angular distribution of nucleons produced in the D-D reactions[1]. Following this suggestion Wolfenstein[2] was able to show that, because of this spin-orbit force, the nucleons produced should be polarized even if both the incident particles and target nuclei are initially unpolarized. Thus the $D(d,n)^3He$ reaction became one of the first sources of polarized fast neutrons, which were used in the early polarization measurements[3], and a great attention was paid to it, where several measurements of the polarization of neutrons produced in this reaction were carried out over nearly all the range of neutron energies the reaction produces.

The principle of measuring neutron polarization is well known[4]. In a typical arrangement, fig. 1, a beam of unpolarized deuterons from an accelerator is incident on target A_1, where a reaction takes place and neutrons emitted, at angle θ_1 are partially polarized in direction n perpendicular to the reaction plane. If these neutrons are scattered by scatterer A_2, then to the right of it will be scattered neutrons with spins parallel to n and to the left of it will be scattered those of the opposite direction. The number of neutrons scattered to either side of A_2 with azimuthal
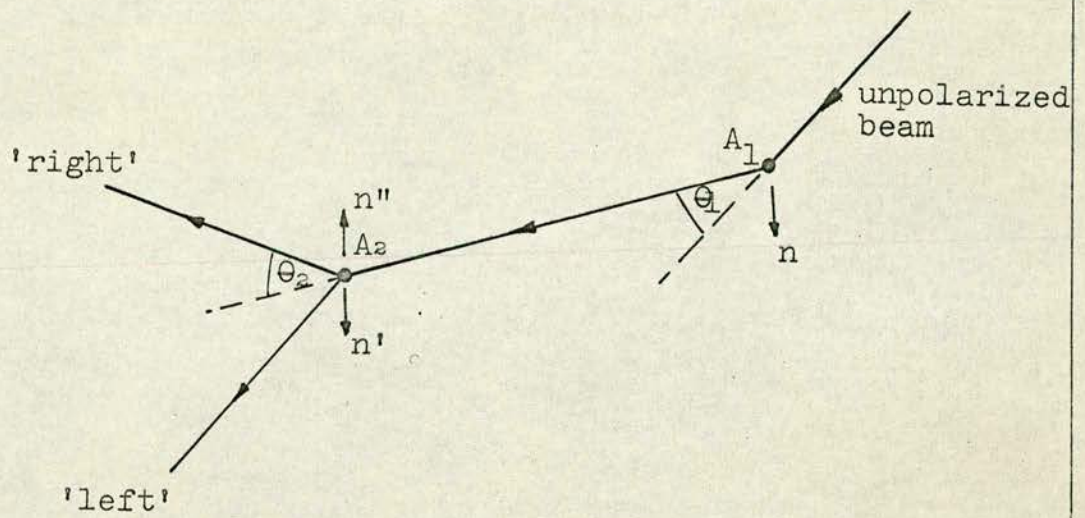
Fig. 1. Typical arrangement for measuring
neutron polarization

angle ϕ is:

$$N(\Theta_2,\phi) \sim \sigma_2(E_n,\Theta_2)[1+P_n(E,\Theta_1)P(E_n,\Theta_2)\cos\phi] \qquad (1.1.1)$$

where $\sigma_2(E_n,\Theta_2)$ is the differential scattering cross-section for unpolarized neutrons and $P_n(E,\Theta_1)$, $P(E_n,\Theta_2)$ are the polarizations resulting from the reaction and scattering by A_2 respectively. The number of neutrons scattered in a given time to 'right' ($\phi = 0$) and to 'left' ($\phi = \pi$), say N_R and N_L respectively, are related to P_n and P as follows:

$$\mathcal{E} = (N_R - N_L)/(N_R + N_L) = P_n P \qquad (1.1.2)$$

Thus the product $P_n P$ is equal to the asymmetry in scattering $\mathcal{E}$ and if either P_n or P is known, the other one can be determined. P is usually called the analysing power of scatterer A_2. Now if appropriate neutron detectors are set at angle Θ_2, to detect neutrons scattered to both sides of A_2, the asymmetry can be determined. In that case when it is required to determine the polarization of neutrons emitted from the reaction, a scatterer A_2, usually called analyser, should be used for which the analysing power can be determined; it is either one of the spin-zero nuclei or a heavier one. Types of analysers, usually used, will be discussed in the following sections with emphasis on two of them used during the $D(d,n)^3He$ polarization measurements described in this thesis.

1.2. Polarization Detection using Scattering from Helium

If one of the spin-zero nuclei (such as ^4He, ^{12}C, ...etc.) is used for analysing the neutron beam emitted from the reaction the

analysing power is calculated from the phase-shifts derived from the scattering cross-sections.   The phase-shifts are best known for scattering of neutrons by ^{4}He, ^{12}C and ^{16}O[4].   Carbon was used in the first experiments demonstrating that the polarization of nucleons, emitted from the reaction, can be detected using scattering from spin-zero nuclei[5-7].

While scattering from ^{4}He takes place, up to neutron energies ~20 MeV, without excitation of internal degrees of freedom of the particles, and consequently the resulting polarization is a monotonic function of energy[8], it is not the same case with either ^{12}C or ^{16}O. Accordingly the phase-shift analysis, when scattering is by ^{4}He, is simpler than in the case of the other two scatterers.   Because of this, the n-^{4}He phase-shifts are the least uncertain[9,10,11] and scattering from helium is the most commonly used for detecting neutron polarization.   The neutron differential scattering cross-section was first calculated, for helium, by Bloch[12] while the resulting polarization was given by Schwinger[13] and Lepore[14].

The most convenient expression for calculating polarization P resulting in scattering from spin-zero nuclei, was given by Baumgartner et al.[15].   It is given in the nomenclature of ref.[4] by:

$$P = \frac{-2 \, \text{Im} \, (g^* h)}{|g|^2 + |h|^2} \tag{1.2.1}$$

$$g = (1/k) \sum_\ell P_\ell (\cos \theta)[(\ell+1)\sin\delta_\ell^+ e^{i\delta_\ell^+} + \ell\sin\delta_\ell^- e^{i\delta_\ell^-}]$$

$$h = (1/k) \sum_\ell P_\ell^{(1)} \sin(\delta_\ell^+ - \delta_\ell^-) e^{i(\delta_\ell^+ + \delta_\ell^-)}$$

where P_ℓ and $P_\ell^{(1)}$ — are the Legendre and associated polynomials

δ_ℓ^+ and δ_ℓ^- — are the phase-shifts for $J = \ell + \frac{1}{2}$ and

$J = \ell - \frac{1}{2}$ respectively.

1.2.1. <u>The existing n-^{4}He phase-shifts</u>

The first nucleon-^{4}He phase-shifts were calculated by
Critchfield and Dodder[16], from published p-^{4}He differential cross-
sections; they covered the energy range from 0.95 - 3.58 MeV, and
only accounted for phases with $\ell < 2$.

Two basic sets of n-^{4}He phase-shifts were further deduced from
p-^{4}He scattering data:

a) The DGS phase-shifts, originally deduced by Dodder and
Gammel[17] from p-^{4}He scattering data at 5.81 and 9.78 MeV
and were then supported by n-^{4}He cross-section measure-
ments carried by Seagrave[18] up to 14 MeV incident neutron
energy.

b) The GTP phase-shifts, deduced by Gammel, Thaler and
Perkins[19] for neutron energies > 10 MeV.

Two approaches were used to test these two sets of n-^{4}He phase-
shifts. One approach was to compare measured cross-sections with
those deduced from the phase-shifts and this procedure usually con-
firmed the DGS set within the experimental accuracy. The other
approach was by comparing phase-shifts deduced from experimental
data with DGS values, where such comparison resulted in disagreement,
particularly for the energy region below 4 MeV.

Thus a number of measurements on n-^{4}He scattering cross-sections

were carried out to test n-^{4}He phase-shifts deduced from p-^{4}He scattering data.   Work prior to 1962 were surveyed by Austin and Barschall[20], who also contributed a set of n-^{4}He phase shifts which covered the energy range up to 8 MeV.   The Austin and Barschall (AB) set of phase-shifts was further extended by Hoop and Barschall[21] (HB) in 1966 where they surveyed the situation again.

The (HB) set of phase-shifts which covered neutron energies up to 30 MeV, was based on two independent sets of previously determined n-^{4}He phase-shifts and was supported as well by angular distributions measured between 6-30 MeV.   This set of phase-shifts is in satis-factory agreement with the DGS set below 10 MeV and with that set of n-^{4}He phase-shifts calculated by Weitkamp and Haeberli[22], from p-^{4}He phase-shifts above 14 MeV.

The phase-shifts derived by Sawers et al.[23], at 1.01 and 2.44 MeV, from their polarization data, disagreed somewhat with both DGS and HB values.

Morgan et al.[24], measured relative differential cross-sections for n-^{4}He scattering at 22 neutron energies between 0.2 and 7.0 MeV and accordingly represented another set of phase-shifts.   For the mentioned energy range they concluded that the n-^{4}He scattering is satisfactorily described without a need to include, in the analysis, phase shifts with $\ell > 1$.

Using an optical model fit, Satchler et al.[25], predicted another set of phase-shifts both for n-^{4}He and p-^{4}He scattering. For n-^{4}He scattering their optical model fit, primarily based on the experimental data of Morgan et al.[24], was applied up to incident neutron energy 18 MeV.

Recently were published two sets of phase-shifts, obtained from fitting together the existing experimental data. One of them, published by Arndt and Roper[26], covered neutron energies up to 20 MeV, is based on the existing data in this energy range but excluding some of them; the cross-sections of Adair[27], Demanins et al.[28], Seagrave[18] except at 4.53 and 14.3 MeV and Hoop et al.[21] at 2.02 MeV and the value of polarization reported by White and Farley[29] at 3 MeV and 90° were excluded.

The other one deduced by Stammbach and Walter[30], where they used additional information that could be extracted from data on charge symmetric p-^{4}He scattering. For this purpose they included in a search first available n-^{4}He data up to 20 MeV, then p-^{4}He data and lastly connected the two systems, where they also included additional n-^{4}He polarization[31] and cross-section data[32] between 11-21 MeV as well as more p-^{4}He polarization data[33]. Their description of both nucleon-^{4}He systems is the more complete in the mentioned energy range.

1.2.2. The degree of agreement between different n-^{4}He phase-shifts

In order to examine the degree of agreement between the main sets of phase-shifts in the energy range <10 MeV, the ^{4}He analysing power, as a function of lab. scattering angle, was computed (using the expressions (1.2.1)) applying different sets of phase-shifts. Some of the computed angular distributions are represented in Figs. 2a and 2b for neutron energies 4 and 7 MeV respectively, where for this purpose were used the phase-shifts of Morgan et al.[24],
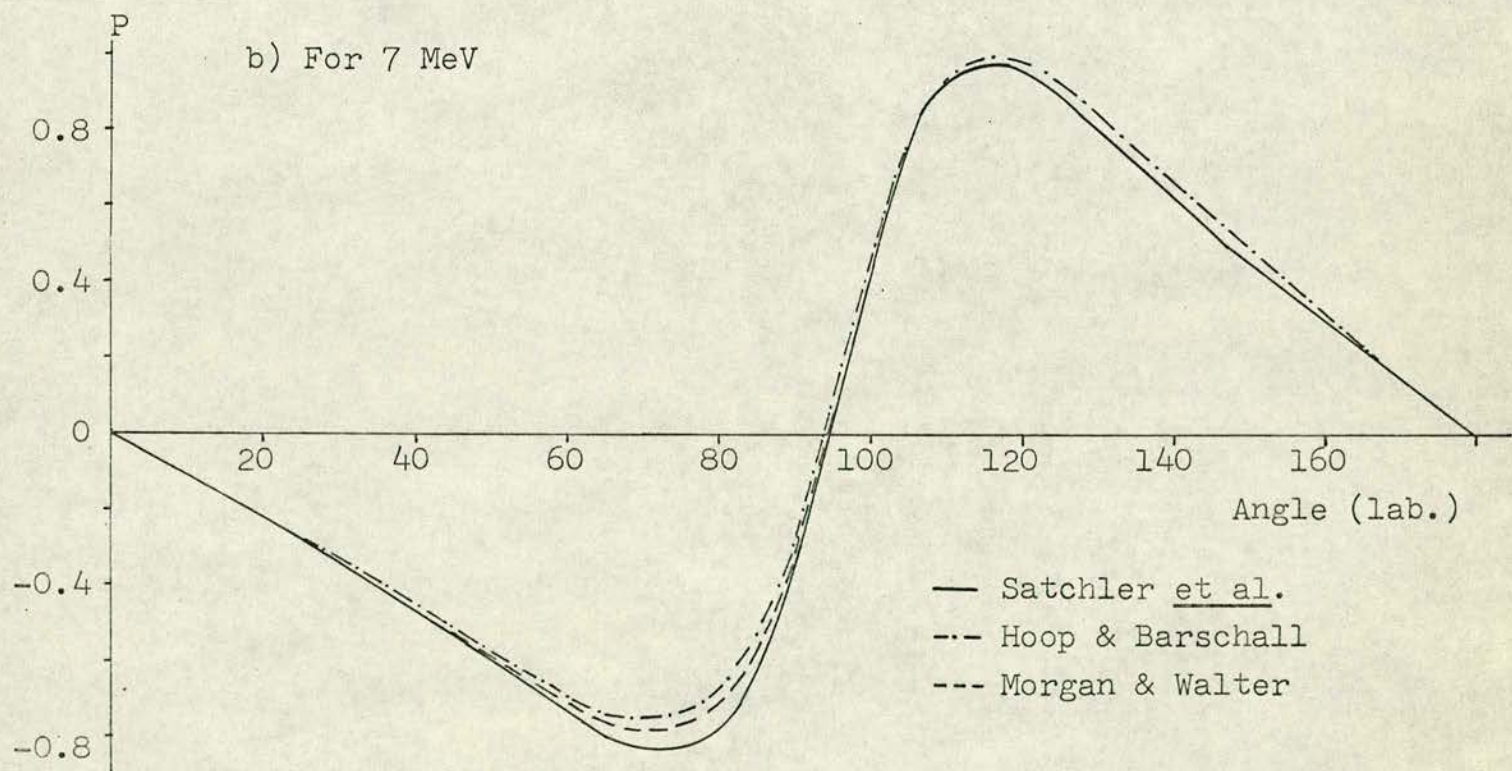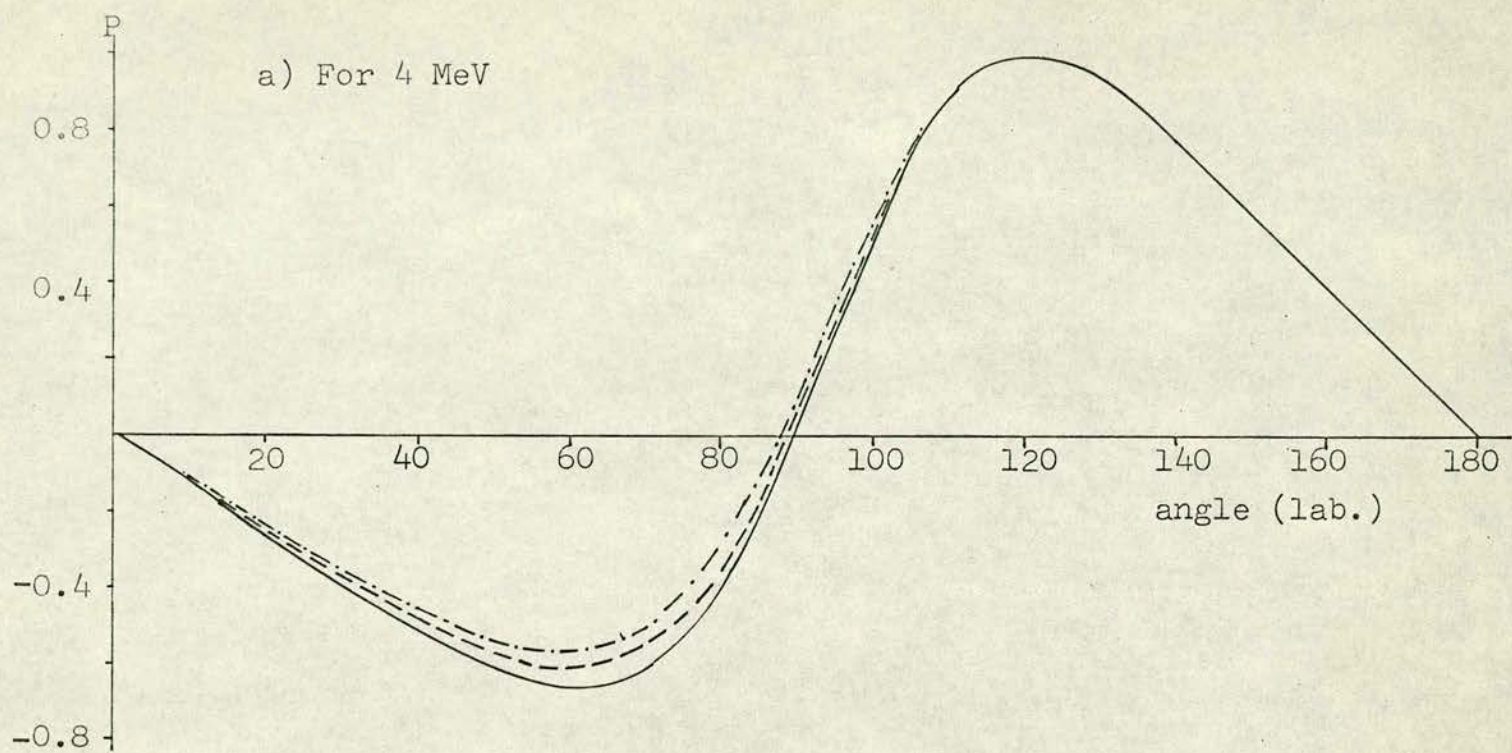
Fig. 2.   The analyzing power as function of angle, according
to three different sets of phase-shifts.

Hoop et al.[21] and Satchler et al.[25].

In general, the disagreement between the analysing powers, related to different phase-shifts is more for forward scattering angles (around 60°) where minimum analysing power occurs, than for backward scattering angles (around 120°) where the maximum analysing power exists.

For example the disagreement for the forward minimum at 4.0 MeV amounts to 20% and 0.65% at the backward maximum (Fig. 2a), while at 7.0 MeV the disagreement amounts to 10% at the forward minimum and 3% at the backward maximum (Fig. 2b). Thus the uncertainty in the helium analysing power is smaller for scattering angles in the neighbourhood of 120° Lab. rather than at 60°. Besides the analysing power at 120° is nearly 1 over most of the energy range (≤ 10 MeV), which is not the case at other angles (Fig. 3).

1.3. Polarization Detection Using Scattering From Heavy Nuclei

Elastic scattering of neutrons by medium and heavy nuclei is also used for measuring the degree of polarization in the neutron beam emitted from the reaction. By scattering of 400 KeV neutrons through 90° from 11 elements (from Cu to Bi) Adair et al.[34] found that the main features observed for the variation of polarization are described by including a spin-orbit coupling term in the optical model potential. This was further supported by Remund[35], where he measured and calculated theoretically the differential cross-sections and azimuthal asymmetries for elastic scattering of 3.3 MeV neutrons by Cu, Ta, Pb and Bi at intervals of 15°, between 30°-150°,

Fig. 3. P_{He} as function of neutron energy, at 4 different scattering angles.
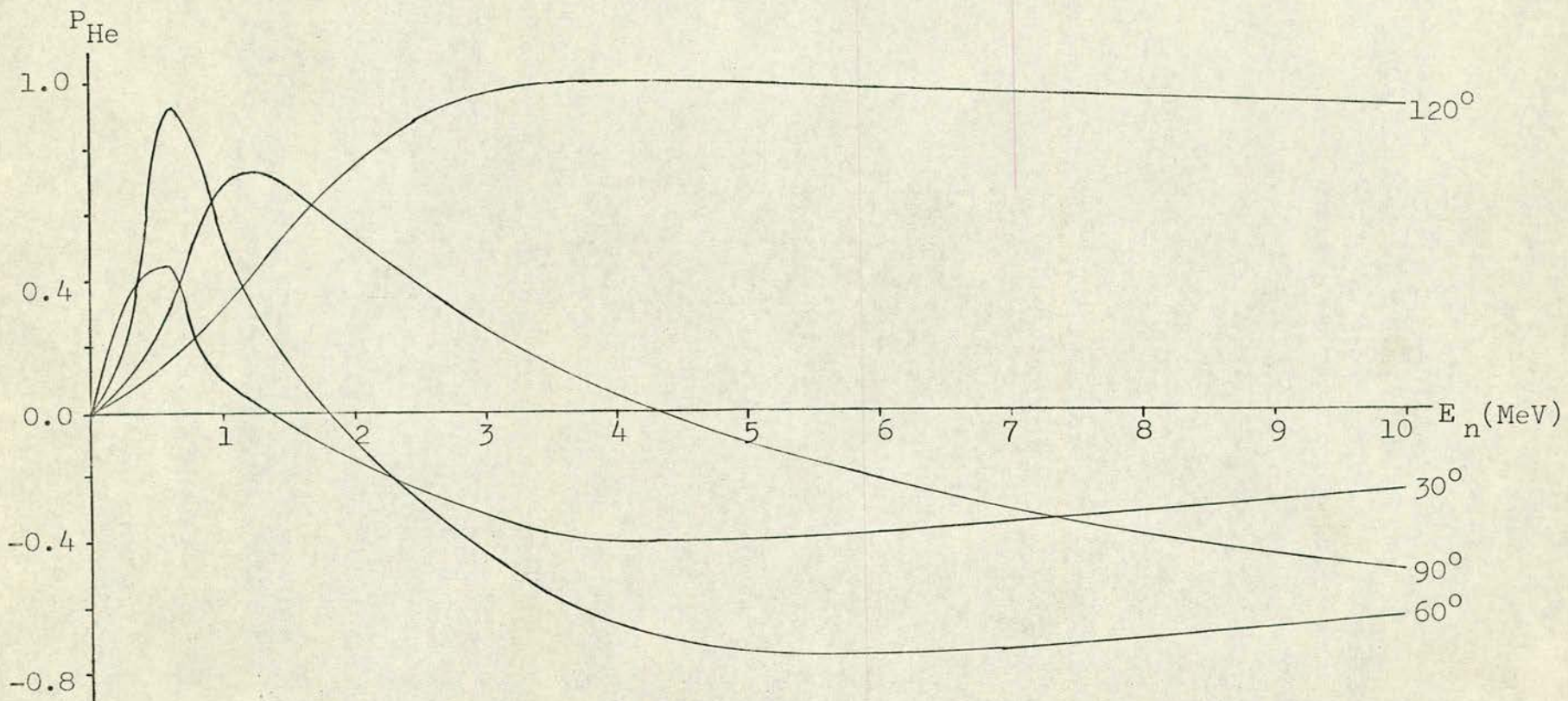
and found that the variations of polarization with atomic number appear similar to those predicted from his calculations based on the optical model.

Other measurements of qualitative nature followed; These were mainly for comparison with optical model fits. Examples of such comparisons are by Olness et al.[36] who scattered 1.5 MeV neutrons through 51.5° by 18 elements, by Ferguson et al.[37] who scattered 0.4, 0.7 and 1.0 MeV neutrons through 55° by 14 elements, by Gorlov et al.[38,39] who scattered 4 MeV neutrons by 12 elements through different angles varying from 10°-170°, and by Mahajan[40], who scattered 4.4, 5.0 and 5.5 MeV neutrons through 40°, 60° and 90° by elements from Ti to Bi. Besides, Morozov et al.[41], recently scattered 4 MeV neutrons through angles in the range 146-177° by In, Sn, Pb, Bi and U, where they find the backward peak of the differential cross-section, predicted by the optical model, for all scatterers except U, but the measured values did not agree with the calculated ones.

More detailed studies of angular dependence of polarization are discussed recently by Galloway[42].

Elastic scattering of neutrons by heavy and medium nuclei at forward small angles (< 10°) is of particular interest; Other interactions, spin orbit ones, take place along with the purely nuclear one. One of them, so called Mott-Schwinger scattering, which leads to large polarization of scattered neutrons will be discussed in the following section.

1.3.1. Mott-Schwinger Scattering

When neutrons are scattered by either heavy or medium nuclei at considerably large angles (> 10°), the short range nuclear interaction between the scattered neutron and the scattering nucleus, which is satisfactorily described by the optical model of nucleus[43,44], is the predominant one.

At angles smaller than 10°, another long range interaction takes place; this one arises between the magnetic moment of scattered neutron and the Coulomb field of scattering nucleus.

This long range interaction was firstly studied by Schwinger[45], where he pointed out that due to such spin-orbit interaction the scattered neutrons are polarized. As a similar effect was predicted by Mott[46] for the case when electrons are scattered, it is usually called Mott-Schwinger scattering. As the major part of such interaction should take place outside the nucleus, and within the screening radius of atomic electrons, the range of scattering angles where it can be observed is restricted by[45]:

$$1/ka \ll 2 \sin \theta/2 \ll 1/kR \qquad (1.3.1)$$

where k, a, θ and R are the neutron's wave number, the screening radius of the atom, scattering angle and radius of the nucleus respectively.

Applying the Born approximation Schwinger was able to show that the amplitude of such scattering is:

$$f_{sh}(\theta) = \tfrac{1}{2} i \, \sigma.n \cot \theta/2 \, (\hbar/Mc)(Ze^2/\hbar c) \qquad (1.3.2)$$

where n is the unit vector defined by $KxK_o = n \, k^2 \sin \theta$.

The substantial contribution of Schwinger scattering to the

differential cross-section $\sigma(\Theta)$ for unpolarized neutron is:

$$\sigma_{sh}(\Theta) = \gamma^2 \cot^2 \Theta/2 \qquad (1.3.3)$$

$$[\ \gamma = \tfrac{1}{2} \mu_n (\hbar/Mc)(Ze^2/\hbar c) \ ]$$

The polarization resulting from Mott-Schwinger scattering is given by:

$$P_{sh}(\Theta) = \frac{-k \ \sigma_t \gamma \cot \Theta/2}{2\pi\sigma(\Theta)} \qquad (1.3.4)$$

where σ_t is the total interaction cross-section.

Thus the polarization resulting in scattering at small angles can be determined from the experiment, once both the total and differential scattering cross-sections are measured. As the differential cross-section is a value of importance when determining $P_{sh}(\Theta)$ it is discussed in more detail in the following section.

1.3.2. The differential scattering cross-section at small angles

When neutrons are elastically scattered by medium and heavy nuclei at small angles ($\leq 10^{\circ}$), other long range interactions have to be considered, along with the short range nuclear interaction, in the total potential of the interaction of neutron with the nucleus. One of these long range interactions is the one, mentioned before, due to Schwinger scattering. This interaction was first studied by Schwinger for the case when the incident neutron beam is initially unpolarized and by Sample[47] for 100 per cent polarized beam, where he applied his formula for the cross-section, slightly different from Schwinger's, for calculating the cross-section of 3.1 MeV neutrons scattered by Pb. The differential cross-section as calculated by

Sample is represented in Fig. 4, where it is remarkable that the differential cross-section is appreciably polarization sensitive for scattering angles $< 10°$.

Another two long range components were suggested, to partici-pate in the interaction. One of them, suggested by Fox[48], on the assumption that the nuclear interaction will not decrease as rapidly with increasing distance from the nucleus, was criticized and excluded by Wilmore and Hodgson[49]. The other one is caused by the interaction of the induced electric dipole moment of the neutron $P = \alpha_n E$ (E is the electric field intensity at the neutron's position) with the Coulomb field of the nucleus and was suggested by Aleksandrov and Bondarenko[50].

The amplitude of such scattering (called polarization scatter-ing), according to the Born approximation, is

$$f_{pol}(\theta) = \alpha_n Z^2 \frac{Me^2}{\hbar R} [1 - \frac{\pi}{4} gR + (gR)^2 \sum_{m=0}^{\infty} \frac{(-1)^m (gR)^{2m}}{(2m+1)(2m+3)}] \qquad (1.3.5)$$

where α_n and R are respectively the polarizability coefficient and radius of the nucleus scatterer; $g = 2k \sin \theta/2$

Such amplitude should lead, assuming that the amplitude of nuclear scattering is purely imaginary, to the appearance of the term $\sigma_{pol}(\theta) = f_{pol}(\theta)^2$ in the total differential scattering cross-section $\sigma(\theta)$.

As the effect is connected with the Coulomb field, its contri-bution to the total scattering cross-section should be at small scattering angles and should manifest itself when neutrons are scattered by heavy nuclei. It was also suggested that the effect
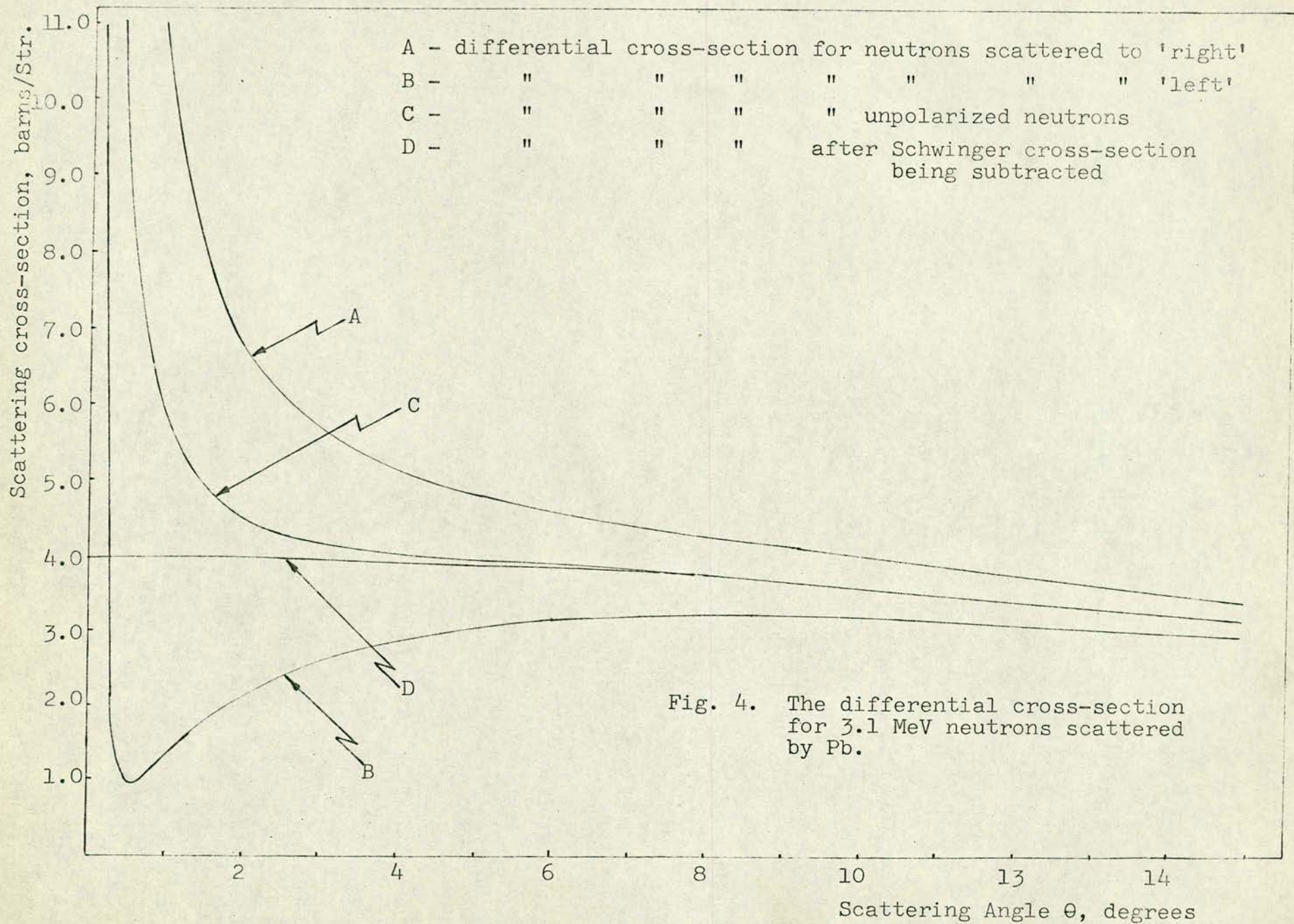
Fig. 4. The differential cross-section
for 3.1 MeV neutrons scattered
by Pb.

should increase with diminishing neutron energy[50].

Thus the total scattering amplitude $f(\theta)$ is usually represented as a summation of amplitudes due to scattering on each of the total potential's components separately:

$$f(\theta) = f_{nucl.}(\theta) + f_{sh}(\theta) + f_{pol.}(\theta) \qquad (1.3.6)$$

For neutrons with $E_n \leq 5$ MeV, this solution is valid[51,52] for scattering angles $\theta \geq 10'$ and $\leq 8\text{-}10^{\circ}$.

However, Weisskopf and Feshbach[53] were able to show that, in the range of studied energies, the optical model for heavy nuclei yields a negative real part of the amplitude of elastic nuclear scattering and therefore the cross-section due to the neutron's polarizability must be characterized by two terms:

$$\sigma_{pol.}(\theta) + 2 \text{ Re } f_{nucl.}(\theta) f_{pol.}(\theta) \qquad (1.3.7)$$

Thus for incident unpolarized neutron beam the differential scattering cross-section is[54]:

$$\sigma(\theta) = \sigma_{nucl.}(\theta) + \sigma_{sh}(\theta) + \sigma_{pol.}(\theta) + 2 \text{ Re } f_{nucl.}(\theta) f_{pol.}(\theta) \qquad (1.3.8)$$

While $f_{pol.}(\theta)$ can be calculated according to formula (1.3.5) and is positive at small scattering angles, the real part of the nuclear amplitude Re $f(\theta)$ is calculated within the framework of the optical model[55]. As there is still not agreement concerning the analytic form and the parameters of the optical potential, the estimate of Re $f_{nucl.}(\theta)$ is likewise somewhat indefinite[56]. The quantity Re $f_{nucl.}(\theta)$ is usually negative for heavy nuclei, at small scattering angles, and accordingly the two terms of expression

(1.3.7) may cancel each other partially or perhaps completely depending on the value of α_n. Thus the contribution of the quantity, represented by expression (1.3.7), in the differential cross-section depend on the relationship between $f_{pol.}(\Theta)$ and Re $f_{nucl.}(\Theta)$ and can be negative at Re $f_{nucl.}(\Theta) < 0$.

In Fig. 5. is illustrated the contribution of expression (1.3.7) in the differential cross-section as calculated by Walt and Fossan[57], for scattering of 570 KeV neutrons by Uranium, applying different values of α.

1.3.3. Models used for describing the scattering cross-section

The interpretation of the experimental data about the differential scattering cross-section require knowledge of $\sigma_{nucl.}(\Theta)$ from the theory, which in its turn depend on the applied model. Different models were applied at different stages to describe $\sigma_{nucl.}(\Theta)$.

Aleksandrov et al.[58,59] assumed that $\sigma_{nucl.}(\Theta)$ can be described with a sufficient degree of accuracy by means of the expression:

$$\sigma_{nucl.}(\Theta) = A \cos \Theta - B \quad (A > o; \; B > o) \qquad (1.3.9)$$

which was usually normalised using values of $\sigma(\Theta)$ at scattering angles $\Theta > 10^\circ$, where the contribution of the long range components is assumed small.

Dukarevich and Dyumin[60] described the cross-section for nuclear scattering by the expression for diffraction of neutrons by a "black" nucleus:

$$\sigma_{nucl.}(\Theta) = A \left[J_1 \left(\frac{R + \lambda}{\lambda} \Theta \right) \Big/ \frac{R + \lambda}{\lambda} \Theta \right] \qquad (1.3.10)$$
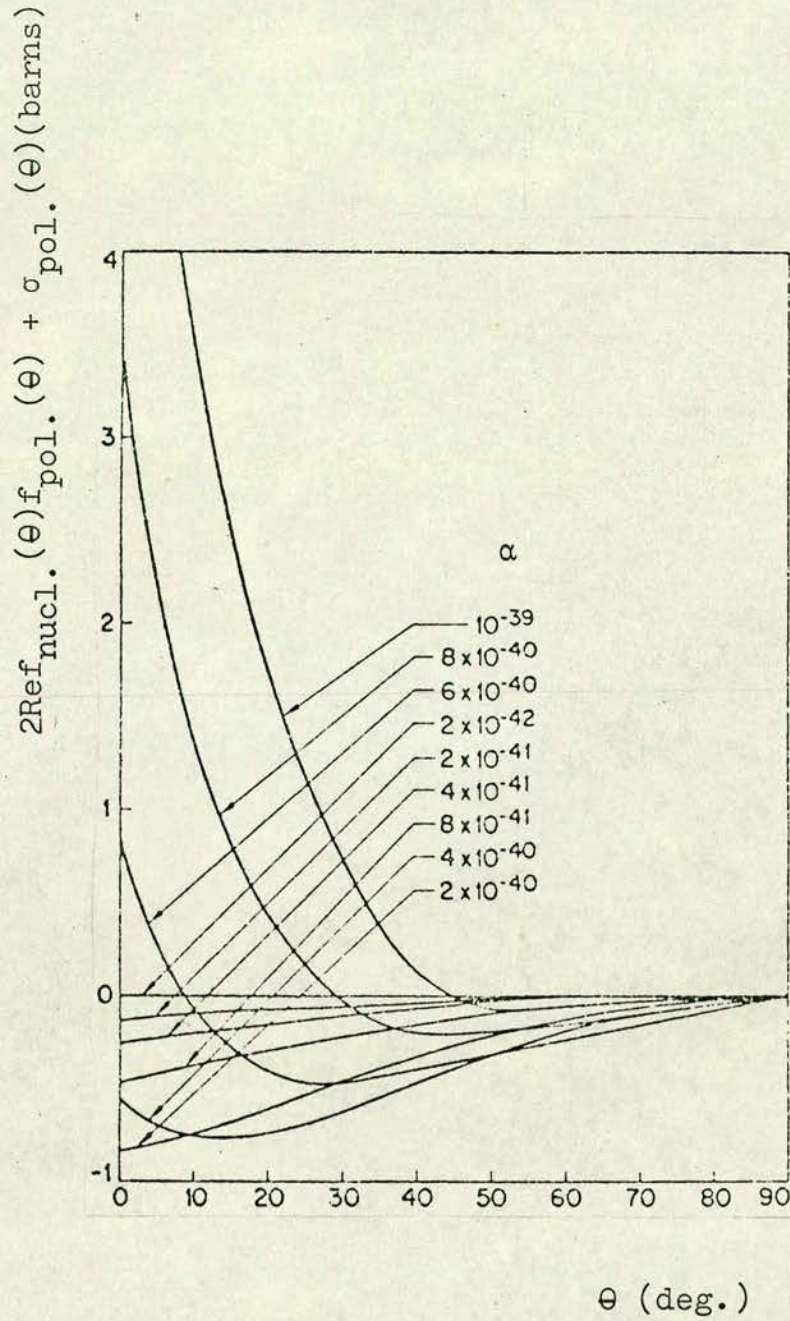
Fig. 5. The term $2\text{Re}f_{\text{nucl.}}(\Theta)f_{\text{pol.}}(\Theta) + \sigma_{\text{pol.}}(\Theta)$ as calculated for different values of α.

where R is the radius of the nucleus; λ is the neutron wave length; the coefficients A and R were usually normalised from the experimental data.

As the optical model was successful in describing $\sigma_{nucl.}(\theta)$, as applied by Wilmore and Hodgson[44] including compound elastic scattering for neutron energies < 5 MeV, it was applied in further works according to various modifications of the model.

Further development in the application of the optical model was by Monahan et al.[61], where they developed a method, for calculating the scattering cross-section at small angles, based on the use of a potential which includes all the three components and applied their method for the case when neutrons of energy 830 KeV are scattered by Uranium through scattering angles in the range 10° - 150° as well as for angles[62] between 1.65°-10°. Such an approach allowed simultaneous evaluation of nuclear and electromagnetic interactions and was further developed and generalised by Redmond[52] and Hogan and Seyler[63].

Thus there still exists uncertainty about the value of $\sigma_{nucl.}(\theta)$, as predicted by the optical model, which makes it determined within 10-20% accuracy[43]. Because of such uncertainty, the shape of the differential cross-section curve (i.e. $\sigma_{nucl.}(\theta)/\sigma_{nucl.}(o)$ as a function of scattering angle) as predicted theoretically in the small angles range is used to allow extrapolation of the experimental cross-section from large scattering angles (where $\sigma_{nucl.}(\theta)$ is the predominant) to the small angles range (up to 0°).

For scattering angles $\theta < 8$-10°, the degree of agreement

between experiment and theory can be tested by the value Δ determined as [54]:

$$\Delta = \sigma(\Theta) - \sigma_{sh}(\Theta) - \sigma_{th}(\Theta) \tag{1.3.11}$$

where $\sigma_{th}(\Theta)$ is the cross-section, associated with the particular model adopted. Accordingly the existing situation about the degree of agreement between the experiment and theory is represented in table 1.1, for scattering of neutrons of several MeV. The optical model was applied by all the authors except those of references[58-60] where either of the two models, given by expressions (1.3.9) and (1.3.10), was used for interpreting the experimental data.

When studying table 1.1, one finds that the neutron differential cross-section of scattering by nuclei of medium atomic weight is satisfactorily described by different models of nuclear scattering as well as by the optical model of the nucleus. For heavy nuclei (such as U, Th, etc.) such agreement between theory and experiment was not achieved by all the workers in this field. Such anomalies in the scattering of neutrons by such nuclei[58,59,60,62,65,66,71] were related either to the fission process[62], e.g. in the case when scattering is by U, or to polarization scattering[71]. That the effect is due to fission process is no more valid assumption as both investigations of the angular distribution of fission neutrons[69], at small angles, and measurements, carried out by the same authors who suggested the existence of the effect, within better statistical accuracy[68] did not confirm it.

The assumption about the existence of polarization scattering (discussed recently by Gorlov et al.[54] and Lebedeva et al.[72])

Table 1.1: The values of Δ (given by eqn (1.3.11) for available published data.

Reference	En MeV	The value of Δ for the given element										
		Cu	Cd	In	Sn	W	Au	Pb	Bi	Th	U	Pu
Alexandrov[58]	2.0	O			O			>0	0		>0	>0
Alexandrov et al.[59]	0.8	O								0	0	
"	2.8	O								>0	>0	
Dukarevich et al.[60]	14.2						O	0	0	>0	>0	
Walt et al.[64]	0.57										0	
Alexandrov et al.[65,66]	0.575										>0	
"	1.3	O						<0			<0	
"	2.45	O						<0			<0	
"	4.5	O						>0			>0	
"	5.6										0	
"	8.4							≶0			>0	
"	14.2							<0			≶0	
Gorlov et al.[67]	4.0	O		O	O			0	0		0	
Kuchnir et al.[68]	0.6						O			0	0	
"	0.84					O	O	O		0	0	
"	1.00		O			O				0	0	
"	1.2					O				0	0	
"	1.6									0	0	
Adam et al.[69]	14.7										0	
Anikin et al.[56]	0.575										0	
"	1.33	O						0			0	
"	2.45	O						0			0	
"	4.5	O						0			0	
"	5.6	O						0			0	
"	8.4	O						0			0	
Palla[70]	14.7										0	
"	15									0		

could produce an increase in $\sigma(\Theta)$ at scattering angles $\Theta < 15^{\circ}$, where the magnitude of the increase depend on the electric polarizability coefficient α. Such scattering should occur, following from the general ideas of theory [73,74], for 1-5 MeV neutrons, if α is with a value of several times more than $2 \times 10^{-42} cm^3$ [58].

The value of α, obtained by Aleksandrov[71], interpreting his experimental data at 2.8 MeV in terms of polarization scattering, is $8 \times 10^{-41} cm^3$; Thaler[75], analysing low energy data of Langsdorf et al.[76], gave an upper limit for α which is $4 \times 10^{-41} cm^3$. At the mean time the values of α obtained from theory, e.g. the values reported by Barashenkov[78], Moroz et al.[74] and Breit et al.[77], are substantially smaller than those obtained from experimental data.

Besides Fossan and Walt[57] calculated the contribution of polarization scattering in the differential cross-section, for the case when 0.570 MeV neutrons are scattered by Uranium, assuming different values of α, Fig. 5, where they found that a value of $\alpha < 2 \times 10^{-40}$ (even zero) is consistent with their experimentally measured cross-section at the mentioned energy[64].

Thus the assumption, that the anomalous scattering is due to the neutron polarizability, is not yet confirmed. It is more likely that these anomalies are due to the models used for interpreting the experimental data; some of the observed anomalies disappeared when the same data were reinterpreted by a different model (e.g. data of Dakarevich et al.[69] for U at 14.2 MeV, when reinterpreted by Aleksandrov et al.[66] and for Th as reinterpreted by Palla[70] (see

table 1.1).

However the analysis carried by Anikin and Kotukhov[56], for their data, within the framework of the optical model leads to the view that the agreement between the measured angular distributions and the calculated ones can be noticeably improved by introducing a small correction to the nuclear potential, corresponding to α in the order of $2 \times 10^{-40} cm^3$; This value seems to be consistent with that one, mentioned before, of Walt and Fossan[64].

1.3.4. The polarization resulting in Mott-Schwinger scattering

Schwinger[45] predicted that practically complete polarization would result from the scattering of 1 MeV neutrons, initially un-polarized, by lead through a scattering angle $\theta = 1.5^o$, and that the polarization will decrease to $P(\theta) = 0.32$ at $\theta = 9^o$.

The first attempts to measure the polarization of a neutron beam, using Mott-Schwinger scattering, were by Longley et al.[79] and Sample et al.[80] for few MeV neutron energies, and did not lead to conclusive results.

First demonstration of the effect was by Voss and Wilson[81] where they detected the polarization of 100 MeV neutrons scattered by Uranium through angles below 1°. This was supported by Hillman et al.[82] where they detected again the effect, using slightly different technique, through $\frac{1}{5}^o$.

Further calculations of the effect were carried out by Baz[83] for neutrons of few MeV scattered by Pb. He applied in his calcu-lations optical model parameters based on Pb experimental cross-sections published by Rhein[84] and obtained the value of polarization

as a function of both the incident neutron energy and scattering
angle.   His calculations, presented in Fig. 6, lead to a much
more rapid decrease of the neutron polarization with increasing
scattering angle.   Besides the values he obtained for 1 MeV
neutrons are lower than those obtained by Schwinger.   These calcu-
lations were supported by the experimental measurements carried out
by Gorlov et al.[85] for the case of scattering of 4 MeV neutrons by
Pb.

The Mott-Schwinger effect was demonstrated, for neutrons of
several MeV, by Gorlov et al.[67,86,87] where they detected polari-
zation in scattering of 4 MeV neutrons by U, Cu, Su, Pb, Bi and In
at scattering angles 2°, 4° and 6°, by Elwyn et al.[62] where they
detected polarization in scattering of 0.83 MeV neutrons from
Uranium through angles 1.65^o, 2.35^o, 4.6^o and 10° and by Kuchnir
et al.[68] where they scattered neutrons of different energies,
between 0.6 – 1.6 MeV, by U, Th, Au, Pb and W through scattering
angles 1.75^o, 2.5^o, 4.0^o, 4.5^o, 6°, 8.0^o, 10° and 15°.

Measurements carried out by Elwyn et al. for 1 MeV neutrons
scattered from several nuclei, with Z in the neighbourhood of 40,
indicated a polarization effect at a scattering angle as large as
24°.   While in these measurements the differential cross-sections
did not exhibit any anomalous behaviour, at the mentioned angle, nor
did the polarizations observed at other angles (56°, 86°, 118° and
150°).   In order to explain this, as the previous calculations
restricted Mott-Schwinger scattering by angles $\leq 10^o$, Monahan et al.[61]
carried out calculations of the effect using more generalised Born
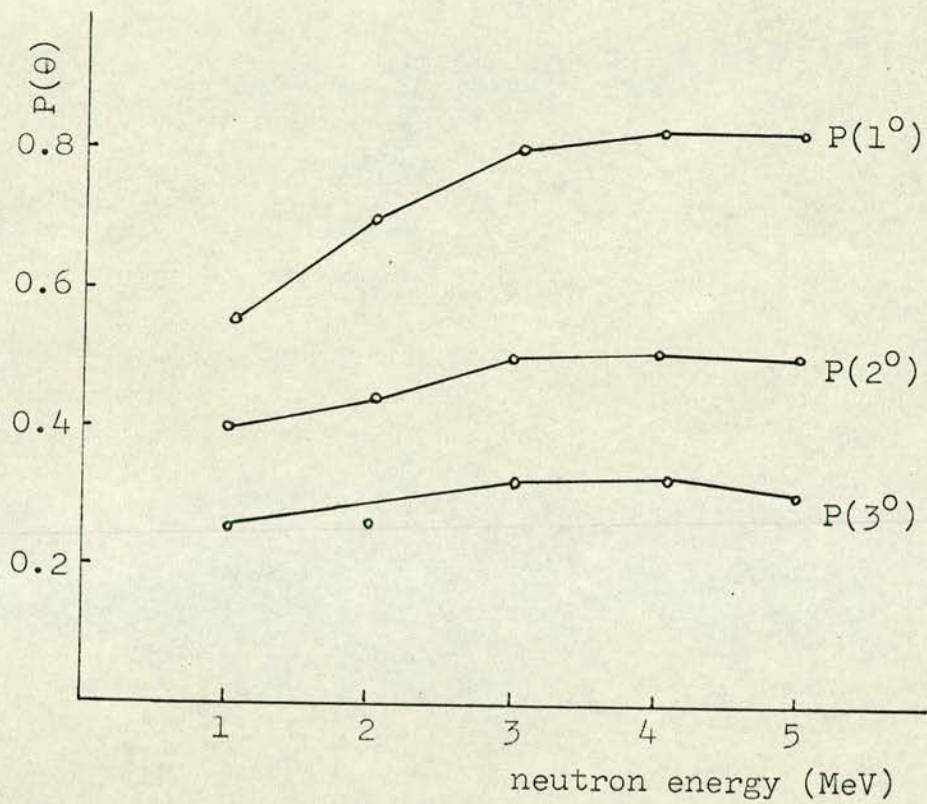
Fig. 6. The lead analyzing power as function
of both the neutron energy and
scattering angle

approximation; allowed for simultaneous evaluation of nucleon and electromagnetic interactions. Such an approach could account for a substantial part of the polarization they observed at 24°, even when neutrons are scattered from nuclei with moderate charge ($Z \gtrsim 40$). This approach was further developed by Redmond[52] and Hogan and Seylor[63] where it was concluded that the polarization can be influenced by Mott-Schwinger scattering at angles much greater than had been previously considered.

Thus calculations, carried out so far, of the polarization resulting in Mott-Schwinger scattering lead to different conclusions concerning both the amplitude of the effect and the range of angles where its influence extends. However, beside the fact that the effect has been demonstrated experimentally, all calculations agree about its influence at angles $\leq 10^{\circ}$.

1.4. Polarization of Neutrons Emitted from the $D(d,n)^3He$ Reaction.

The polarization of neutrons emitted from the $D(d,n)^3He$ reaction was first observed in 1953 by Baumgartner and Huber[15,89] as well as by Ricamo[6,7], where in these experiments Carbon was used as polarization analyser.

Actual measurements of neutron polarization in the $D(d,n)^3He$ reaction followed by Meier et al.[90], where he measured the polarization of neutrons emitted at several angles from a thin D_2O target bombarded by 600 KeV deuterons, and by McCormac et al.[91], who used a thick target at deuteron energies between 500 and 700 KeV. Again in these measurements ^{12}C was used for analysing the emitted neutrons.

In order to avoid background difficulties and because of the uncertainty involved in the phase-shift analysis, when carbon is used as polarization analyser, Levintov et al.[8] used scattering from helium for detecting polarization. In their measurements, covering the energy range from 600 - 1800 KeV, the recoil nuclei in ^{4}He counters with directional properties, were detected instead of the scattered neutrons.

At about the same time, 1956, Pasma[92] employed ^{4}He as polarization analyser in a technique, where scattered neutrons were recorded in coincidence with helium recoil nuclei. For this purpose he developed a helium gas scintillation counter in which the light pulses accompanying the recoil α-particles are detected.

Since then helium has been widely used as polarization analyser, in most of the D(d,n)^{3}He polarization measurements to date (see table 1.2). This is due to the fact that building a He gas scintillator does not involve so many technical difficulties as in the case of the liquid one[4,23,93,94]. Liquid helium is a more efficient scatterer scintillator[95-98], but it demands, beside a liquid helium source for 'topping up' as loss rates are of the order of 12 ccs / hour[99], very low temperature techniques. Besides the use of liquid helium is connected with complications, when analysing the experimental data, of the need for multiple scattering corrections which may well be larger than those required for finite geometry[100,101]. However with the recent improvements of the resolution of liquid helium scintillators the application of a spin precession solenoid between the ^{4}He scatterer and the neutron producing target, for interchanging the role of the detectors, is becoming very attractive[102].

Table 1.2: The experimental arrangements so far used for measuring polarization from the $D(d,n)^3He$ reaction.

Reference	Target	Analyser	Experimental details
Meier et al.[90]	D_2O	^{12}C	2 neutron detectors
McCormac et al.[91]	"Drive in" Cu	^{12}C	2 neutron detectors
Levintov et al.[8]	Zr-D, 150 KeV and thick	^4He	He recoil in directional proportional counters
Pasma[92]	D_2O, 50KeV	^4He	He gas scintill., 2 interchangeable neutron detectors
Kane[133]	"Drive in" Al	^{12}C	1 neutron side detector
Ot-Stavnov[103]	D_2O	^4He	He recoil in directional proportional counters
Steuer et al.[104]	D_2O, thick	^{12}C	
Boersma et al.[105]	TiD, 50KeV	^4He	He gas scint., 2 neutron detectors with P.S.D., solenoid
Rogers et al.[106]	D_2O thick	^{12}C	Accelerated beam not analysed, 2 neutron detectors
Hansgen et al.[107]	D_2O thick	^{12}C	2 neutron detectors with P.S.D.
Mulder[108]	D_2O, 50KeV	^4He	Diffusion cloud chamber
Behof et al.[109]	D_2O, thick	^4He	He gas scint., 2 interchangeable neutron detectors with γ-rejection by timing
Stoppenhagen et al.[110]	TiD, thick	^{12}C	Associated ^3He time of flight, solenoid
Thomas et al.[111]	TiD, 400 μg/cm²	^4He	He gas scint., 2 neutron detectors

Table 1.2 (Contd.)

Reference	Target	Analyser	Experimental details
Prade et al.[112]	TiD, thick	^{4}He ^{12}C	Expansion cloud chamber Associated ^{3}He coincidence, 1 neutron side detector
Roding et al.[113]	TiD, 186 μg/cm²	^{4}He	He gas scint., 2 neutron side detectors with γ-rejection by timing.
Daehnick[114]	Deuter. gas	^{4}He	^{2}He proportional counters, a scatterer, 2 interchangeable neutron detectors
Baicker et al.[99]	gas	^{4}He	Pulsed beam time of flight, liquid He scatterer, 1 neutron side detector
Avignon et al.[115]	gas	^{4}He	He gas scint., 2 interchangeable neutron detectors
Dubbledam et al.[116]	gas 175-350KeV	^{4}He	Solenoid, He gas scint., 2 neutron detectors
May et al.[117]	gas	^{4}He	Solenoid, He gas scint., 2 neutron detectors
Niewodniczdanski et al.[118]	gas	^{4}He	He gas scint., 2 neutron detectors (interchangeable)
Trostin et al.[119]	Zr-D, 19 mg/cm²		
Babenko[120]	gas	^{4}He	He gas scint., 2 interchangeable neutron detectors
Bondarenko et al.[121]		^{4}He	He recoil in directional proportional counter
Purser et al.[122]	gas	^{4}He	He gas scint., 2 neutron detectors

Table 1.2 (Contd.)

Reference	Target	Analyser	Experimental details
Miller[123]		^{4}He	Pulsed beam time of flight, liquid He scint., 2 neutron detectors (interchangeable)
Lam et al.[124]		^{4}He	Pulsed beam time of flight, liquid He scint., 2 neutron detectors (interchangeable) with P.S.D., simultaneous real and random coincidences
Drigo et al.[125]	TiD	^{4}He	He recoil detection in triple proportional counter
Gorlov et al.[85,86,134]	D$_2$O,400KeV	U, Cu, Pb, In, Sn and Bi	Using Mott-Schwinger scattering at 2^0, 4^0 and 6^0
Davie[126]	TiD, thin	^{4}He	He gas scint., 2 neutron detectors (inter-change-able) with P.S.D., simultaneous real and random coincidences
Spalek et al.[127]	gas,150KeV	^{4}He	Solenoid, He gas scint., in coincidence with two side detectors (plastic scint.)
Gorlov[128]		In,Pb, Sn and Bi	Using scattering from In, Pb, Sn and Bi at large backward angles (146^0 - 177^0)
Smith et al.[129]	gas,300-400KeV	^{4}He	Liquid ^{4}He, 2 neutron detectors associated with time of flight technique

As the measurements described in this thesis are in the deuteron energy range below 10 MeV, the experimental arrangements used in the $D(d,n)^3He$ polarization measurements, so far reported in the mentioned range, are presented in table 1.2. The state of neutron polarization in the $D(d,n)^3He$ reaction was reviewed on several occasions; It was reviewed by Haeberli[4] in 1961, Alekseev[3] in 1964, Meyerhof and Tombrello[130] in 1968, and recently by Galloway[131] and by Walter[132].

Neutron polarization, so far reported for deuteron energies ≤ 10 MeV and reaction angle = $45° \pm 5°$, are represented in Fig. 7, where some of the reported data, e.g. data of Hansgen et al.[107], Thomas et al.[111], Prade et al.[112] and Rogers et al.[106], are omitted for clarity.

These data, not represented in Fig. 7, are in the energy range below 1 MeV and support the existence of a peak in the polarization at deuteron energy $\sim$ 100 KeV.

The existence of such a peak was discussed by Fick[135,136] where he relates it to a narrow resonance in the D-D system. Such an explanation was not confirmed by the experiments carried out by Ad'eseirch et al.[137] using polarized deuterons.

Existing theories[138-143] do not account for a peak in the energy dependence of the polarization in the region below 200 KeV. Besides Hansgen and Nitzsche[144], as a result of a new set of measurements in the same energy range using scattering from ^{12}C, do not relate it completely to the $D(d,n)^3He$ reaction. In this recent explanation they relate the low energy part of the peak to the increase of the $D(d,n)$ reaction's polarization and the high

Fig. 7. The D(d,n)^{3}He neutron polarization at reaction angle = $45^\circ \pm 5^\circ$ lab.

Legend:
- ⊙ Pasma[92]
- ○ Meier et al.[90]
- ◐ Daehnick[114]
- ○ Davie[126]
- ⊖ Trostin et al.[119]
- ▲ Boersma[105]
- ▽ Stoppenhagen et al.[110]
- ▼ Levintov et al.[8]
- ◈ Steuer et al.[104]
- ◆ Avignon et al.[115]
- ◆ Purser et al.[122]
- ◇ Dubbeldam et al.[116]
- ▫ Mulder[108]
- ▣ Behof et al.[109]
- ▣ McCormac et al.[91]
- ▣ Spalek et al.[127]
- ✕ Smith et al.[129]
- ▽ Roding et al.[113]
- ⬠ Bondarenko et al.[121]
- ▽ Baicker et al.[99]

P_n(%)

Ed(MeV)

32

energy part to the rapid decrease of the ^{12}C analysing power.

Although these low energy data were excluded from representation in Fig. 7, discrepancies between results reported by different authors are remarkable over the whole range; a situation difficult to explain. Nevertheless it is worth noting the general trend of most of them; if one excludes data of Pasma[92], Meier et al.[90], McCormac et al.[91], Roding et al.[113], Baicker et al.[99], Avignon et al.[115] and that point of Dachnick[114]. The remaining data, excluding that point by Levintov et al.[8] at 400KeV, follow a trend which supports, at deuteron energy < 1 MeV, the theory of Boersma. There is more basis to support such a trend than the trend of the excluded data. For example the data of Pasma[92] were criticised by Boersma[105] where he suggested that they should be corrected for instrumental asymmetry and even though Walter[132], agreeing with Pasma, excluded them in his recent review. The other points were obtained either using scattering from ^{12}C, e.g. those of Meier and McCormac, where the phase-shifts are not as well known as for helium[131], or using scattering from helium. Nevertheless one has to bear in mind that the data of Roding et al. must have been obtained by scattering from helium at an angle where the analysing power is poor, this becomes obvious when one compares the low asymmetries they report with their polarization values[113] and that the data of Baicker et al. was obtained using scattering from liquid helium where such a technique was still at a preliminary stage, e.g. high background and poor resolution.

Concerning the D(d,n)^{3}He polarization measurements, using Mott-

Schwinger scattering, there is only one measurement; it was carried out by Gorlov et al.[85,86,134] by scattering 1.2 MeV deuterons, through angles 2°, 4° and 6°, from U, Cu, Pb, In, Su and Bi. This measurement, as well as the measurements reported recently by Gorlov[128] and carried out by scattering neutrons, produced at deuteron energies 1.2, 2, 2.38 and 2.7 MeV, from In, Su, Pb and Bi through backward angles between $146^\circ - 177^\circ$, is not represented in Fig. 7 as the reaction angle was 37°.

1.5. Conclusion

As the present situation of the $D(d,n)^3He$ polarization, below 10 MeV, is not completely settled, it is worth while to produce a set of measurements, as accurately as possible, in this energy range; this would help in resolving the existing discrepancy as well as calibrating one of the main sources of polarized neutrons.

Such a set of measurements will be described in the following chapters of this thesis, where they can be classified as:

a) Measurements below 1 MeV

b) Measurements between 1 - 5 MeV.

Measurements below 1 MeV were carried out using both scattering from helium and the Mott-Schwinger one, while the other set, between 1 - 5 MeV, are by scattering from helium; the most recent measurements, in the latter range, using scattering from helium are those of Smith and Thornton[129] represented in Fig. 7; they became available after completion of the experimental work described in this thesis.

Measurements at deuteron energies below 1 MeV using both the Mott-Schwinger scattering and the helium one should be useful. On the one hand if both the measurements will agree, it should be a further step towards solving the ambiguity about the energy dependence of polarization below 500 KeV.   Beside this there is still a lack of information concerning scattering from heavy nuclei at small angles, so measuring the polarization of the $D(d,n)^3He$ reaction by applying Mott-Schwinger scattering should result in more information about the differential cross-section, of the used scatterers, at small angles.

CHAPTER TWO

D(d,n)^{3}He POLARIZATION MEASUREMENTS USING SCATTERING
FROM HELIUM

CHAPTER TWO
$D(d,n)^3He$ POLARISATION MEASUREMENTS USING SCATTERING FROM HELIUM

The measurements described in this chapter, as well as those described in the rest of this thesis, are with neutrons emitted from the $D(d,n)^3He$ reaction; deuterons accelerated to the desired energy, bombard a deuterium target; neutrons emitted at the angle of interest are then scattered by the analyser, which is helium in these measurements.

Accordingly in the following sections will be described the target arrangement (used during all the measurements described in this thesis) and the cooling system attached to it, then the ^4He polarimeter and finally the actual measurements and their treatment.

2.1. The Target Arrangement

The target used is a TiD (deuterium gas absorbed in titanium layer) on a copper backing foil in the form of a strip, 1.5 cm long and 3 mm wide; it is soft soldered to a specially designed brass holder which provided an arrangement for water cooling of the target. Such cooling is required to prevent thermal out-gassing of deuterium.

The particular design of the target holder (see fig. 8), helped to reduce the scattering background, as the material close to the target is very little. Besides the target could be accurately located, mechanically, relative to the accelerator beam tube and the He polarimeter; once it is aligned, the target holder can be removed for replacing the target without a need for realigning the whole system when it is fitted again.
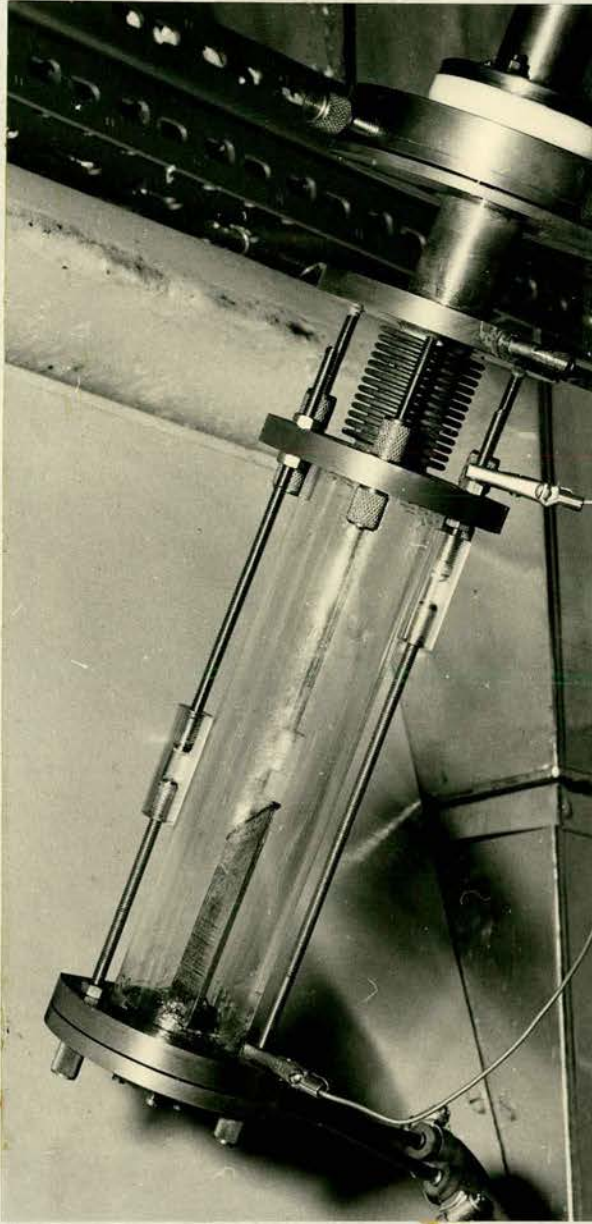
Circulating cooling water
going to the target.

Fig. 8.   Photograph of the target arrangement.

The efficiency of the water cooling system applied to the target was studied, in a specially performed experiment. The experiment is similar to that one carried out by Rethmeier et al.[145], for investigating the variation in the target temperature with the power of the incident beam; a diagram of the experiment is represented in Fig. 9, where heat is conducted through a copper rod, of the same diameter as the deuteron beam, from an electric heating element mounted on its top. The other end of the rod (5 cm long) is soldered, in place of the target, to the top of the cooling system; the whole system is under vacuum. In such arrangement, the target temperature is that one at the contact point between the rod and the cooling system; this was determined from the temperature gradient along the rod. For this purpose a group of thermocouples were employed; six thermocouples were coupled to the rod, through holes specially drilled right to its centre, where a distance 7 mm was kept between each two of them.

For studying the power dissipated by the cooling system, another three thermocouples were employed; one of them was connected to the top of the rod, where the heating element is mounted, see Fig. 9, and the other two were dipped into the ingoing and outgoing cooling water.

All the thermocouples, connected to the system, were then connected, through a switch, to a digital voltmeter (Solartron type), where the measured thermoelectric voltages were typed out. Corresponding temperatures were then determined from calibration chart.

Thus from the measured temperatures, at the six points along
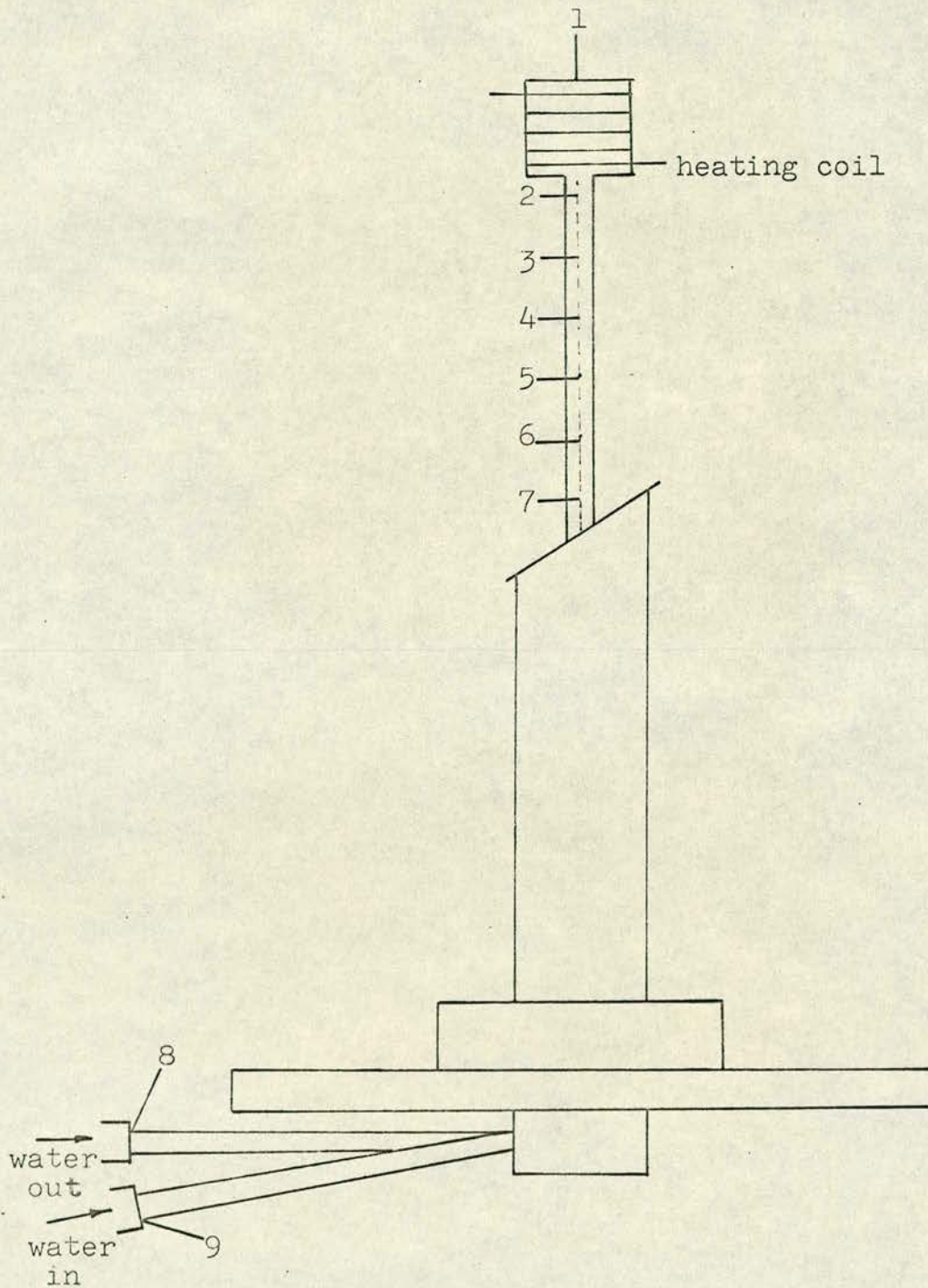
Fig. 9. The arrangement used for studying
the target temperature.

1-9 are the thermocouples connected
to the system.

the rod, the temperature at the contact point, with the cooling system, was determined by extrapolation; the value ΔT is the difference between the temperatures measured by the two thermocouples connected to the cooling water.

Three copper rods representing three different beam cross-sections were used during these measurements; two of them were with circular cross-sections, their diameters are 2.5 and 3.5 mm, and the third rod has a rectangular cross-section (3.5 x 20 mm).

Although the system was kept under vacuum, there was a need to wrap the rod with rectangular cross-section with asbestos in order to prevent heat transfer from its surface; the temperature gradient along it was not linear when asbestos was not used. With asbestos around the rectangular rod the amount of heat transferred from its surface, as estimated from both the power given by the heating element and that one conducted through it to the cooling system, was not more than 3%.

The value Δt was measured for the three rods, varying the water flow at a fixed incident power, and it was found that, for all of them, Δ was steady ($\sim 1°$) at water flows > 7 c.c./sec. Such typical dependency is represented in Fig. 10 for the case when the rod, of diameter 3.5 mm, was used and the incident power was 46 watts; the target-water temperature difference $T_t - T_w$, was constant for such water flows (Fig. 11).

The value of $T_t - T_w$, as a function of the incident power is

$\Delta T(C^{o})$

Fig. 10. ΔT as a function of the water flow at 46 watts.

Water flow (CC/Sec)

$T_r - T_w(C^{o})$

Water flow (CC/Sec)
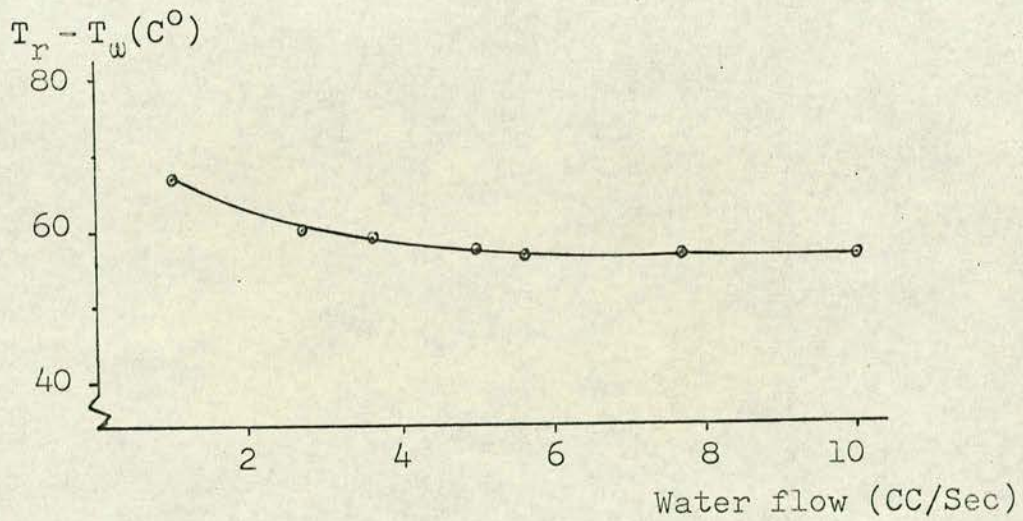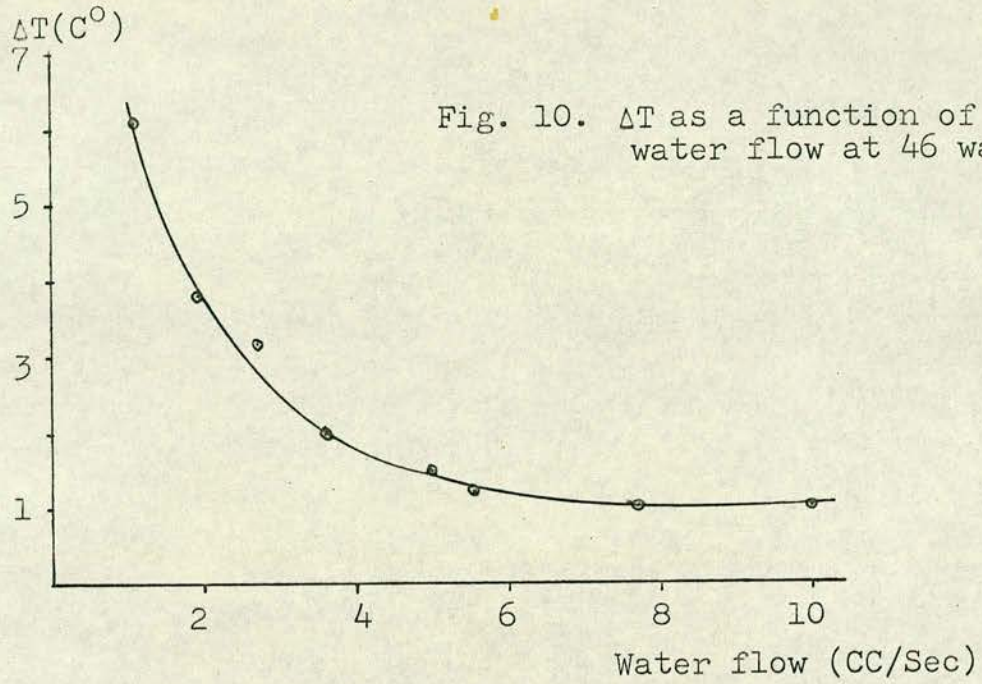
Fig. 11. The target temperature as a function of the water flow at 46 watts.

represented in Fig. 12 for the three beam cross-sections.   Note
that the target temperature, at a particular incident power, is
smaller for the rectangular beam cross-section than the other two
circular ones (see Fig. 12).   The effect of soldering, i.e. a need
to solder the rod to the cooling system with silver, mentioned in
ref.[145] was not found;   the same linearity was obtained (see Fig. 12)
when the soldering was repeated;   the rods were soldered to the
cooling system with usual soft solder.

However the target temperature does not exceed $100^{o}C$ when a
beam with diameter 3.5 mm is incident with power 75 Watts (see Fig.
12);   accordingly this cooling system is highly efficient as the
target temperature is nearly half the permissible limit i.e. $200^{o}C$.

This cooling system proved to be efficient enough, during
actual measurements where a TiD target, with $0.9 \ mg/cm^2$ titanium
layer, was bombarded with a 50 μ A beam of deuterons incident with
0.5 MeV energy;   the neutron yield from the target reduced to 50%
of the original value, only after 50 hours of bombardment;   a figure
of merit representing the life of such target[146,147] is ~ $3 \ m \ Ah/cm^2$;
this value seems to be consistent with the value $2.7 \ m \ Ah/cm^2$ for a
tritium titanium target reported in ref.[147].

2.2.   The Helium Polarimeter

The helium polarimeter, used during the measurements described
in this chapter, is schematically represented in Fig. 13;   neutrons,
emitted from the TiD target, pass through the aperture of a throated
collimator, then scattered by the helium gas scintillator and
detected by the two side detectors.
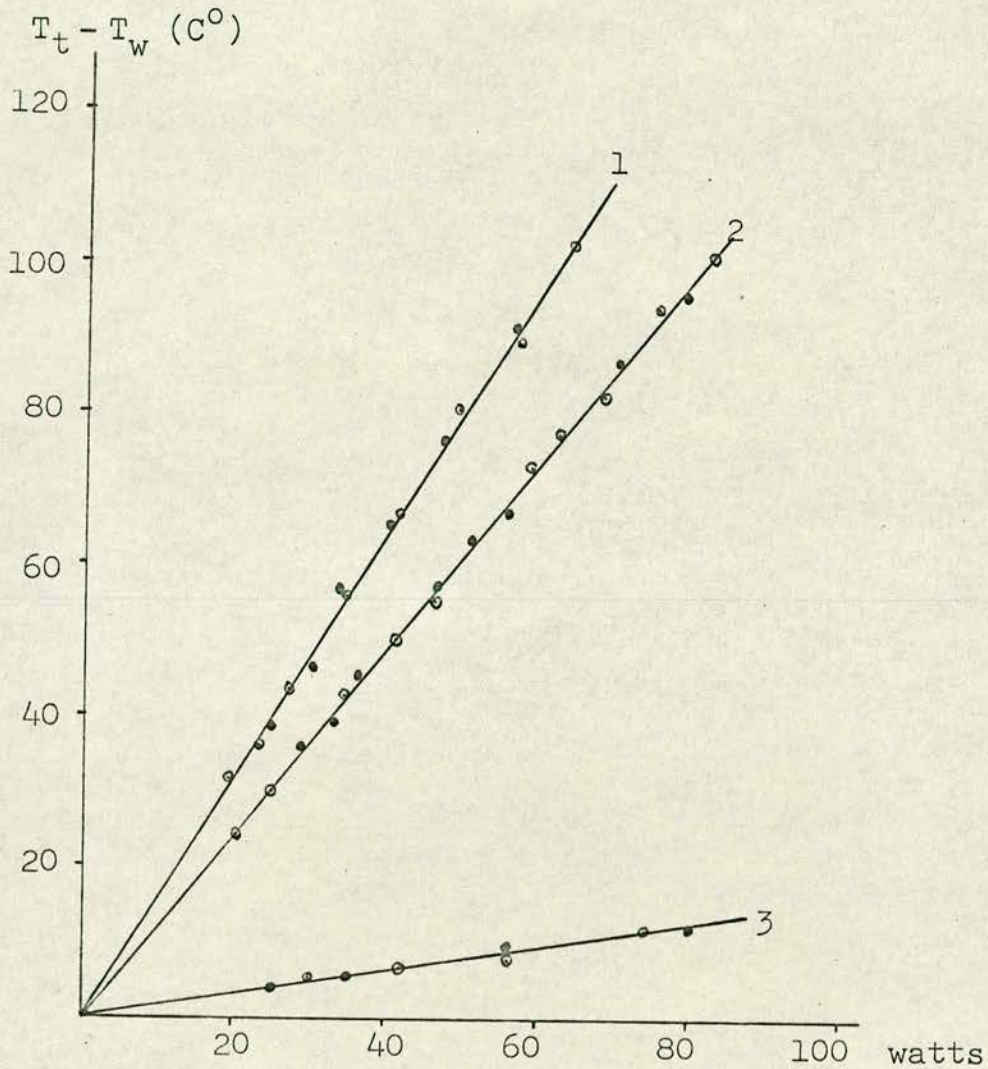
Fig. 12. The target-water temperature difference as a function of incident power.

1 - Circular beam cross-section (2.5 mm diam.)
2 -   "   "   "   "   (3.5 mm diam.)
3 - Rectangular beam cross-section

• - First soldering
⊘ - Second soldering
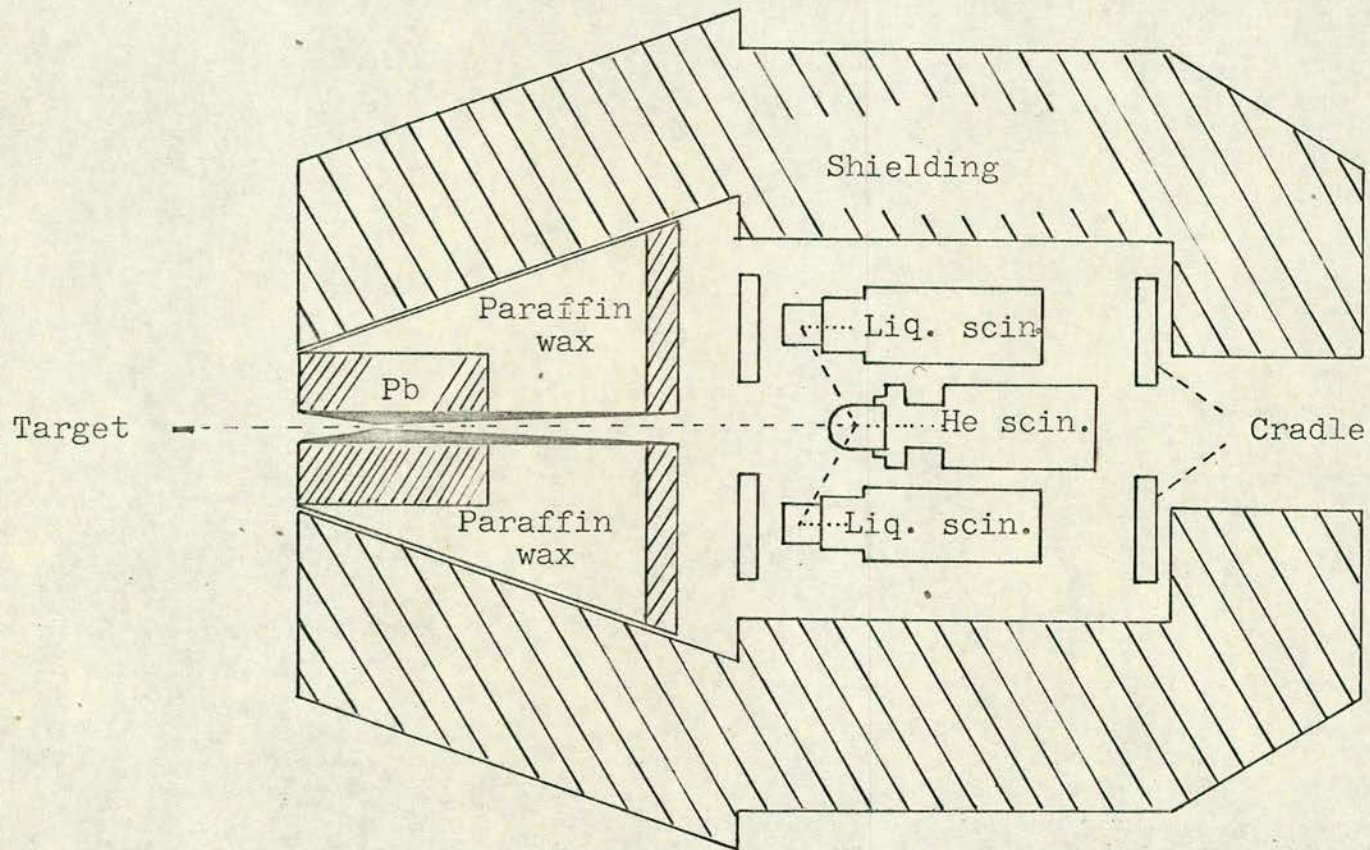
Fig. 13.   The Helium Polarimeter.

The collimator itself is of 46 cm length and constructed of a steel body narrower at the front than the back; such design is meant specially for angular distribution measurements where there is a need to rotate the collimator and polarimeter around the target. Two layers of lead are included in the collimator; the front layer, close to the target, is cylindrical, 20 cm diam. and 20 cm long, and is used to degrade the energy of undesired neutrons by inelastic scattering. The back layer, 5 cm thick, is actually covering the whole back of the collimator; it reduces the γ-ray flux resulting from neutron capture in the paraffin wax filling the space between the two lead layers. The throat of the collimator is formed by brass and polythene inserts, each 5 cm long, so that by varying their number, the position of the throat, and consequently the area of the helium scintillator illuminated by the neutron beam can be changed. The distance between the collimator's throat and the source is usually selected on the basis that the solid angle subtended by the helium gas scintillator at the target is of a value allowing complete illumination of the scintillator by the collimated neutrons; this is in order to avoid false asymmetry which might result, if the dimension of the incident neutron beam, at the centre of the ^{4}He gas, is less than the scintillator's diameter, and if the position of the incident deuteron beam at the target is, for some reason, shifted. Besides it fulfils the requirement for obtaining the highest scattering efficiency of the ^{4}He scintillator.

The ^{4}He gas scintillator in its design is similar to that designed by Shamu[148]; it is a steel container in the form of a

cylinder, 5 cm diameter, where its side facing the collimator is a
hemisphere in shape.   Its axial length is 6 cm;   the thickness of
its wall is 2 mm.   The internal surfaces of the container are
coated with a reflecting layer of aluminium, then with a layer of
magnesium oxide, deposited electrostatically[149] (up to a thickness
~ 2 mm) and finally with a coating of di-phenyl stilbene of similar
density and distribution as described in[150].   The other side of the
container, where it is coupled to the photomultiplier, is a quartz
window, 2.5 cm thick, coated on the side in contact with helium,
with di-phenyl stilbene according to ref.[150].   A cross-section of
the helium gas container is represented in Fig. 14;   it is usually
filled with 5 atm of Xenon and 65 atm of ^{4}He, in order to function as
a scintillator;   it is usually refilled about every six months;
this is due to a slight gas leakage[94].

Each of the two side detectors uses a NE 213 liquid
scintillator, encapsulated in a special bubble free cell, Nuclear
Enterprises Ltd. BA1 modified type, of 5 cm length and 5 cm diameter,
with the nitrogen expansion bubble contained in a coiled capillary
tube on the end face.   The use of a bubble free cell is required
to maintain a detection efficiency unaffected by rotating the two
detectors, e.g. for interchanging their roles, for checking the
existence of instrumental asymmetries in the plane perpendicular to
the reaction plane.

The three detectors, the ^{4}He gas one and the two side
detectors, are mounted on a cradle (see Fig. 15), rotatable accurately
through angles up to 360° in 90° steps, about an axis joining both
the ^{4}He gas scintillator and the neutron producing target;   this

Stainless steel
~ 0.2 cm thick walls

~ 5 cm

quartz win.

Photomultiplier

High pressure valve
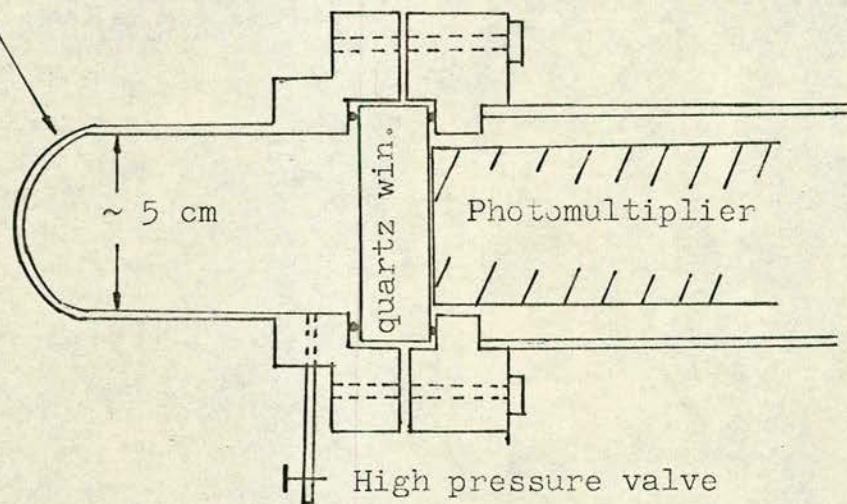
Fig. 14. Cross-section of the ^{4}He gas scintillator.

The rotating cradle
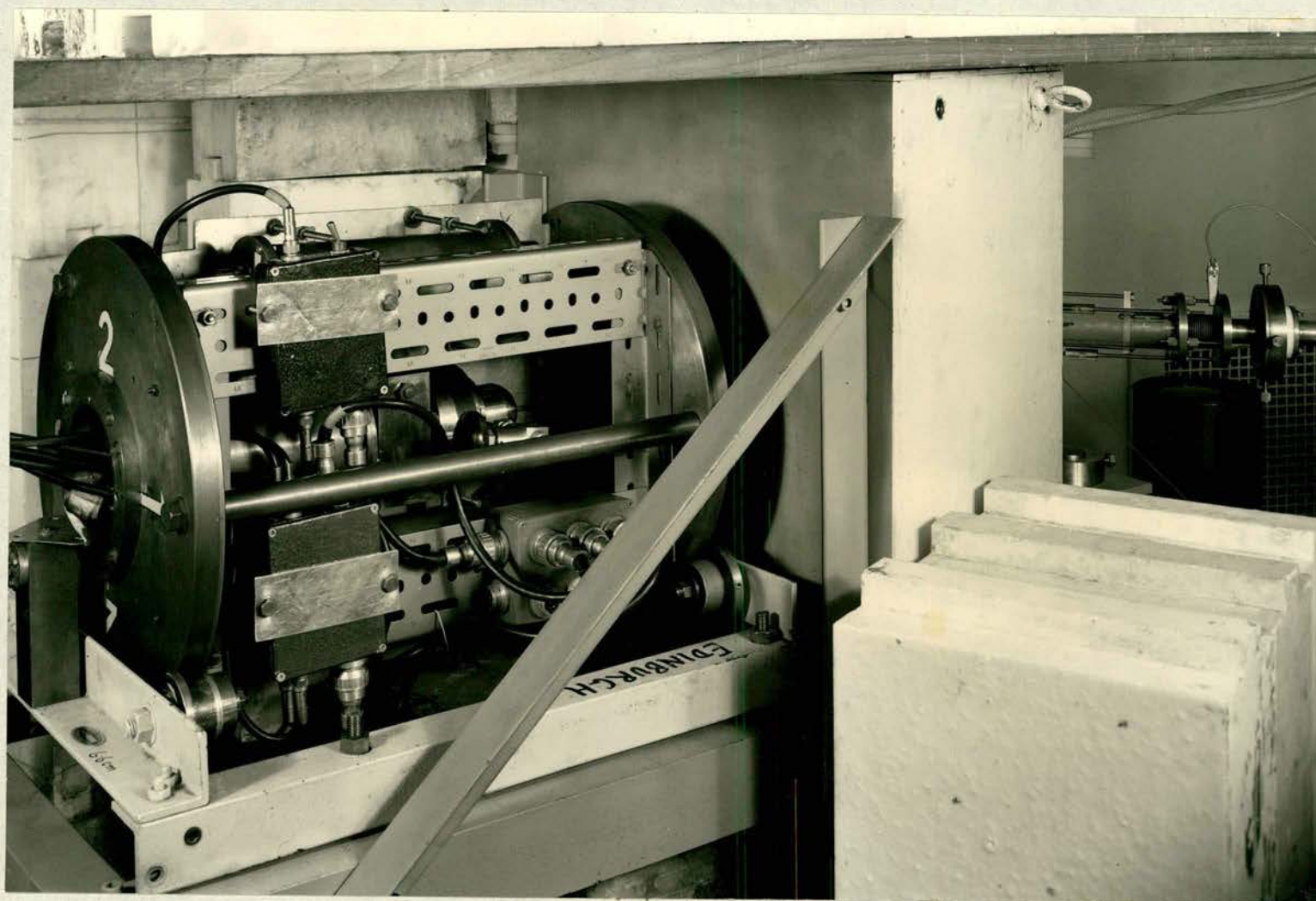
The TiD target holder

Fig. 15. Photograph of the polarimeter.

cradle, with the three detectors, is the same one used before during measurements carried out by Davie below 1 MeV deuteron energy[126].

Although the collimator provides primary shielding, for the side detectors, from neutrons scattered from the neutron producing target, it was not enough to shield them from other neutrons scattered from the laboratory ceiling etc.

In order not to allow other neutrons, rather than those scattered from the helium gas scintillator, to be detected by the side detectors, secondary shielding was used both around the polarimeter and on top of it; the shielding is of about 25 cm thickness, is built up from the available shielding material; blocks of borax loaded resin were used for this purpose (see Fig. 16), during measurements (at incident deuteron energies > 1 MeV) which took place at UK A.E.A, Harwell; Cans filled with either borated water or paraffin wax were used, for the same purpose, during measurements, at Edinburgh University, below 1 MeV.

2.3. Electronic Arrangement of the Polarimeter

The electronic arrangement of the polarimeter was developed by Davie and Galloway[94] and is described in more details in[126]; it applies a coincidence technique to the detection of both the He recoils and scattered neutrons. For this purpose the scintillations in the ^{4}He gas are transferred, through the quartz window, to a 6255 B photomultiplier coupled to the helium container; each of the two liquid scintillators is coupled to a 6262 B, EMI type, photo-multiplier, where a linear signal from the 11th dynode is utilized
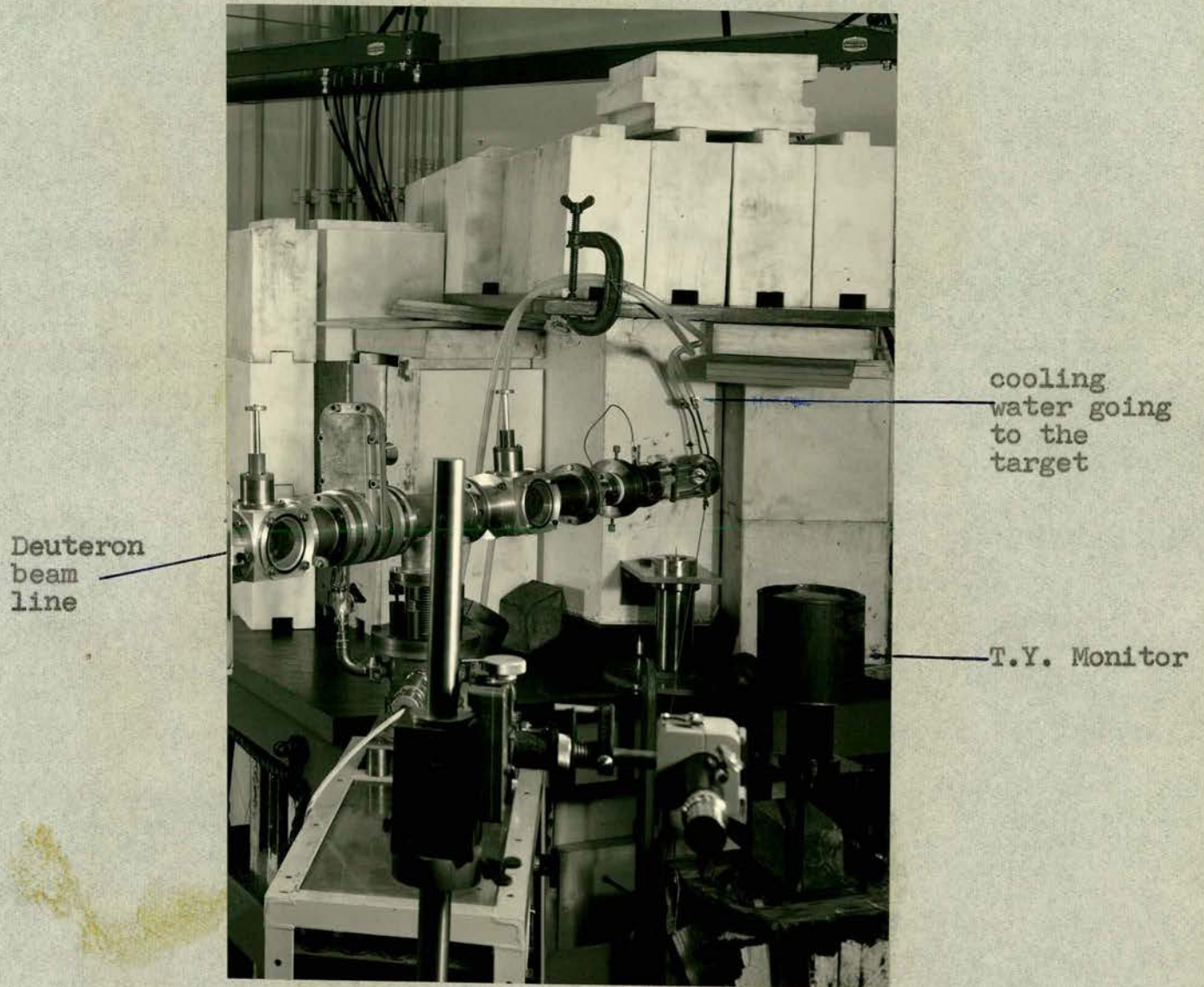
Fig. 16. Photograph of the polarimeter being surrounded
with Borax loaded shielding.

with circuitry of the same type developed by Roush et al.[151], to
provide pulse-shape discrimination against γ-rays resulting from
neutron capture by the shielding material.   Such procedure for
pulse-shape discrimination was applied instead of the Owen[152]
technique as it was found that the latter is affected by rotation
of detectors, around the axis joining the target and the He gas
container which can be a source of false asymmetry.   The linear
pulse from 11th dynode was found not to be affected by rotation[94].

The electronic block diagram is represented in Fig. 17, two
coincidence units, 1 and 3, determine (real + random) coincidences
between the side detectors and the ^{4}He gas scintillator.   The
other two units, 2 and 4, detect the random coincidences only by
delaying the pulses from the He scintillator.

Thus both prompt and delayed coincidences between each side
detector and the He gas scintillator are recorded and used to gate four
pulse height spectra of associated ^{4}He recoils in the gas scintillator.
Triple coincidence unit 1 receives from the "right" side scintillator
an input corresponding to linear signals above 100 KeV electron recoil
energy and simultaneously a neutron identifying input, which are
required to be in coincidence with an input from the ^{4}He gas
scintillator, where a resolving time of ≈ 1 μ sec. is used.

Coincidence unit 2, receives signals identical to unit 1 from
the "right" side scintillator but in coincidence with a delayed input
from the He gas scintillator;   the input from the gas scintillator
is delayed by 3 μ sec. to give outputs which are only due to the
random coincidences.

KEY: EHT – EHT power supply   P/A – Pre-Amplifier
       PSD – P.S Discriminator   AMP – Amplifier
       DIS – Integral Discriminator DEL – Delay
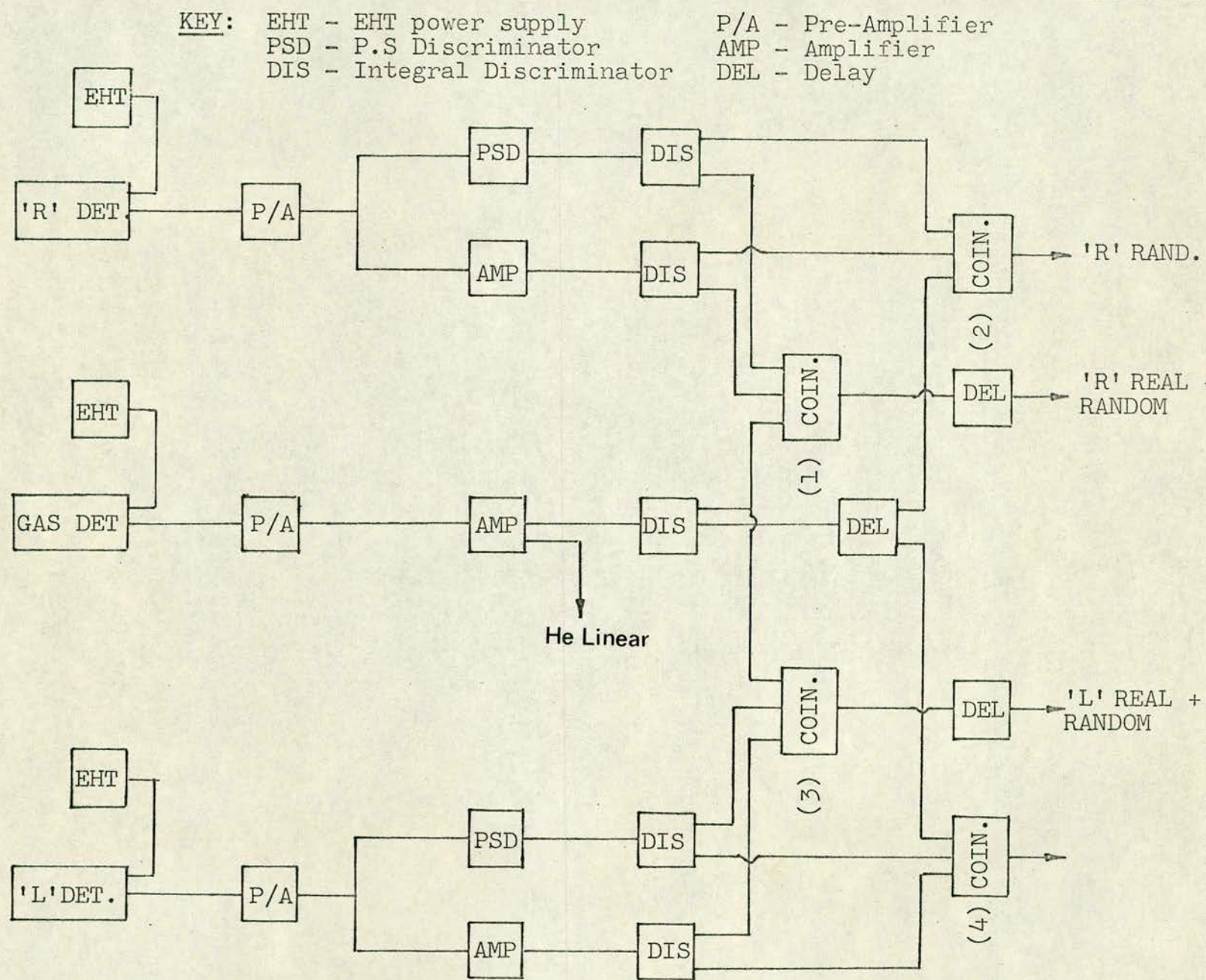
Fig. 17.   The electronic block diagram of the helium polarimeter

Triple coincidence units 3 and 4 operate the same way as units 1 and 2 respectively but for the "left" side detector.

Following after coincidence units 1 and 3 were applied another two delay units, set at 3 μ sec. delay time, to bring all the four coincidence outputs into the same time relation with respect to the linear output from the ^{4}He gas scintillator; this is in order to produce the desired gated spectra.

Thus to the analyser's memory are transferred, through a specially designed routing unit, four spectra; the first two sections of the memory record (real + random) coincidences from both 'right' and 'left' side detectors respectively, while the next two sections record the random coincidences from the same detectors and in the same order. Besides the pulses are transferred, through a shaper coupled to the routing unit to four scalers. Fig. 18 shows typical spectra recorded during measurements for incident deuteron energy 2.5 MeV and neutrons emitted at laboratory angle 75°; they are plotted, in histograms, using a PDP-8 data processor at the UKAEA, where each two spectra, related to one of the side detectors, are overlapped.

During the actual measurements, the analyser is connected to a high speed paper tape punch; this allowed the four spectra, stored in the analyser's memory, to be punched out on a paper tape within less than one minute, at the end of the measurement.

Beside the four scalers, mentioned before, two ratemeters are coupled to the electronics; one of them is usually connected to the output from the helium gas scintillator. The other ratemeter is
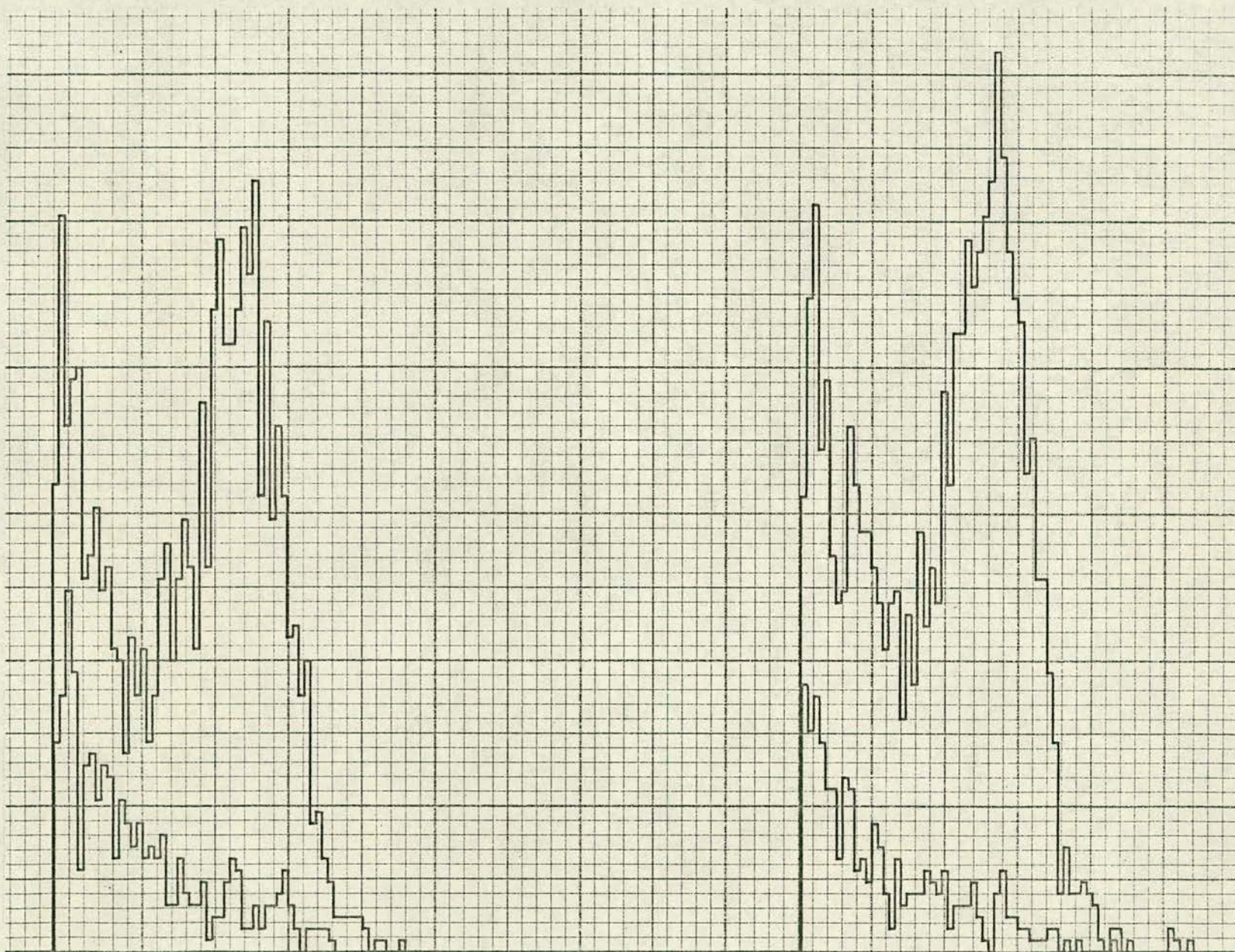
Fig. 18 — Four recoil spectra recorded with
the ^{4}He polarimeter assembled.

connected to the output of a NE-400 scintillator, insensitive to γ-rays, placed as near as possible to the target (see Fig. 16).

The readings of these two ratemeters are used to ensure that the beam is well focused on the target.

Two sets of measurements, with the polarimeter set up, were carried out. One of them was carried out, using the UKAEA 4.5 MeV Van de Graaff, in the deuteron energy range from 1 – 4 MeV; the other one was carried out using the 0.5 MeV Van de Graaff at Edinburgh University. These two sets of measurements will be described in the following sections.

2.4. Measurements Carried Out at Deuteron Energies Higher than 1 MeV.

A set of measurements was carried out, with the polarimeter set up, using the deuteron beam from the 4.5 MeV Van de Graaff; the measurements were carried out in three stages. The first stage, just after the ^{4}He gas scintillator was filled, produced a set of measurements at incident deuteron energies 1.2, 2.0, 3.0 and 4.0 MeV. In these measurements the polarimeter was set to measure the asymmetries resulting when neutrons emitted from the TiD target at laboratory angle 47° were scattered by the ^{4}He gas.

The second stage was fulfilled about three months later, with the same helium gas scintillator filling, and resulted in a set of measurements at incident deuteron energies 1.2 and 2.5 MeV. The measurements were for neutrons emitted from the D(d,n)^{3}He reaction at angles of 27°, 35°, 47°, 55°, 65°, 75° and 89° lab. for both

energies with an additional measurement at 105° for 2.5 MeV.

The third stage was just after the ⁴He gas scintillator was refilled and it resulted in measurements with neutrons emitted at laboratory angle 47°, at incident deuteron energies 2.1, 2.5 and 3.13 MeV and at laboratory angles 55° and 65° for 2.5 MeV.

The deuteron beam currents, used during measurements, ranged between 12 μA and 45 μA for incident deuteron energies between 4.0 and 1.2 MeV respectively.

2.4.1. The experimental procedure

Every time the polarimeter was set to look at the target at an angle Θ with the direction of the incident deuteron beam, both the target and the centre of the helium gas scintillator were optically aligned.

Once the alignment was achieved, the asymmetry measurements started in both the reaction plane and the one perpendicular to it, measurements being also performed with the two side detectors interchanged.

Thus a sequence of four measurements resulted at the end of a complete rotation of the cradle carrying the three detectors; the cradle being rotated in 90° steps through 360°. With the cradle in positions 1 and 3 (see Fig. 15), the asymmetry in the reaction plane is measured; the one in the perpendicular plane is measured with the cradle in positions 2 and 4. Each measurement, with the cradle held in a particular position, lasted 1024 seconds; the four spectra stored in the analyser (Laben 512 channels) were punched

out and the readings of the scalers, coupled to the system, were noted.

Once a complete rotation of the cradle was performed, e.g. starting from position 1 and at the end of the measurement at position 4, it was then rotated backwards; this way the measurements were again repeated up to position 1.

Thus the cradle was rotated, i.e. forward up to position 4 and then backward up to position 1, until a reasonable statistical accuracy was achieved for the measured asymmetry. Readings with the side detectors in the horizontal plane, were interspersed with those taken in the vertical one which allowed a continuous check on the instrumental asymmetry.

2.4.2. The TiD targets

Two thicknesses of TiD targets were used during the measurements , both with copper backings. One of them, used mainly during measurements at incident deuteron energies ≤ 3 MeV, had a titanium layer ~ 0.636 mg/cm^2; the other one, used for measurements at incident deuteron energies 2.1, 3.13 and 4 MeV, had a titanium layer ~ 2.9 mg/cm^2.

Considering that the incident deuteron beam, due to the design of the target system (see Fig. 8), was at an angle $\sim 45°$ to the perpendicular to the target, the thickness of the titanium layer traversed by the incident deuterons is more than the quoted one;

---

* All the TiD targets, used throughout measurements reported in this thesis, were prepared in the radiochemical centre, Amersham.

thus the incident deuterons in fact traversed ⬜ titanium layers 0.9 mg/cm² and 3.0 mg/cm² respectively.

The target thicknesses in KeV[153], i.e. the energy losses in the targets ⬜ are represented in Table 2.1. These values were calculated using the TiD stopping powers given by Coon[154].

Table 2.1.

Ed (MeV)	TiD Thik mg/cm²	Thickness (KeV)
1.2	0.9	200
2.0	0.9	150
2.1	3	450
2.5	0.9	125
3.0	0.9	120
3.13	3	380
4	3	300

2.5. Measurements at 0.5 MeV Deuteron Energy

The polarimeter was set up to measure the asymmetries resulting from scattering of neutrons emitted from the $D(d,n)^3$He reaction at an angle $\Theta = 50^\circ$ lab., with the direction of the incident deuteron beam.

In these measurements deuterons with energy 0.5 MeV, accelerated by the 0.5 MeV Van de Graaff of Edinburgh University, were incident on a TiD target. The target thickness in this case

was about 350 KeV.

The measurements were carried out for comparison with polarization measurements, at the same deuteron energy and with the same TiD target, carried out using Mott-Schwinger scattering; these will be reported in the following chapter.

The geometry of the experiment was basically the same as described in section 2.2.; only the inserts of the collimator, used to form a throat, were rearranged. This is in order to allow for a distance between the target and the collimator aperture twice that during the previous measurements. This arrangement of the inserts was made in such a way that the angle subtended by the helium gas scintillator at the centre of the target remained the same as before, i.e. 3.5^{o}; thus the collimator was no longer throated; it became tapered.

The shielding around the polarimeter, during the measurements, consisted mainly of paraffin wax and borated water.

Following the same experimental procedure, described in the preceding section, measurements were carried out with neutrons incident on the helium gas and emitted directly from the target; the deuteron beam current was about 50 μA, during these measurements.

Another set of measurements were carried out, at the same deuteron energy and beam current, with neutrons emitted from the back of the target at 50° lab. These measurements were carried out in order to check whether the measured asymmetry could be affected by the thickness of brass and circulating cooling water traversed

by neutrons emitted from the target during the measurements at 27° and 35° lab. at deuteron energies 1.2 and 2.5 MeV described in section 2.4. However it was found that neutrons passing through such a thickness of brass and cooling water did not affect the measured asymmetry significantly. The value of the asymmetry (%) measured in the reaction plane for neutrons emitted directly from the target was -11.3 ± 0.5, in good agreement with a value -11.9 ± 0.9, measured with the polarimeter looking at the target from the back.

The check on the existence of any asymmetry in the plane perpendicular to the reaction plane yielded the values $(0.3 \pm 1.3)\%$ and $(0.2 \pm 1.3)\%$ in each case.

2.6. The Rate of Collecting Data

The time required to achieve a statistical accuracy ΔP in the measurement of the $D(d,n)^3He$ polarisation P_n, using scattering from ^4He, in the ideal case e.g. point scatterer and point side detectors, is proportional to[94]:

$$\frac{1 - P_n^2 P_{He}^2}{P_{He}^2 \, \sigma(\Theta)} \quad \frac{1}{(\Delta P)^2} \tag{2.6.1}$$

where $\sigma(\Theta)$ is the differential cross-section of scattering, from ^4He, for unpolarized neutrons at scattering angle Θ.

The denominator of this expression represents a convenient figure of merit[94] and, considering its dependence on the scattering angle Θ, it can be a good guide to the rate of data collection.

Such dependency is represented in Fig. 19, for neutron energies 2.0, 3.8 and 6.0 MeV, as calculated using the phase shifts given by Satchler et al.[25]. It is remarkable that the rate of collecting data, for a particular neutron energy, is maximum at two particular scattering angles; one of them is essentially forward and the other one is backward scattering angle. These two angles are different for different neutron energies (see Fig. 19). While for 2 MeV neutron energy the backward maximum is higher than the forward one (Fig. 19), it is lower than the forward maximum at neutron energies 3.8 and 6.1 MeV.

The scattering angle used in the present ^{4}He polarimeter is a backward one (123°); this angle was chosen because the agreement between the analysing powers, deduced from different sets of phase-shifts, is better than at forward angles (see Section 1.2.2). The rate of collecting data should be slower, considering the energy of the emitted neutrons as related to incident deuteron energies, than is the case when a forward scattering angle is used. Nevertheless it was possible to complete a polarization measurement, for a particular energy, within a time less than 10 hours.

2.7. Treatment of the Experimental Data

The basic steps, required for the treatment of the experimental data, were carried out using a Digital Equipment Corporation PDP-8 computer available in the Department of Physics. Special codes were used during these steps.

The first step was to sum up all the corresponding spectra
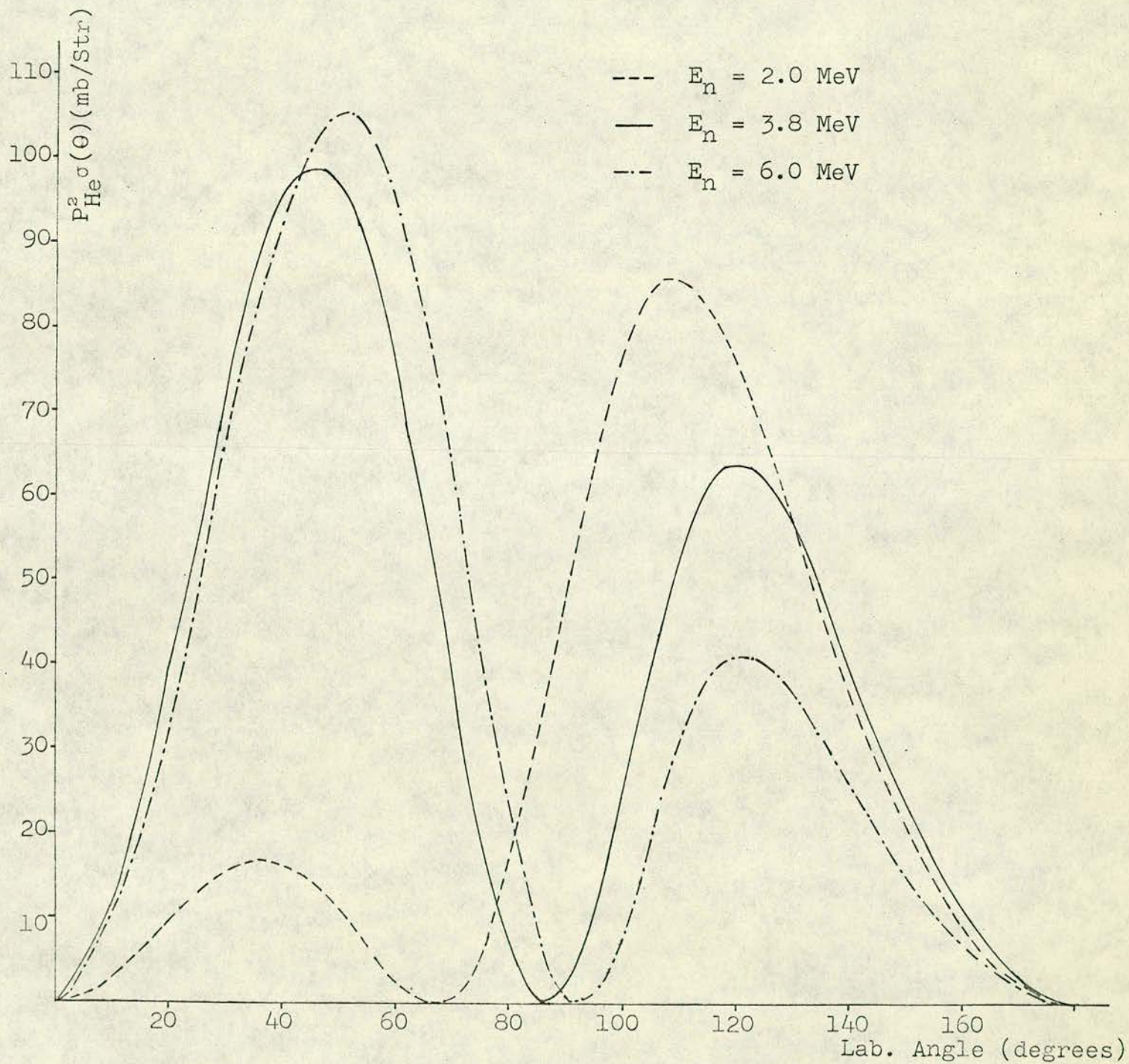
Fig. 19. The rate of collecting data, as function of
scattering angle, for neutrons incident
with different energies.

(recorded on punched paper tape) resulting with the cradle held at a particular position.

The resulting spectra were punched out on the high speed paper tape punch coupled to the computer. In this way all the data tapes produced at one cradle position, during a particular measurement, were summed onto a master tape which had an identifier indicating the cradle position punched onto it at the beginning.

In the treatment of the data taken with a particular deuteron energy and reaction angle θ, this procedure was repeated four times, so producing four master tapes corresponding to the four cradle positions. They were then usually joined together, in the same order, i.e. from position 1-4, in one tape.

The next step was, using another code, to store the data contained in the combined master tape on a magnetic 'Dectape' and a keyword, to allow the data to be called down at convenience, usually preceded the loading of the data onto the Dectape. Thus for a particular polarization measurement 16 spectra were stored on the Dectape; 8 of these spectra were (real + random) ones; the other eight were the corresponding random spectra.

The final step, at this stage, was to plot the 8 real spectra, resulting after the random ones were subtracted. This was carried out, through a special code, with the plotter available at the E.R.C.C. and coupled to the IBM 360/50 computer. The resulting 8 real spectra were plotted with an indication of the statistical standard deviation associated with each point.

Examples of these plottings are shown in figures 20 - 21, for
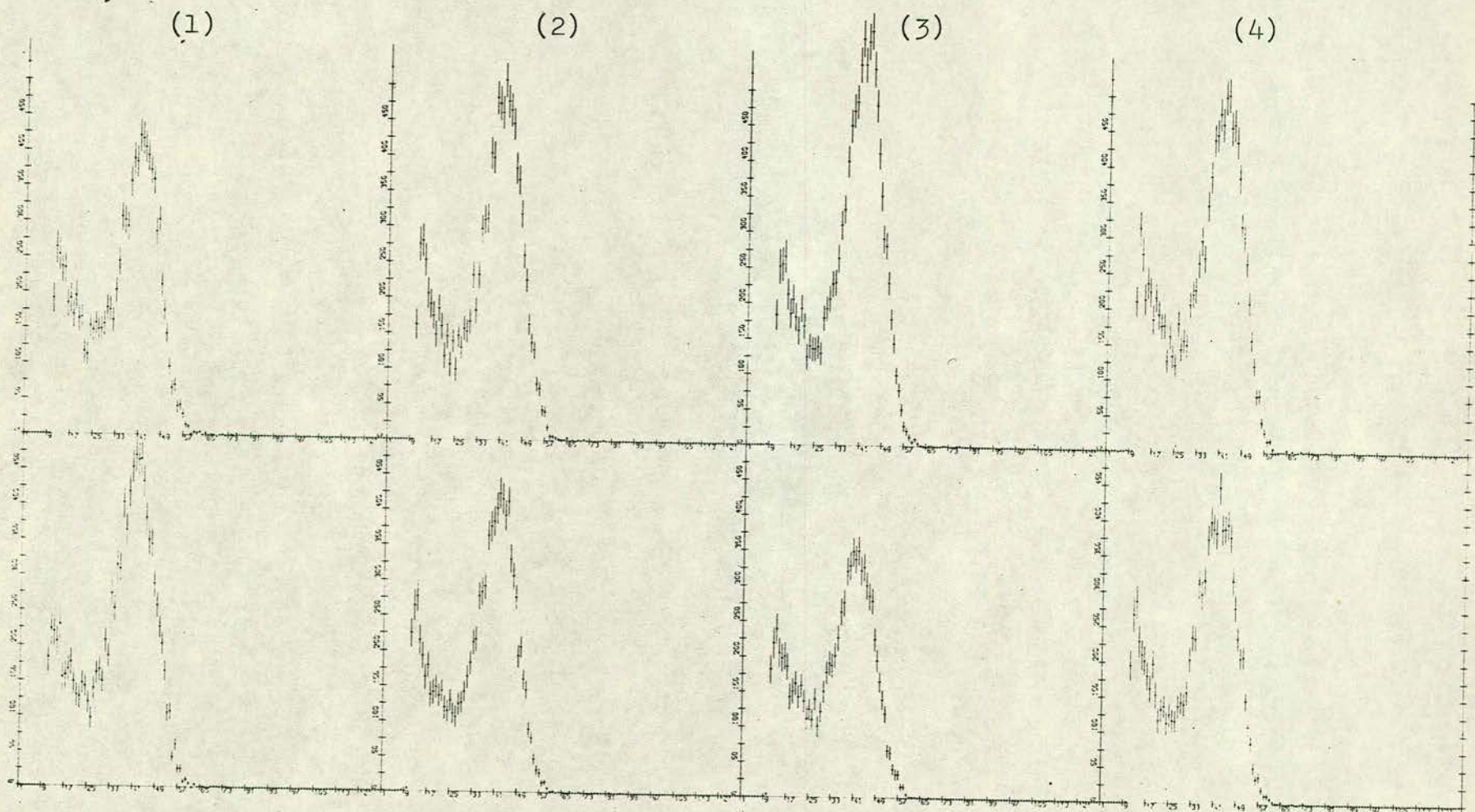
Fig. 20. The recoil spectra resulting when neutrons, emitted from the reaction
with 1.2 MeV deuterons at 55° lab, are incident on the ^{4}He scintillator.
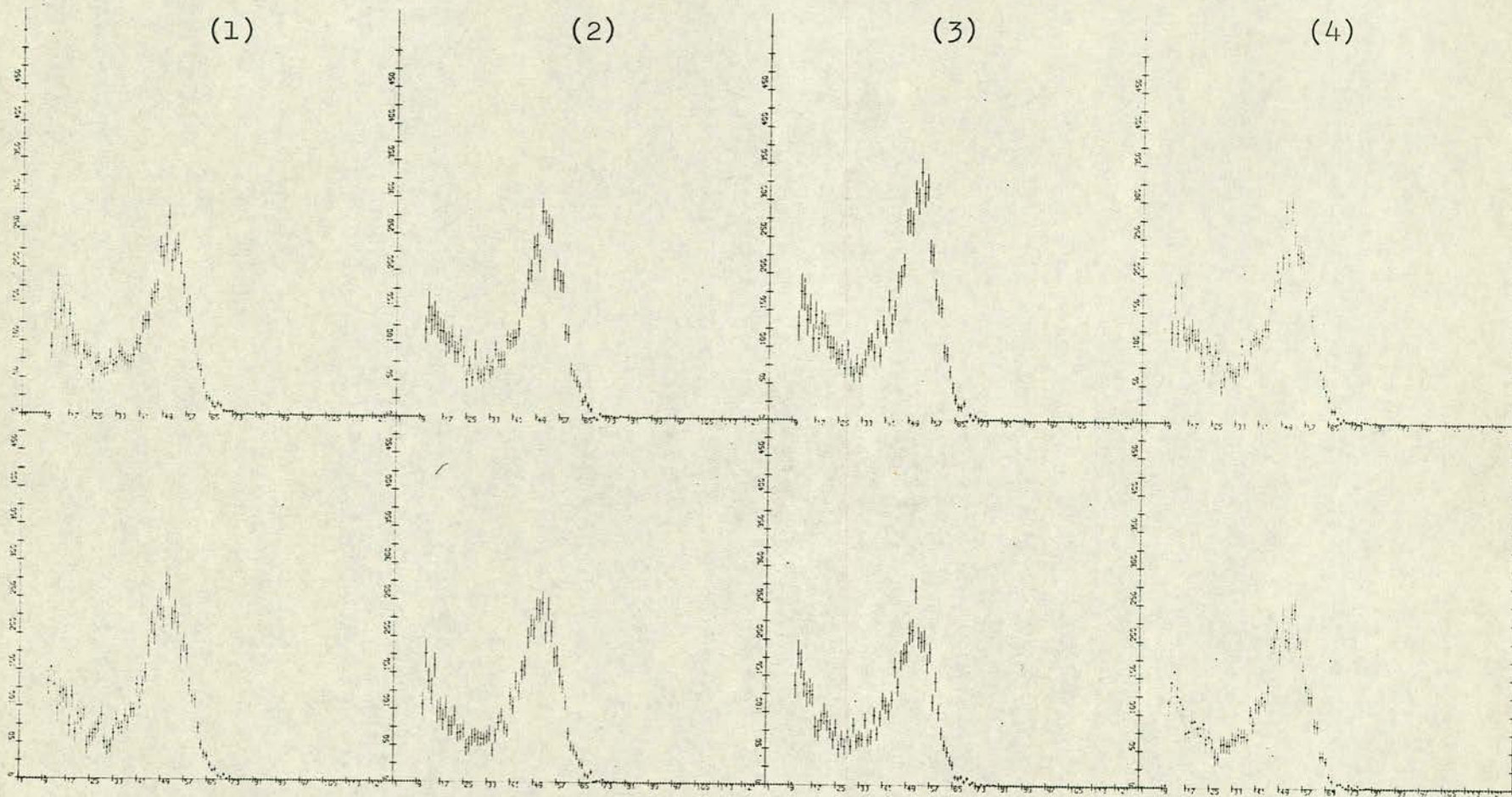
Fig. 21. The recoil spectra resulting when neutrons, emitted from the reaction with 2.5 deuterons at 55° lab., are incident on the ⁴He scintillator.

deuteron energies 1.2 MeV and 2.5 MeV respectively; these measurements were with neutrons emitted from the $D(d,n)^3He$ reaction at 55° lab. In each of these two figures are represented the resulting 8 recoil spectra, where the upper four spectra are for one side detector and the lower four are for the other one.

Such plottings could help in a preliminary judgement about the quality of the measurements. Note that the recoil spectra detected in the reaction plane, marked (1) and (3) on Figs. 20 - 21, are of different heights due to the asymmetry in scattering whereas spectra, detected in the perpendicular plane, marked (2) and (4) are almost the same, as one would expect.

2.7.1. The measured asymmetries

A further stage in the treatment of the experimental data was to evaluate the asymmetry from the recoil spectra; this will be discussed in this section.

If the number of neutrons scattered from the helium, in a given time, to the 'right' is N_R and that to the 'left' is N_L, then the ratio:

$$r = N_R/N_L \qquad (2.7.1)$$

is called the right-left ratio.

From equation (1.1.1) of section 1.1 it follows that:

$$r = (1 + PP_n)/(1 - PP_n) \qquad (2.7.2)$$

Then the measured asymmetry is given by:

$$\varepsilon = PP_n = (r-1)/(r+1) \qquad (2.7.3)$$

As two detectors, in this polarimeter, are used for detecting

neutrons scattered, from the ^{4}He gas scintillator, both to the 'right' and 'left', then r should be calculated using the following expression:

$$r = \sqrt{\frac{N_{R1}}{N_{L1}} \quad \frac{N_{R2}}{N_{L2}}} \tag{2.7.4}$$

where N_{R1} and N_{R2} represent the number of neutrons scattered to the right as measured by each of the two detectors, while those scattered to the left are represented by N_{L1} and N_{L2}. The duration of measurements, as well as the difference in the efficiencies of the two side detectors should cancel entirely[4], when expression (2.7.4) is used for calculating r.

The measured asymmetry was calculated, using a code written for the PDP-8. The code is based on expressions (2.7.3) and (2.7.4). It calls the data, stored on the Dectape, related to a particular measurement, through its keyword. It then sums the counts between any two channel numbers selected by the user, for each of the stored 16 spectra; it prints out the 16 totals along with the two asymmetries accompanied with their standard deviations. One of the asymmetries referred to the horizontal plane, the other to the vertical plane which should be zero within the limits of statistical accuracy. The code allowed this procedure to take place within a few seconds from the selection of the two limits. In order to determine the proper limits to be used for calculating the asymmetry, the behaviour of the asymmetry as calculated by integrating the whole recoil spectrum, i.e. including the tail, and then increasing the lower limit of integration by one channel, was

studied.   For this purpose another two codes were used, written for the IBM 360/50 and loaded on the same Dectape on which the experimental data are stored.   Either of these codes could be sent, through the PDP-8, along with the data of a particular measurement to the IBM 360/50.

One of these two codes allowed the plotting of the recoil spectrum resulting when all the four real spectra detected in the reaction plane were added together, along with each point, was plotted, the absolute value of the asymmetry calculated between the point where the asymmetry is plotted, and another point chosen almost at the end of the upper edge of the spectrum.   The code allowed the absolute values of the asymmetries to be plotted along with the associated statistical accuracies.   This code was applied to all the experimental data described in this chapter resulting in plottings similar to the two represented in Figs. 22-23.   It was noticeable in all such plottings that the calculated asymmetry increased with the increase of the selected channel number;   the increase of the channel number correspond to the decrease of the 'tail' contribution in the calculated asymmetry.

Such common behaviour of the asymmetry further supported the view that the tail is due to multiple scattering processes taking place in the quartz window and metals surrounding the helium gas scintillator, along with scattering by the helium itself[94,126] and that the asymmetry associated only with the tail is very small, either zero or little different from zero.

The other code does the same as the one described above, only
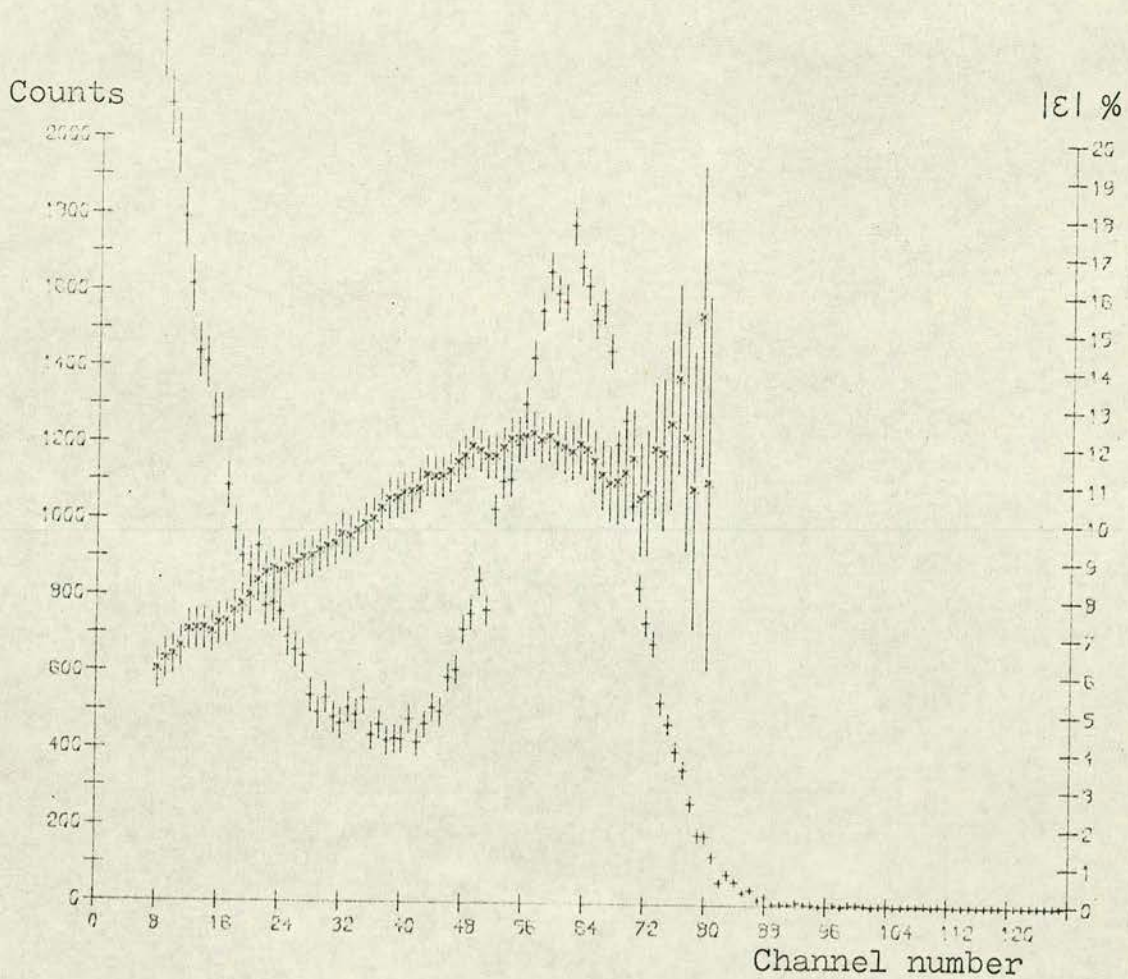
Fig. 22.   The behaviour of the asymmetry along the
recoil spectrum resulting with neutrons
emitted from the reaction at 47° lab.,
and incident deuteron energy 1.2 MeV.
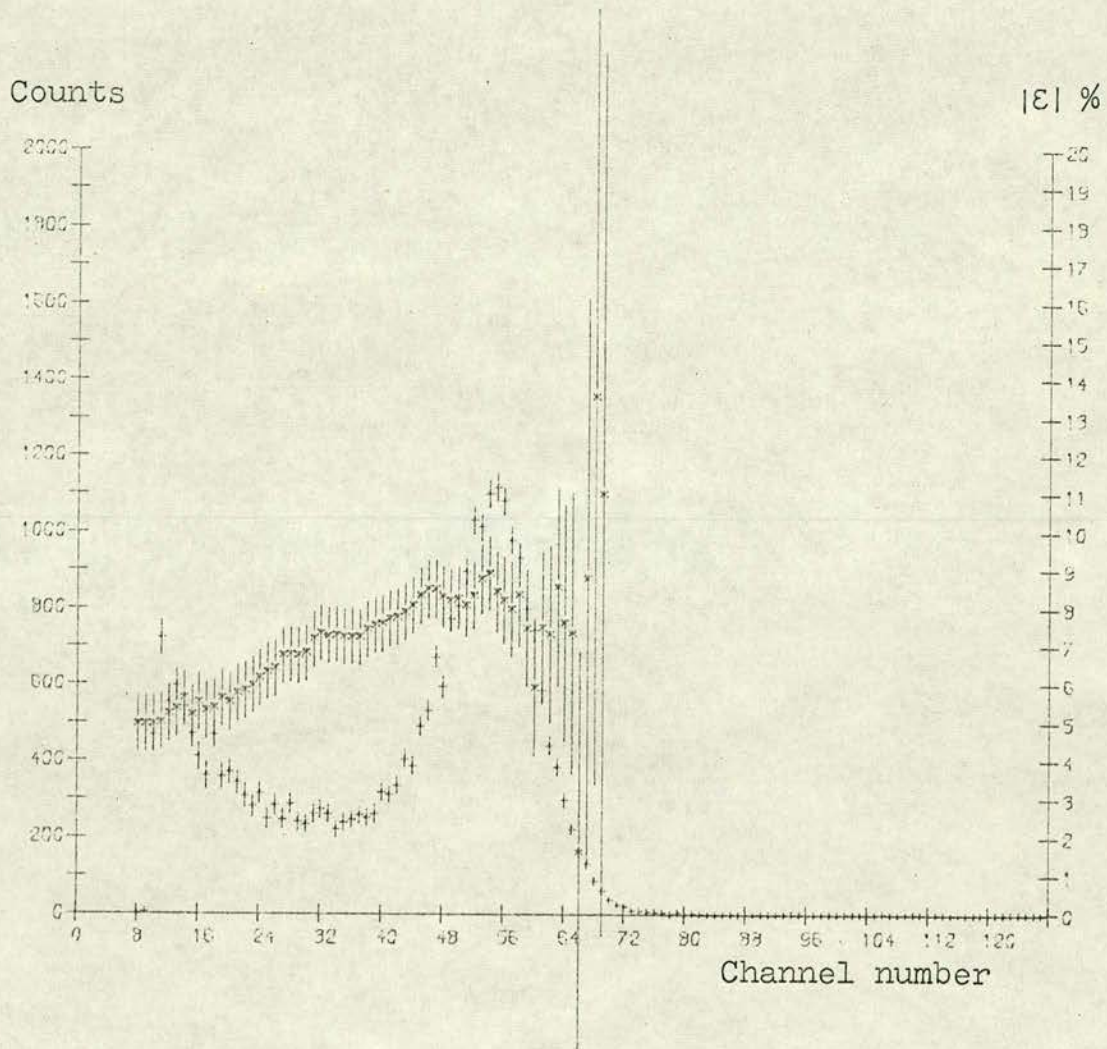
Fig. 23.   The behaviour of the asymmetry along the
           recoil spectrum resulting with neutrons
           emitted from the reaction at 47° lab.
           and incident deuteron energy 2.5 MeV.

with the four spectra associated with the plane perpendicular to the reaction plane. It was applied as well for analysing the obtained experimental data, where a similar picture to that in Figs. 24-25 was repeated. Such plottings served as a good check on the absence of significant instrumental asymmetry which proved to be almost zero in all the measurements described in this chapter.

2.7.2. Correction of the measured asymmetries for the 'tail' effect

For a start a Monte Carlo code, developed by Davie[126], for simulating the spectra resulting after neutrons incident on the helium scintillator are scattered through different routes, was used. The code, being amended, calculated three spectra, uncorrected for the finite resolution of the helium scintillator. These spectra are:

(i) The energy spectrum of the helium recoils in the gas scintillator for incident neutrons which are scattered into the side detector.

(ii) The energy spectrum of the helium recoils in the gas scintillator, due to neutrons which first collide with the helium, then with the metal and the quartz volume around the rear of the scintillator volume before being detected by the side detector.

(iii) The energy spectrum of the helium recoils in the helium gas scintillator, due to neutrons which first strike the metal and quartz, at the rear of the scintillator, then recoil off helium into the side detector.

In calculating these three spectra it is assumed that the
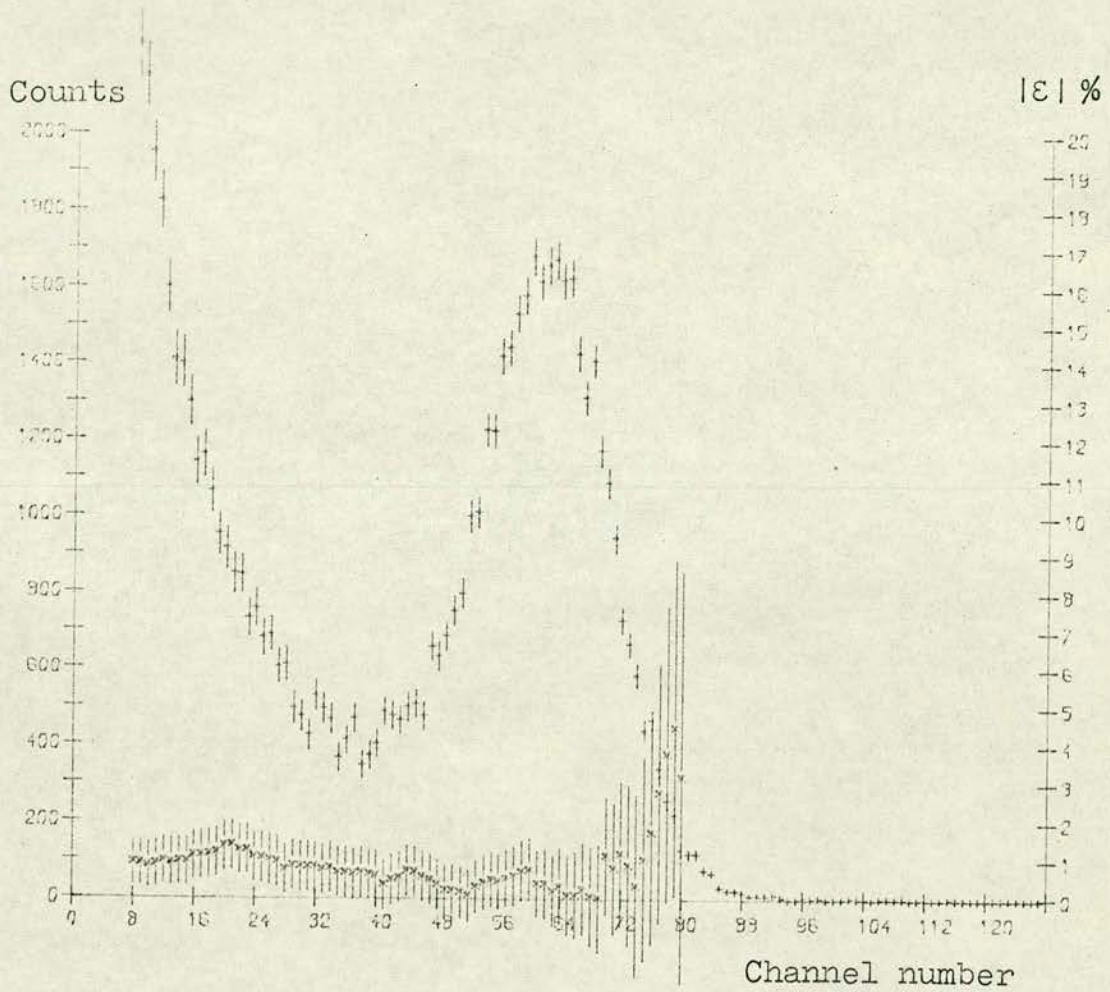
Fig. 24.   The behaviour of the instrumental asymmetry
associated with measurements at Ed = 1.2 MeV,
where neutrons are emitted at 47° lab.

Counts

|ε| %

Channel number
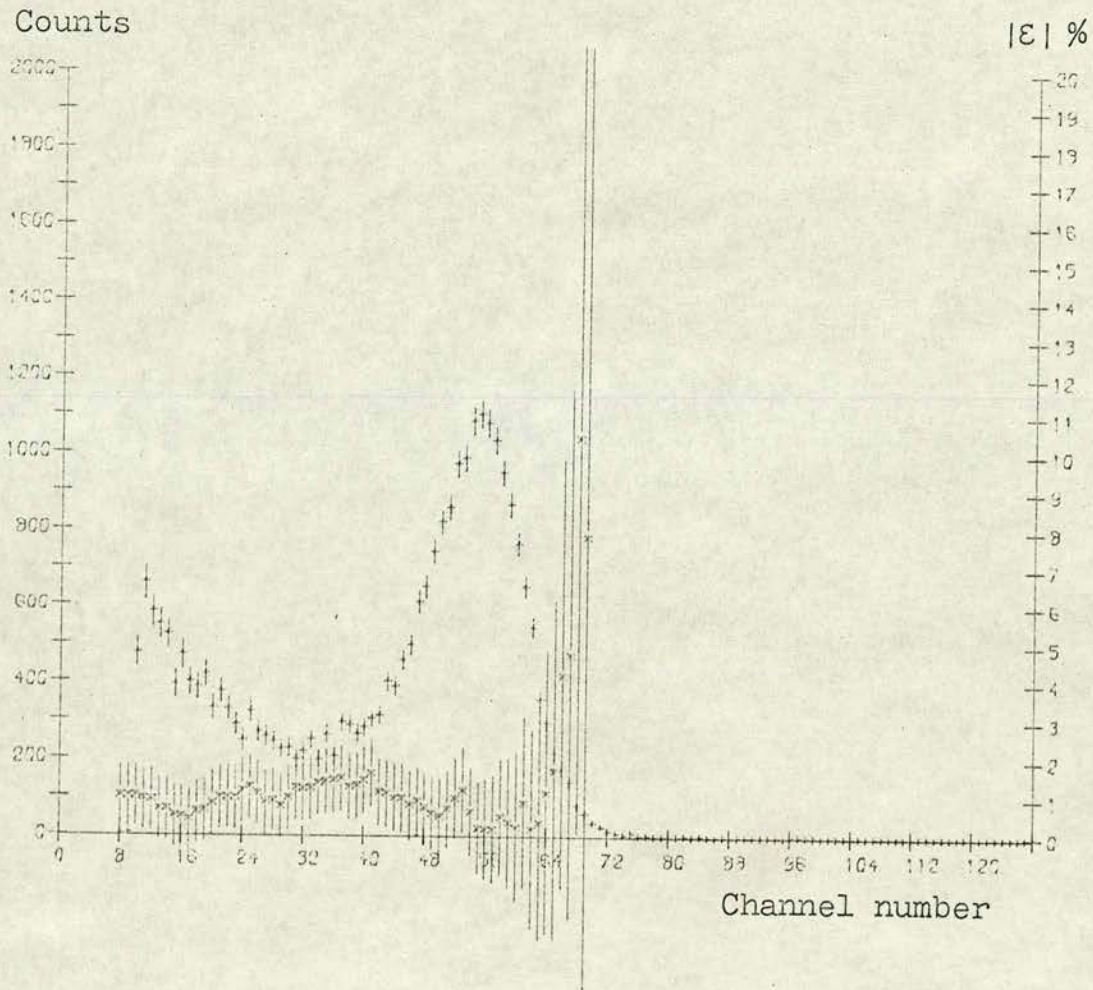
Fig. 25.   The behaviour of the instrumental asymmetry
associated with measurements at Ed = 2.5 MeV,
where neutrons are emitted at 47° lab.

differential cross-section for the scattering in the metal and quartz is a constant, no energy loss takes place in the scatter and absorption of the neutron flux in the metal and quartz is ignored.

The results of calculations, applying the code, are represented in Fig. 26, for the case when neutrons of energy 3.8 MeV are incident on the helium gas scintillator. The phase shifts required for the calculation were obtained by interpolation from those of Satchler et al.[25]. After all the three spectra were gaussian smeared, with a F.W.H.M. resolution ~ 30%, spectra (i) and (ii) were added and the resulting one is represented in Fig. 26 where it is marked as (a). The spectrum resulting after adding the calculated helium recoil spectrum (marked as (b)) to spectrum (a) is represented as (c) on the same figure. Spectrum (c) is very similar to the one obtained experimentally and represented in Fig. 26. Such a simulated spectrum is calculated ignoring contributions of other different routes of scattering (e.g. scattering from the aluminium mounting plate beneath the helium gas scintillator, scattering from the photomultiplier of the side detector and its brass container etc.). Thus one cannot rely completely on such a simulated spectrum when extrapolating the experimentally observed tails as it is a very crude spectrum.

The asymmetries were calculated by integrating an area of the recoil spectrum taken as:

(a) The area of the spectrum between the midpoint of the low energy edge of the peak and the midpoint of the high energy edge.

A: The helium recoil as detected for neutron energy 3.8 MeV

B: The simulated spectra as calculated for neutron energy 3.8 MeV

75
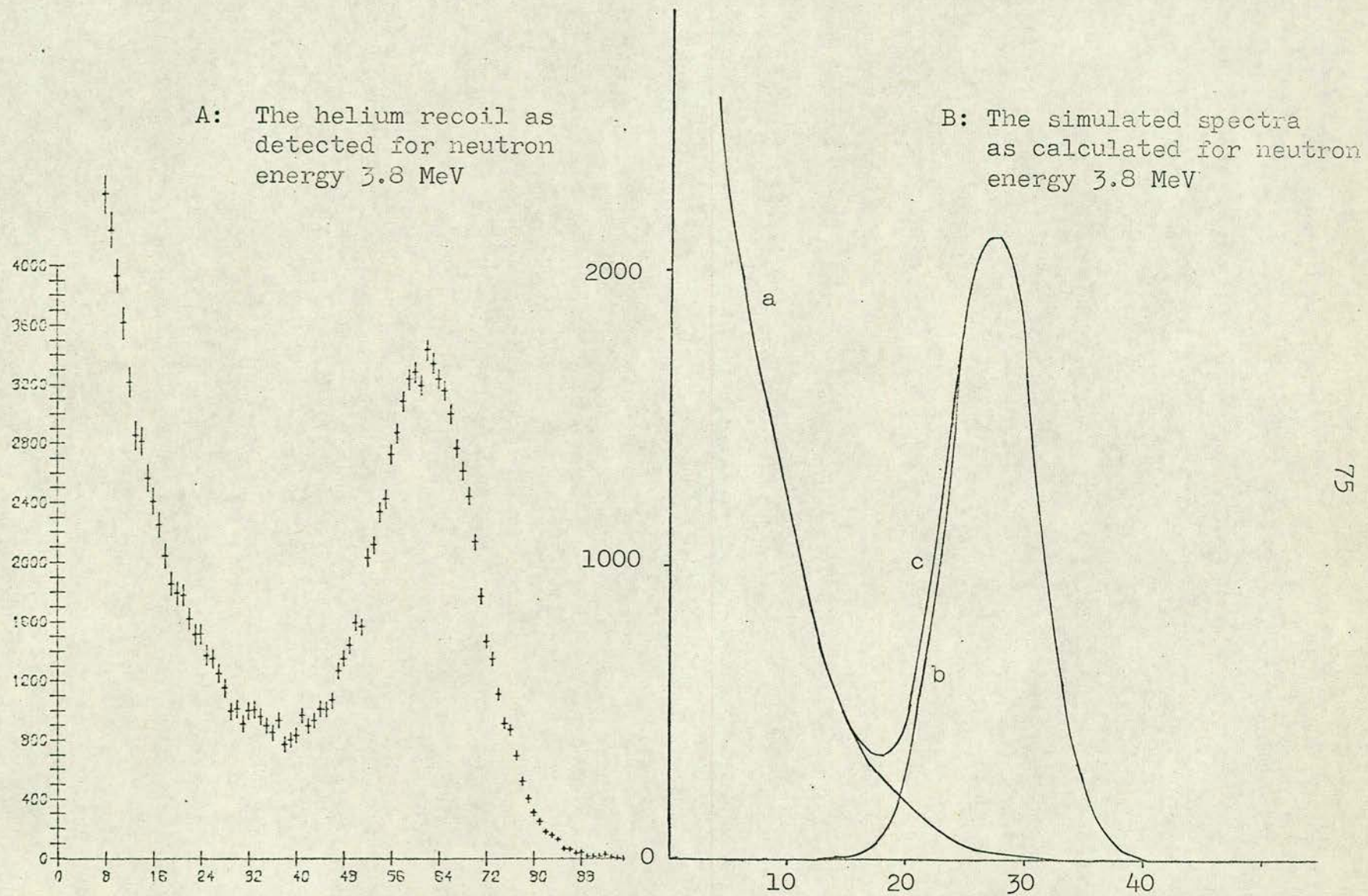
Fig. 26. The recoil spectra both as detected and calculated at neutron energy 3.8 MeV.

(b) The area between the midpoint of the low energy edge and
the summit of the peak.

(c) The area between the summit of the peak and midpoint
of the high energy edge.

While the asymmetry obtained by integrating area (c) agreed, within
the statistical accuracy, with the one calculated from (a) it was
significantly higher than the asymmetry related to (b) and so
supported the assumption that the tail falls off under the peak.

The correction for the effect of unpolarized tail was intro-
duced to the experimentally measured asymmetry by subtracting the
area under the tail from the selected area of the spectrum.   The
tails were extrapolated in the fashion represented in Fig. 27.

In this way the corrected asymmetry calculated from a selected
area of the recoil spectrum, between any two limits, agreed, within
the statistical accuracy, with another one calculated for two
different limits;   the limits being selected in the area of the
spectrum starting from the midpoint of the lower edge and ending
within a few channels after the midpoint of the upper edge.

2.7.3. The corrected asymmetries

The existence of the low energy tail put some limitations on
the selection of the area of the recoil spectrum under the peak to
be integrated for evaluation of the asymmetry;   one has to obtain
asymmetry with the least uncertainty and this can be achieved only
by reducing the applied correction.   As the resolution of the helium
gas scintillator deteriorated with time, the tail effect increased.
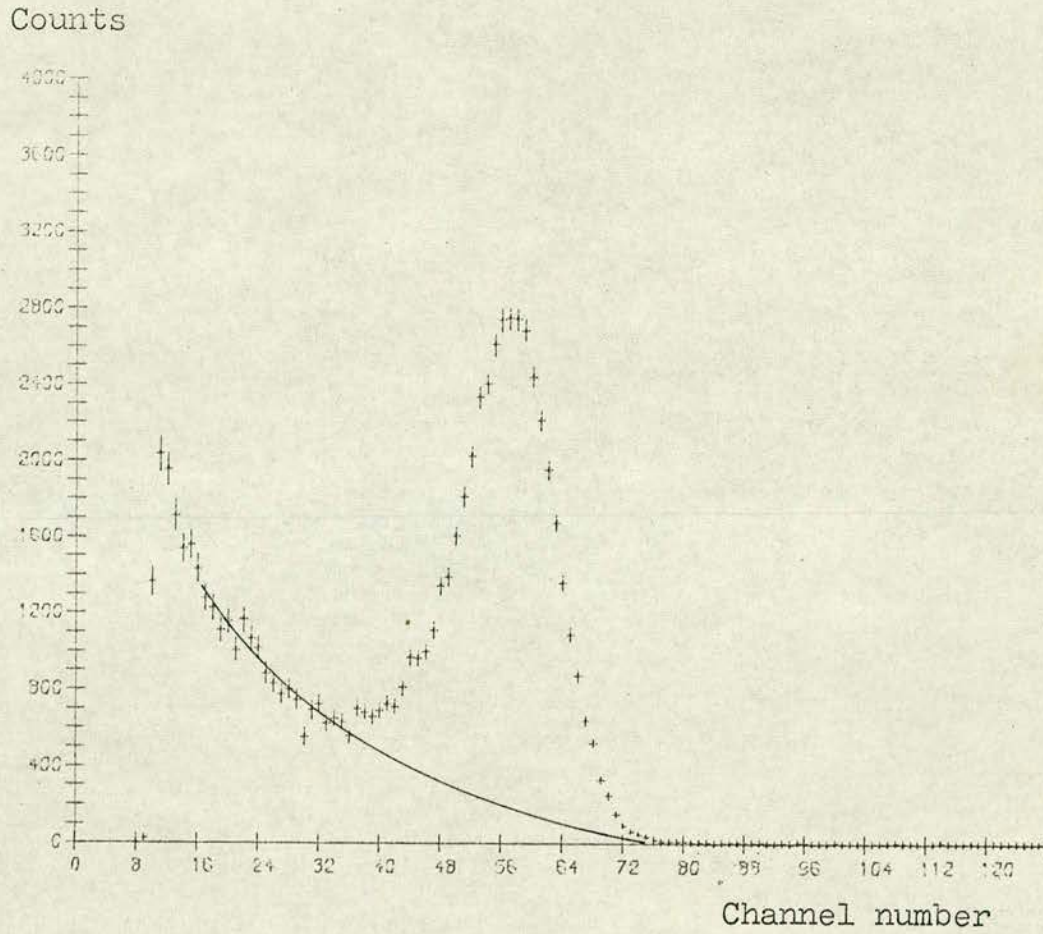
Fig. 27. The helium recoil spectrum for neutrons emitted at 35° from reaction with 2.5 MeV deuterons. The solid line showing the tail extrapolation.

Measurements carried out with the helium gas just after being filled resulted in tails different from those obtained with the scintillator a few months after.   An example is represented in Fig. 28, where a recoil spectrum for neutrons of 3.8 MeV energy (Fig. 28a) and another spectrum detected after three months for neutrons of 3.6 MeV energy (Fig. 28b) are compared.   The correction required for the latter (Fig. 28b) is more than that for the first spectrum.

On the one hand the tail effect proved to be smaller for the asymmetry calculated from the area of the spectrum between the summit of the peak and the midpoint of the higher energy edge, than for the one evaluated from the area between the summit of the peak and the midpoint of the lower edge.   However one does not wish to lose much of the statistical accuracy.   Thus the asymmetry was calculated from an area of the spectrum between the midpoint of the lower edge and few channels after the midpoint of the high energy edge.   All the asymmetries obtained with such criteria in mind are introduced in Table 2.2.   In Table 2.2. are given the incident deuteron energies, in the first column, followed by the reaction angles, the measured asymmetry $\varepsilon(\%)$, the asymmetry detected in the plane perpendicular to the reaction's one $\overline{\varepsilon}(\%)$, the correction factor χ applied to ε and the corrected $\varepsilon(\%)$ is given in the last column.

a) The recoil spectrum
obtained with the helium
scintillator just filled
at neutron energy 3.8 MeV

b) The recoil spectrum
obtained few months
later at neutron
energy 3.6 MeV

79
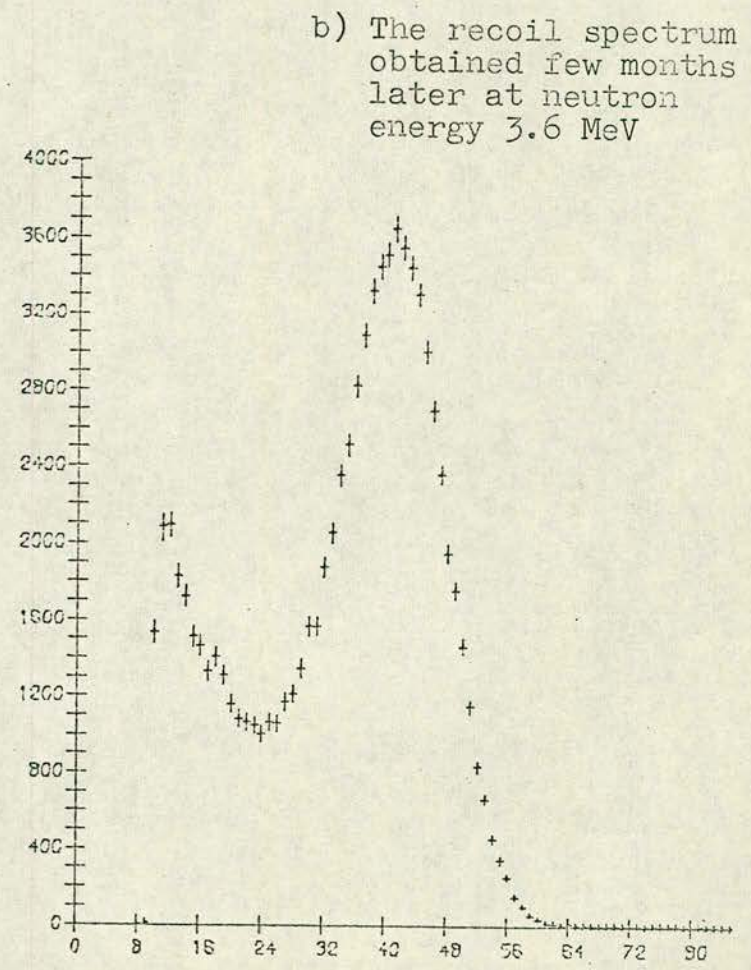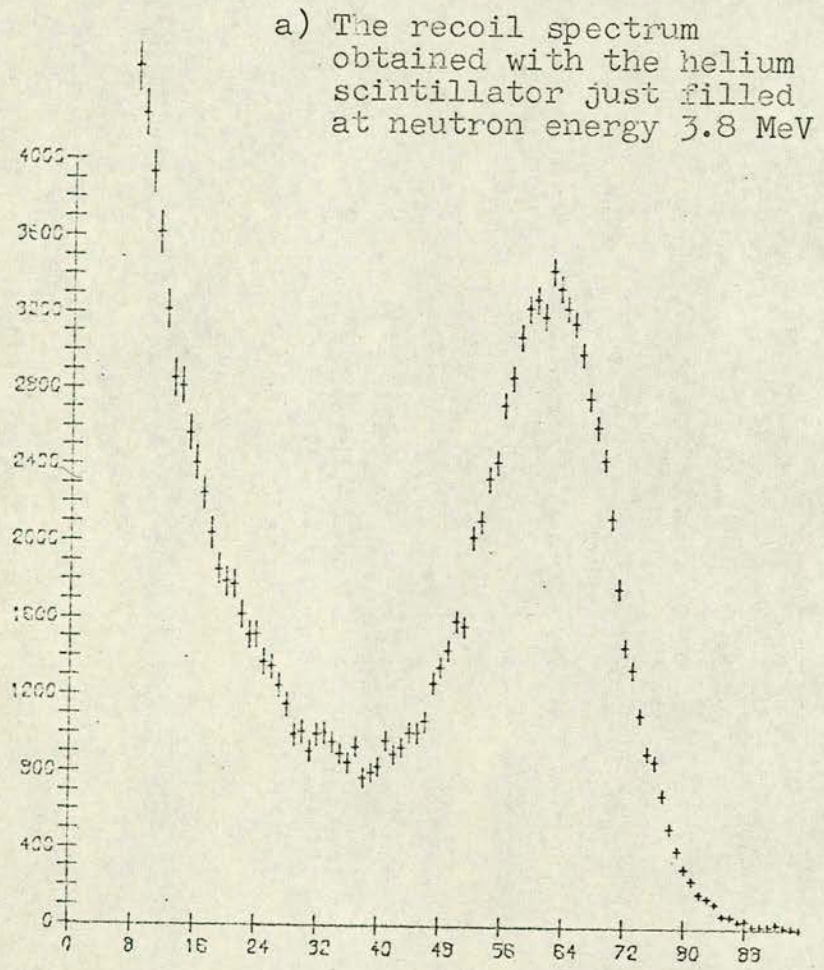
Fig. 28.   The helium recoil spectra obtained at neutron energies 3.8 and
3.6 MeV.

Table 2.2: The asymmetries obtained.

Ed (MeV)	θ Lab.	Measured ε (%)	ε̄ (%)	Correction factor χ	Corrected ε (%)
0.5	50°	-11.3 ± 0.5	0.3 ± 1.3	1.09	-12.3 ± 0.5
1.2	27°	-6.8 ± 0.5	1.0 ± 0.7	1.10	-7.5 ± 0.6
	35°	-8.5 ± 0.5	0.3 ± 0.6	1.13	-9.6 ± 0.6
	47°	-12.0 ± 0.7	0.5 ± 0.7	1.13	-13.6 ± 0.8
	55°	-13.5 ± 0.7	0.1 ± 0.7	1.16	-15.7 ± 0.8
	65°	-10.8 ± 0.8	-0.3 ± 0.8	1.10	-11.9 ± 0.8
	75°	-4.4 ± 0.8	0.7 ± 0.8	1.10	-4.8 ± 0.9
	89°	8.2 ± 1.7	-2.5 ± 2.5	1.10	9.0 ± 1.9
2.0	47°	-13.0 ± 1.0	0.8 ± 1.0	1.12	-14.6 ± 1.1
2.1	47°	-13.6 ± 0.9	0.5 ± 1.6	1.09	-14.8 ± 1.0
2.5	27°	-2.4 ± 1.0	2.4 ± 1.9	1.12	-2.7 ± 1.1
	35°	-5.7 ± 0.9	2.0 ± 1.6	1.12	-6.4 ± 1.0
	47°	-9.8 ± 1.1	0.6 ± 1.5	1.15	-11.3 ± 1.3
	47°	-12.3 ± 1.2	-2.6 ± 2.6	1.06	-13.0 ± 1.3
	55°	-9.9 ± 1.0	-0.6 ± 0.9	1.13	-11.2 ± 1.1
	55°	-8.9 ± 1.3	0.6 ± 1.9	1.08	-9.6 ± 1.4
	65°	-6.4 ± 0.8	-0.7 ± 0.8	1.19	-7.6 ± 0.9
	65°	-7.2 ± 1.6	0.0 ± 2.8	1.07	-7.7 ± 1.7
	75°	0.8 ± 0.9	-0.2 ± 0.8	1.17	0.9 ± 1.0
	89°	8.3 ± 1.2	-0.2 ± 1.3	1.15	9.5 ± 1.4
	105°	10.8 ± 2.1	0.6 ± 2.1	1.10	11.9 ± 2.3
3.0	47°	-8.7 ± 1.3	0.3 ± 1.5	1.14	-9.9 ± 1.5
3.1	47°	-8.0 ± 1.1	-0.5 ± 2.1	1.10	-8.8 ± 1.2
4.0	47°	-6.6 ± 1.5	1.9 ± 1.7	1.14	-7.6 ± 1.7

2.8. Calculation of the Mean Analysing Power

The helium analysing power P is required, according to formula (1.1.2) of section 1.1, in order to calculate the neutron polarization P_n from the measured asymmetry. When applying expressions (1.2.1), given in section 1.2, to calculate P account must be taken of the scattering angles involved due to the finite sizes of both the helium gas scintillator and the side detectors as well as of the variation in the $D(d,n)^3He$ cross-section when accounting for the solid angle subtended by the helium gas scintillator at the target. The analysing power calculated with account of these factors is called the mean analysing power <P> and will be discussed in what follows.

For a uniform monoenergetic neutron flux Ψ, incident on the ^4He scintillator, the number of neutrons detected per second by a small element volume dv of the 'right' detector after being scattered by volume dv' of the helium gas, according to formula (1.1.2) given in section 1.1, is given by:

$$n_r = \frac{\Psi P_r n \sigma(\theta) [1 + PP_n \cos\phi] dv dv'}{\eta^2} \qquad (2.8.1)$$

where P_r is the probability of a scattered neutron being detected, n is the number of ^4He nuclei per unit volume and η is the distance between dv and dv'. In practice the target is located at a definite distance from the helium scintillator and one has to consider the neutron flux Ψ in such a case. For a neutron emerging from the target at distance ℓ and scattered at a point (x,y,z), from the origin of coordinates (X,Y,Z) which is located at the rear of the ^4He scintillator, the reaction angle θ will be:

$$\Theta = <\Theta> - \frac{y}{z + \ell} \qquad (2.8.2)$$

where $<\Theta>$ is the mean reaction angle.   Considering that the fractional variation of the $D(d,n)^3He$ reaction cross-section is a constant, say Δ for small deviations from $<\Theta>$, the neutron flux Ψ at a point (x,y,z) within the gas scintillator will be given by[126]:

$$\Psi = \frac{\Psi'}{x^2 + y^2 + z^2} \left(1 - \frac{\Delta y}{z + \ell}\right) \qquad (2.8.3)$$

where Ψ' is the mean neutron flux from the target as $\ell \gg |x|$, $|y|$, $|z|$ expression (2.8.3) can be approximated by:

$$\Psi = \Psi'' (1 + \alpha y) \qquad (2.8.4)$$

for a parallel neutron flux, where α is the fractional variation of the $D(d,n)^3He$ cross-section per unit length traversed in the y direction in the ^4He scintillator; α is calculated at the centre of the helium gas scintillator and depends on both the deuteron energy and the geometry of the polarimeter.

Substituting Ψ as given by expression (2.8.4) in expression (2.8.1) the latter becomes:

$$n_r = \frac{\Psi'' P_r n \sigma(\Theta) (1 + \alpha y)(1 + PP_n \cos \phi) \, dvdv'}{\eta^2} \qquad (2.8.5)$$

The total number of neutrons detected per second by the 'right' detector after scattering by the ^4He scintillator is:

$$N_r = \Psi'' P_r n \int \frac{\sigma(\Theta)(1 + \alpha y)(1 + PP_n \cos \phi) dvdv'}{\eta^2} \qquad (2.8.6)$$

This total number for the 'left' detector, which is symmetrical to the 'right' one, will be:

$$N_\ell = \Psi'' \, P_\ell \, n \int \frac{\sigma(\Theta)(1 - \alpha y)(1 - PP_n \cos \phi)}{\eta^2} \, dv dv' \qquad (2.8.7)$$

As the asymmetry is calculated using expressions (2.7.3) and (2.7.4) of section 2.7.1 where the side detectors efficiencies cancel entirely, the measured asymmetry, given by expression (2.7.3), will be:

$$\varepsilon = P_n \left[\frac{\int \frac{\sigma(\Theta) \, P \cos \phi}{\eta^2} \, dv dv' + \frac{\alpha}{P_n} \int \frac{y\sigma(\Theta)}{\eta^2} \, dv dv'}{\int \frac{\sigma(\Theta)}{\eta^2} \, dv dv' + \alpha P_n \int \frac{y\sigma(\Theta) \, P \cos \phi}{\eta^2} \, dv dv'} \right]$$

$$= P_n \left[\frac{I_1 + \frac{\alpha}{P_n} I_1'}{I_2 + \alpha P_n I_2'} \right] = P_n < P > \qquad (2.8.8)$$

where I_1, I_1', I_2 and I_2' are double volume integrals calculated throughout the volumes of both the ^{4}He scintillator and side detectors.

Thus the expression for $< P >$ includes both corrections for finite geometry as well as the variation of the $D(d,n)^3$He cross-section with angle and can be approximated[126] as:

$$\varepsilon = P_n \frac{I_1}{I_2} + \alpha \frac{I_1'}{I_2}$$

$$= P_n < P_1 > + \omega \qquad (2.8.9)$$

where ω is the 'false' asymmetry due to the variation of the reaction angle and $< P_1 >$ is the analysing power corrected only

for the finite geometry.

A Monte Carlo program, used before by Davie[126], based on expressions (2.8.8) and (2.8.9), was applied for evaluating the mean analysing power $< P >$ in which the volumes of both the ^{4}He scintillator and side detector are sampled in a random way. The sampling process uses a 'rectangular' random distribution generated by a power residue method[155]. According to formula (2.8.8), the code should be supplied with an estimation of P_n, with n-^{4}He phase-shifts, as well as the fractional variation of the $D(d,n)^3$He cross-section. The measured asymmetries were used as estimations of P_n and this proved to give $< P >$ with enough accuracy. When trying the value of P_n obtained from this $< P >$ as a more accurate esti-mation of polarization, the calculation did not result in a signifi-cant difference in the value of $< P >$.

The fractional variation of the $D(d,n)^3$He differential cross-section α was evaluated from the cross-sections given by Brolley and Fowler[156] for each incident deuteron energy and particular reaction angle. As the angle subtended by the target at the centre of the helium gas scintillator was about 3.5°, the value of α was, in general, small.

The n-^{4}He phase-shifts, supplied to the code, were obtained by interpolation, for each resulting neutron energy, from those of Satchler et al.[25].

A calculation, using the code, resulted in values of $< P_1 >$, $< P >$ and ω with the value of ω usually small, less than the statistical accuracy involved, for all the cases under consideration.

2.9. The Effect of the Tail Correction on the Resulting Polarization

In this section will be discussed, how far different values of the asymmetry, obtained as a result of different tail extrapolations, can affect the resulting polarization P_n. The following discussion is concerning the asymmetry resulting in the scattering of neutrons emitted from the reaction, with deuterons of incident energy 1.2 MeV, at a laboratory angle 47°.

The tail of the resulting recoil spectrum can be extended under the peak according to three, obvious, extrapolations (Fig. 29).

The tail extrapolation, marked as 1 in Fig. 29, is the one which would result assuming that the tail falls off completely within the low energy edge of the spectrum, i.e. the tail effect does not extend to the area under the upper edge; extrapolation 2 is according to the simulated tail represented in Fig. 26B; extrapolation 3 is the extrapolation used for correcting the asymmetries reported in the previous section and given in Table 2.2. First step was to calculate the asymmetry by integrating first the area between the midpoint of the lower edge and the summit of the peak, then by integrating the area between the summit of the peak and the midpoint of the upper edge and finally by integrating the one between the two midpoints.

Second step was to evaluate the correction factors τ_1, τ_2 and τ_3 for the extrapolations 1-3 respectively; then multiply the values of τ_1 by the measured asymmetries, as calculated from the three areas, to obtain asymmetries ε_1. The same procedure was repeated for extrapolations 2 and 3 where asymmetries ε_2 and ε_3
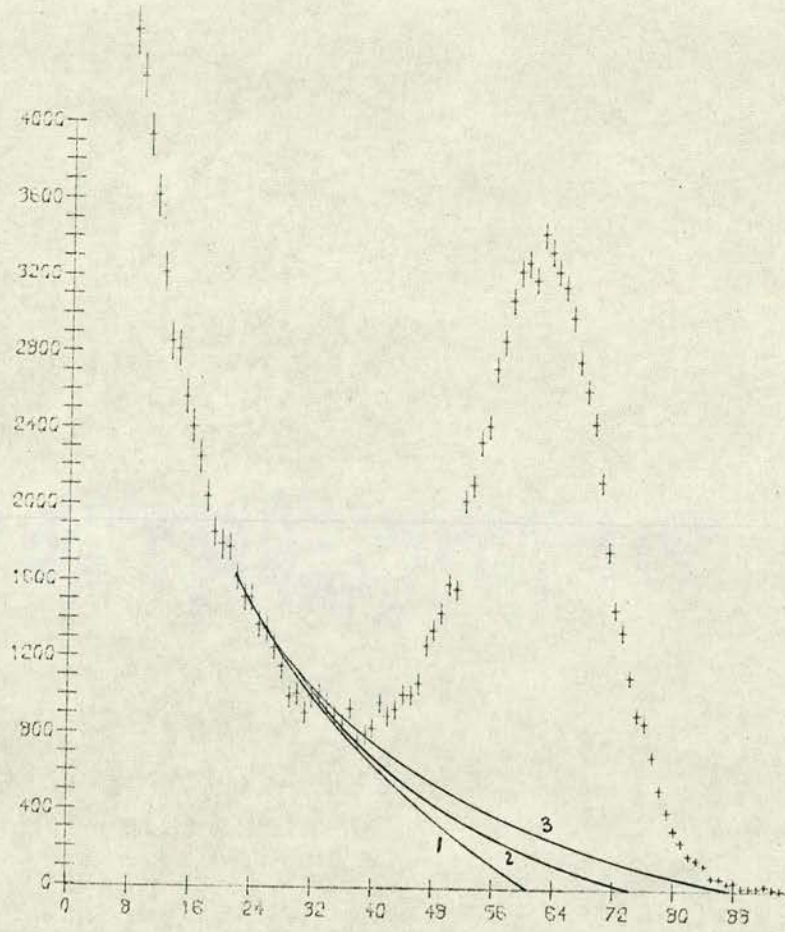
Fig. 29.   Different extrapolations
of the tail.

were obtained.

Finally the corrected asymmetries (i.e. ε_1, ε_2 and ε_3) were divided by the mean analysing power $< P >$, calculated as described in the previous section, to obtain polarization P_n. The results of such calculations are given in Table 2.3; in Table 2.3. are given the corrected asymmetries ε_1, ε_2 and ε_3 where each of them is preceded by its correction factor τ and followed by the resulting polarization value. It is remarkable that the three polarization values, obtained as a result of a particular extrapolation, agree well within the statistical accuracies.

Calculation of the polarization P_n obtained from the asymmetry, evaluated from the area under the peak and between the two midpoints, without applying any tail correction, yielded a value of P_n(%) -12.8 ± 0.8; it is significantly different from a value -14.5 ± 0.9 resulting when the most likely tail correction is applied.

2.10. The Resulting D(d,n)^{3}He Polarizations

It has been proved[126] that other corrections which might contribute to the measured polarization, e.g. multiple scattering in the ^{4}He gas scintillator, scattering in the target assembly etc., are insignificant; accounting for them should give an upper limit far smaller than the obtained statistical accuracies.

Thus the polarization, resulting in the D(d,n)^{3}He reaction, can be evaluated from the corrected asymmetries, given in Table 2.2., and the mean analysing power calculated as described in Section 2.8.

Table 2.3. Values of polarization P_n obtained according to different tail corrections.

Area of Integration	Un-corrected ε	τ_1	ε_1	$P_n(\%)$	τ_2	ε_2	$P_n(\%)$	τ_3	ε_3	$P_n(\%)$
Lower edge	-11.77 ± 1.13	1.06	-12.5 ± 1.2	-13.3 ± 1.3	1.10	-12.9 ± 1.2	-13.7 ± 1.3	1.17	-13.8 ± 1.3	-14.7 ± 1.4
Upper edge	-12.43 ± 0.91	1.00	-12.4 ± 0.9	-13.2 ± 1.0	1.05	-13.1 ± 1.0	-13.9 ± 1.1	1.09	-13.5 ± 1.0	-14.4 ± 1.1
Between the two edges	-12.00 ± 0.73	1.03	-12.4 ± 0.8	-13.2 ± 0.9	1.08	-13.0 ± 0.8	-13.8 ± 0.9	1.13	-13.6 ± 0.8	-14.5 ± 0.9

The resulting polarizations are given in Table 2.4; in the first column of Table 2.4 are given the incident deuteron energies; in the following columns are given the mean deuteron energies, calculated considering the energy losses in the targets given in Table 2.1, the reaction angles θ, the mean analysing powers and finally the resulting $D(d,n)^3He$ polarizations (%).

Average values of the corrected measured asymmetries at deuteron energy 2.5 MeV, given in Table 2.2. at reaction angles 47°, 55° and 65°, were used along with the mean analysing powers to obtain the values of P_n given in Table 2.4.

As for the incident deuteron energies 2.0, 2.1, 3.0 and 3.13 MeV the mean energies are the same, i.e. a mean energy ~ 1.9 MeV for incident deuteron energies 2.0 and 2.1 MeV and 2.94 for 3.0 and 3.13 MeV, the values of P_n can be averaged. Thus an average value of P_n(%) for mean deuteron energy 1.9 MeV will be -15.8 ± 0.8; for mean deuteron energy 2.94 MeV such average value will be -10.3 ± 1.03. These average values will be used in the discussion of the obtained results in Chapter IV.

Table 2.4. The resulting D(d,n)^{3}He polarizations.

Ed (MeV)	< Ed > (MeV)	θ (Lab)	< P >	P_n(%)
0.5	0.33	50°	0.89	−13.8 ± 0.6
1.2	1.1	27°	0.93	− 8.0 ± 0.6
		35°	0.94	−10.2 ± 0.6
		47°	0.94	−14.5 ± 0.9
		55°	0.94	−16.6 ± 0.8
		65°	0.93	−12.8 ± 0.9
		75°	0.92	−5.2 ± 1.0
		89°	0.89	10.2 ± 2.1
2.0	1.90	47°	0.93	−15.6 ± 1.2
2.1	1.90	47°	0.93	−16.0 ± 1.1
2.5	2.44	27°	0.91	−3.0 ± 1.2
		35°	0.91	−7.0 ± 1.1
		47°	0.92	−13.3 ± 1.0
		55°	0.93	−11.2 ± 1.0
		65°	0.94	−8.2 ± 1.0
		75°	0.94	1.0 ± 1.1
		89°	0.92	10.4 ± 1.5
		105°	0.94	12.7 ± 2.4
3.0	2.94	47°	0.91	−10.9 ± 1.6
3.13	2.94	47°	0.91	−9.7 ± 1.3
4.0	3.85	47°	0.90	−8.4 ± 1.9

CHAPTER THREE

$\underline{D(d,n)^3He}$ POLARIZATION MEASUREMENTS USING

MOTT-SCHWINGER SCATTERING

CHAPTER THREE

$D(d,n)^3He$ POLARIZATION MEASUREMENTS USING MOTT-SCHWINGER SCATTERING.

Although Mott-Schwinger scattering, described in section (1.3.1), can be a good alternative to scattering from spin-zero nuclei for detecting polarization from the $D(d,n)^3He$ reaction, it is still not as commonly used as scattering from helium.

In this chapter two sets of $D(d,n)^3He$ polarization measurements using a Mott-Schwinger polarimeter will be described. The first measurement was carried out using the deuteron beam from the 1 MeV Cockcroft-Walton accelerator. The other set was carried out using the same polarimeter, being reset with different geometrical arrangement, where the deuteron beam was produced by the 0.5 MeV Van de Graaff. These two sets of measurements will be described in the following sections.

3.1. The Experimental Arrangement

The experimental arrangement used during measurements with the deuteron beam from the Cockcroft-Walton accelerator, was described before[157,158], where it was mainly used for differential cross-section measurements at small angles. It is shown in Fig. 30, in elevation which gives the relative positions of the TiD target, scatterer and monitors. In this arrangement, the vertical ion beam from the accelerator, analysed magnetically through 30° (see Fig. 30), provided a deuteron beam incident on the TiD target. The target holder, and cooling system attached to it, is of the same design
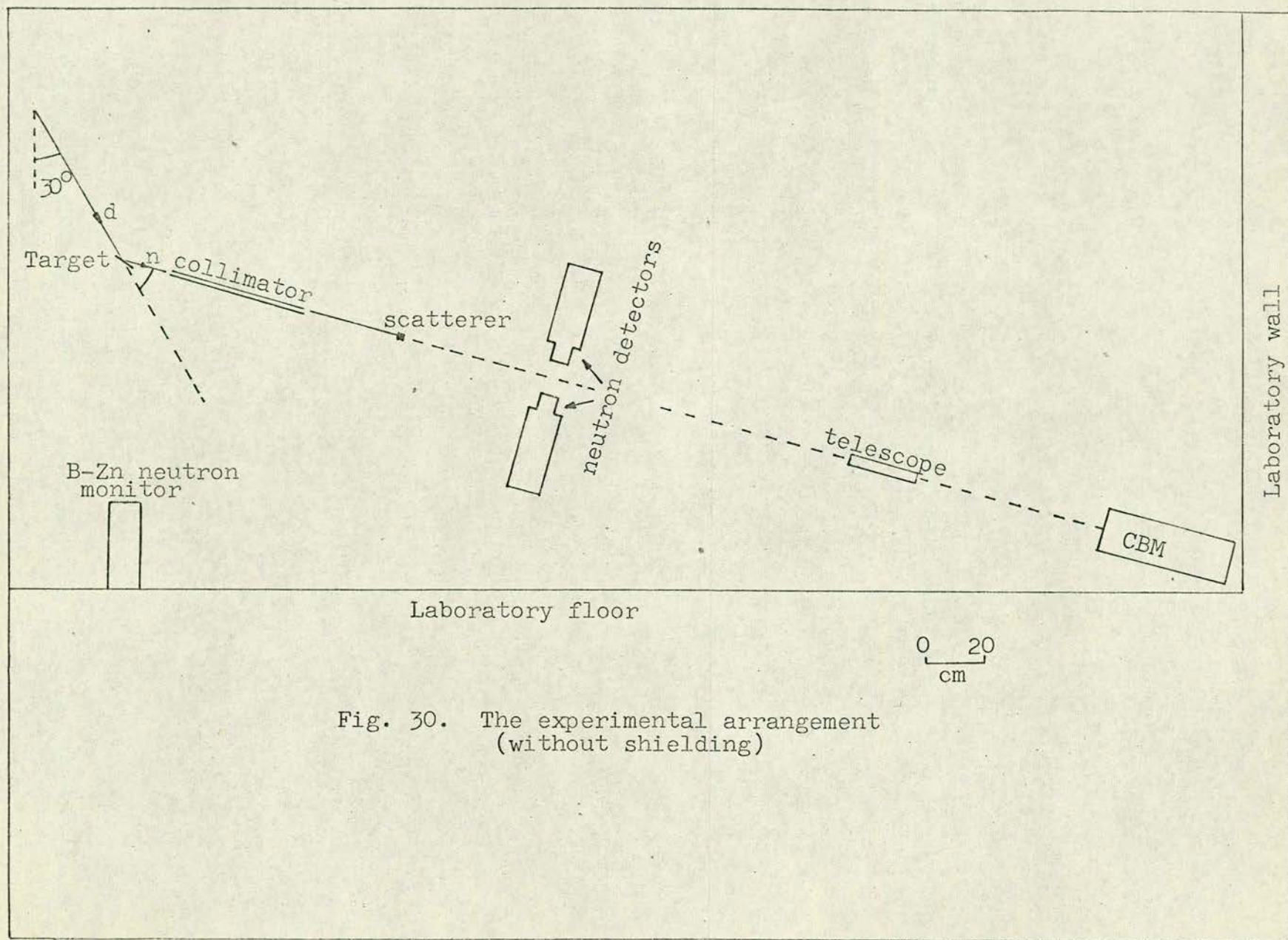
Fig. 30.   The experimental arrangement
          (without shielding)

described in section 2.1.

Neutrons resulting from the $D(d,n)^3He$ reaction and emitted
at angle 46° lab. to the beam direction, pass through a collimator,
then are scattered by the scatterer to the side detectors.   The
collimator (50 cm long) is formed from five cylindrical pieces
of polythene, each is 5 cm in diameter with a 7 mm diameter axial
hole, fitted together in a brass tube.   The scatterer is located
35 cm from the collimator exit; its diameter (1.2 cm) is slightly
larger than the neutron beam at this point.

The two side detectors, for detecting the scattered neutrons,
are mounted on a special arrangement (Fig. 31) at a distance about
57 cm from the scattering sample.   Each of the two side detectors
is a 5 mm x 20 mm x 30 mm stilbene crystal with its 20 x 30 mm face
coupled to a photomultiplier.   The 30 mm edges of the crystals are
parallel to the collimated neutron beam axis so that the 5 mm thick-
ness determines the spread in the scattering angle subtended at the
scatterer.   The arrangement, carrying the detectors (Fig. 31), is
a special rig with which the detectors can be moved by screw drivers,
on accurately machined rails and in this way they can be set to
detect neutrons scattered at a particular angle.   Besides the rig
itself is rotatable; this allows measurements in either of the
scattering planes.

In order to prevent neutrons emitted from the target to be
detected by the side detectors, the collimator was built into
shielding between the target and the detectors, consisting of 90 cm
of paraffin wax and borated water contained in sealed polythene bags
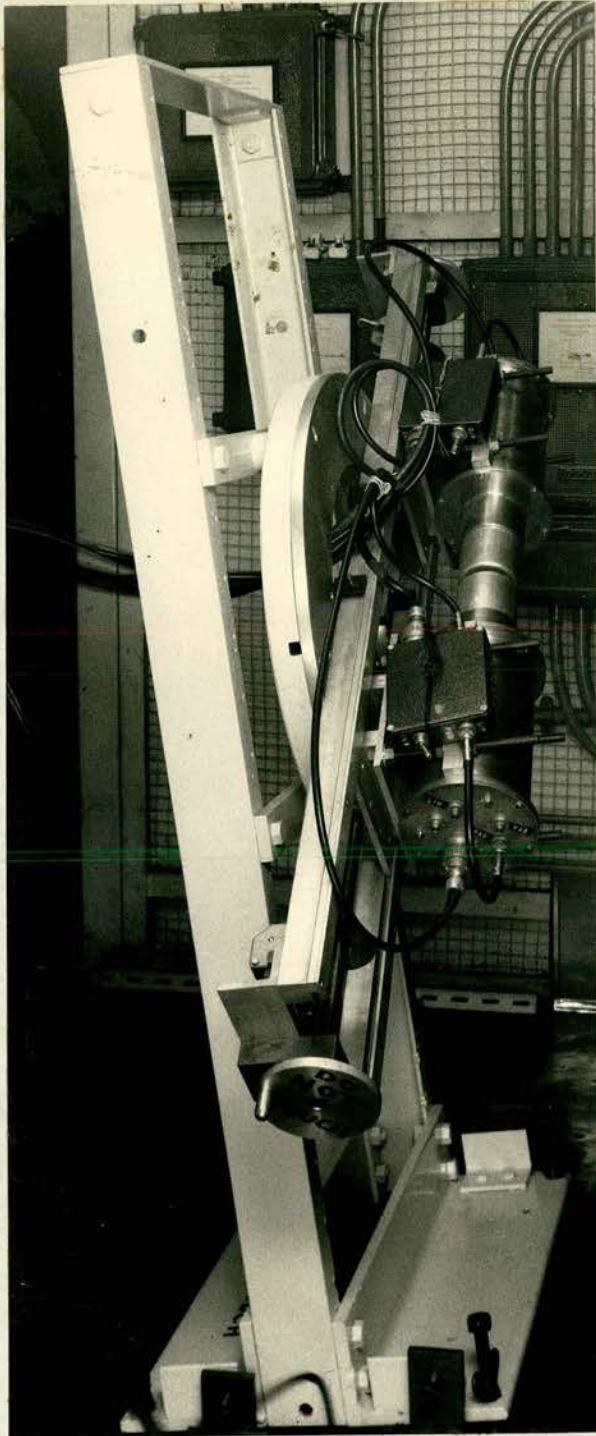
Fig. 31. Photograph of the rig carrying the two stilbene detectors.

inside tin cans.   Besides a wall of lead and iron (18 cm thick)
was applied to reduce γ-ray background.   The whole detector
mounting is surrounded by the laboratory wall on one side and
45 cm of paraffin wax and borated water, as well as 6 cm of lead
and iron, on the other sides (Fig. 32).   Similar shielding was
applied above the rig, and in this way a well shielded chamber
results.   In its backwall is a hole of 15 cm diameter along the
collimator's axis which allows the neutron beam to pass through to
a detector which is used for monitoring the collimated beam.

3.2.   The Electronic Set-up

The electronic set-up is based on four detectors.   Two of
them, mentioned in section 3.1, are for detecting neutrons scattered
from the sample, hereafter called stilbene detectors;   the other
two are for monitoring neutrons from the target.

Each of the two stilbene detectors has   its stilbene
crystal mounted with its 20 mm x 30 mm face in optical contact with the
photocathode of a 56 AVP (Mullard type) photomultiplier.   The
other faces of the crystal are coated with titanium dioxide paint
as diffuse reflector, with a thin (0.5 mm) aluminium can used as
light-tight cover.

One of the other two detectors is set up to monitor neutrons
coming through the collimator, hereafter called the collimated beam
monitor (CBM);   the other one, placed just under the target, is for
monitoring the neutron yield from the target and will be called here-
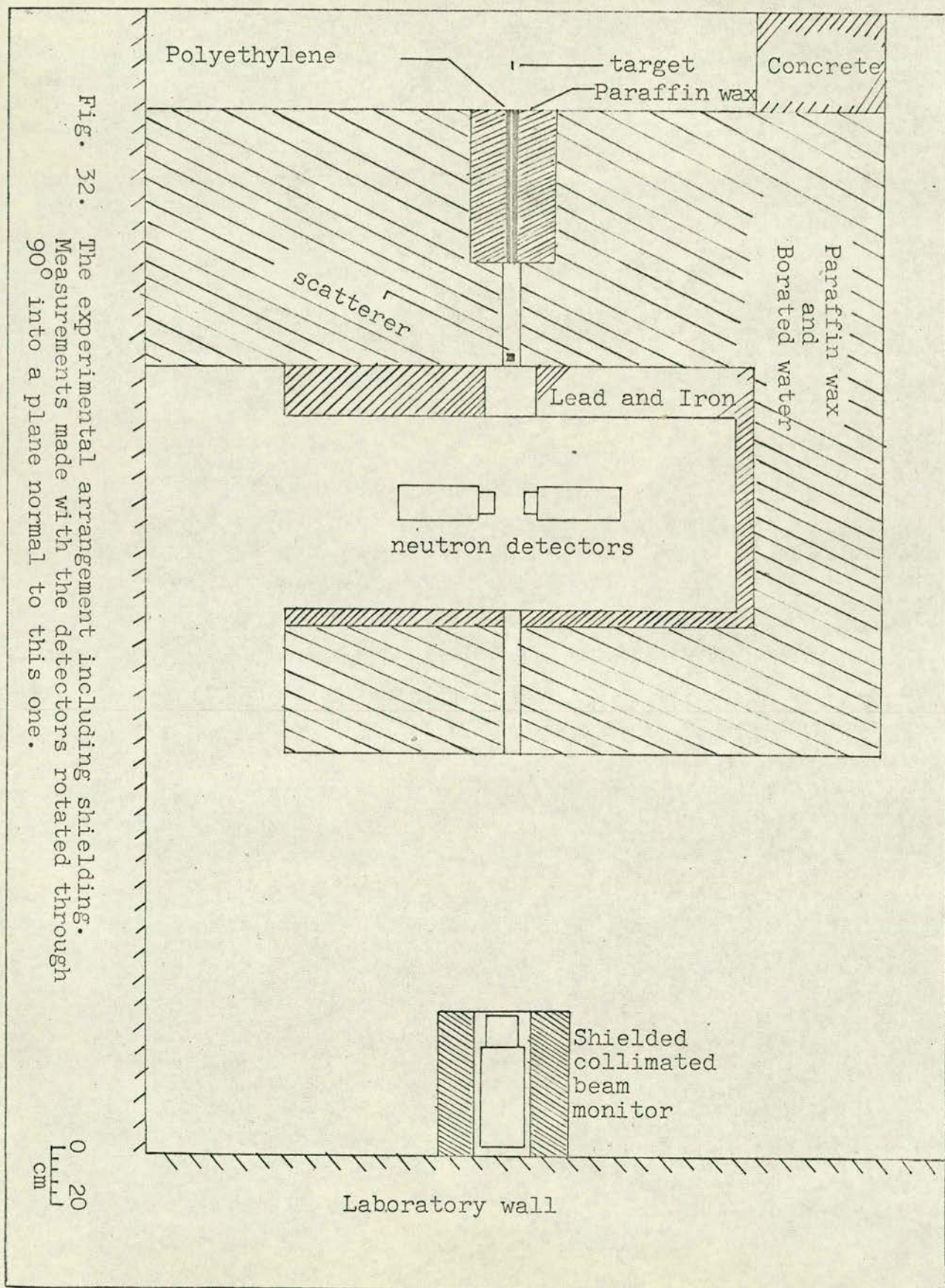after the target yield monitor (TYM).

Fig. 32. The experimental arrangement including shielding. Measurements made with the detectors rotated through 90° into a plane normal to this one.

96

The CBM is a NE 213 liquid organic scintillator coupled to EMI type 6262 B photomultiplier.

The two stilbene detectors and the CBM are coupled to dynode chains, suitable for pulse shape discrimination of neutrons against γ-rays. The pulse shape discrimination technique employed, for all the three detectors, is the Owen technique[152].

The principle of the Owen technique, utilizes the properties of the scintillators used in these three detectors. These scintillators, when excited, emit light which decays with fast and slow components. The relative intensities of the fast and slow components depend upon the nature of the incident exciting radiation. For neutrons, this ratio of the slow component to the fast is larger than for γ-rays. This difference results in voltage pulses, from the photomultiplier, of different shapes according to the nature of the radiation. Allowing saturation of the current between the last dynode and the anode of the photomultiplier, the difference between the shapes of the pulses is translated into a pronounced difference in voltage pulse heights for neutron and gamma signals. For the two stilbene detectors this was achieved by biasing the anode, a few volts positive, with respect to the last dynode, by connecting a suitable resistor between them; for the CBM a separate supply was used. About 3.5 volts (positive) were enough to obtain the desired effect.

A typical electronic circuit, coupled to any of the three detectors, based on this technique is represented in Fig. 33. According to such a circuit two outputs, linear and saturated, are taken from

P/A - Preamplifier   AMP - Amplifier   DIS - discriminator
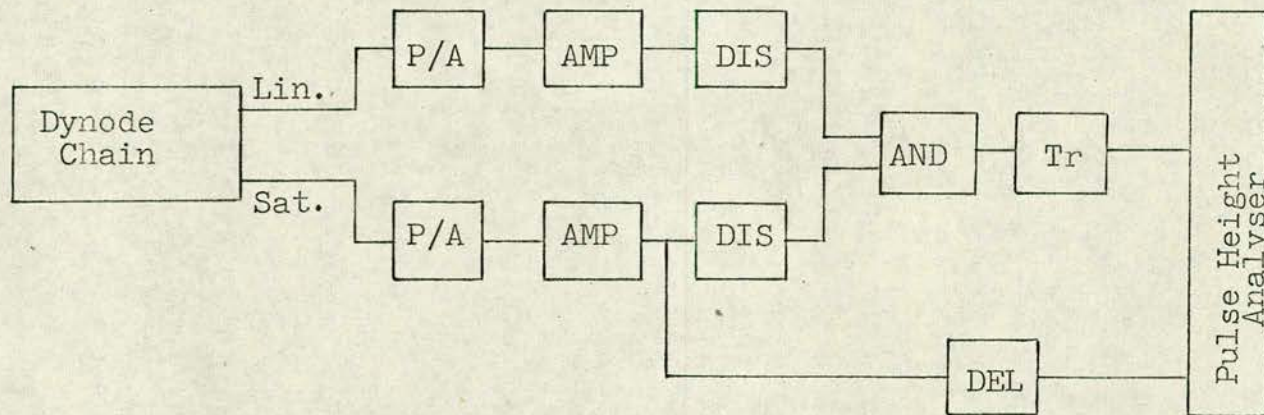

Fig. 33.   A typical electronic circuit used to
            set up pulse-shape discrimination

the dynode chain.   The linear one is usually taken from one of the dynodes before the last.   The saturated output is from the last dynode, which is biased a few volts negative with respect to the anode. Both the two outputs are coupled to suitable preamplifiers and amplifiers.

The discriminator following the amplifier of the linear output was usually set at a discrimination level to reject 0.3 MeV γ-rays; this was checked using ^{22}Na-γ source.

Pulses corresponding to coincidence between the output of this linear discriminator and the corresponding discriminator on the saturated output were obtained from the "AND" unit (see Fig. 33). Such pulses indicated neutrons above a set energy level and after a logic conversion ("Tr" unit in Fig. 33) could be used to gate the pulse height analyser.

The following step is to vary the bias applied to the anode and observe the resulting pulse height spectrum on the analyser's screen, using a 100 mCu ^{210}Po-Be source.   When the best pulse shape discrimination is achieved (Fig. 34a), the anode will then be at the required bias.

The final step is to set the discriminator following the saturated output at such a level as to reject most γ-rays without rejecting neutrons.   By suitable setting of the delay units attached to the two discriminators, it is possible to inhibit the analysis of high energy gamma pulses and the peak due to γ-rays is thus significantly reduced (Fig. 34b).

This set-up procedure established optimum gamma rejection and neutron acceptance for the two stilbene detectors and CBM.

Fig. 34. Pulse shape discrimination spectra obtained with the CBM
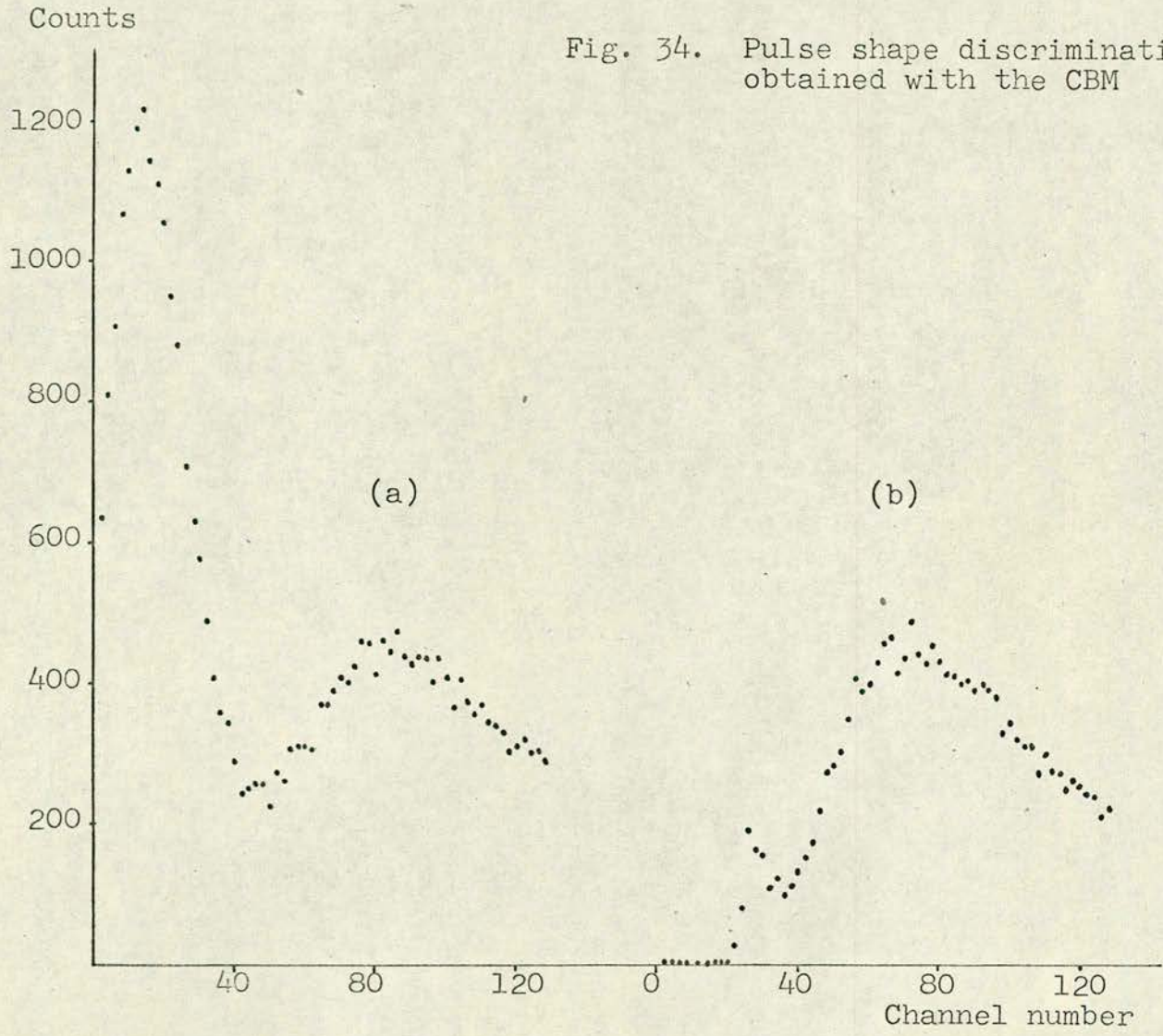
The TYM is a NE 400 scintillator, insensitive to γ-rays, coupled to EMI 6079 B photomultiplier; NE 400 type of scintillator consists of a grooved disc of Boron polyester, with ZnS as scintillator, of 25 mm diameter and 1.2 mm active layer.

As such a type of detector is mainly for slow neutrons, it is surrounded by 10 cm of paraffin wax to slow down fast neutrons.

The electronic block diagram is represented in Fig. 35. Both the stilbene detectors, as well as the CBM, have got identical circuitry. Thus pulses from the four detectors are fed to the pulse height analyser (Laben - 512 channels), through its mixer, where in the four sections of its memory can be accumulated, during a particular time of measurement, four spectra coming from the two stilbene detectors, CBM and TYM.

Besides collection of spectra, the pulses from the CBM and TYM are also fed to scalers and ratemeters. The scalers are controlled by a special "stop start" unit attached to the analyser so that counts registered correspond to the interval during which spectra are collected.

For the CBM, as with stilbene detectors, 2 discriminators and an 'AND' unit are used to signal neutron pulses above an energy threshold, but in addition a third discriminator is coupled to the saturated O/P amplifier with a higher γ-rejection setting of 1000 γ-rays received to 3 accepted. The discriminator pulses, are then fed to the CBM scaler (Fig. 35). The TYM scaler is attached directly to its discriminator as shown.

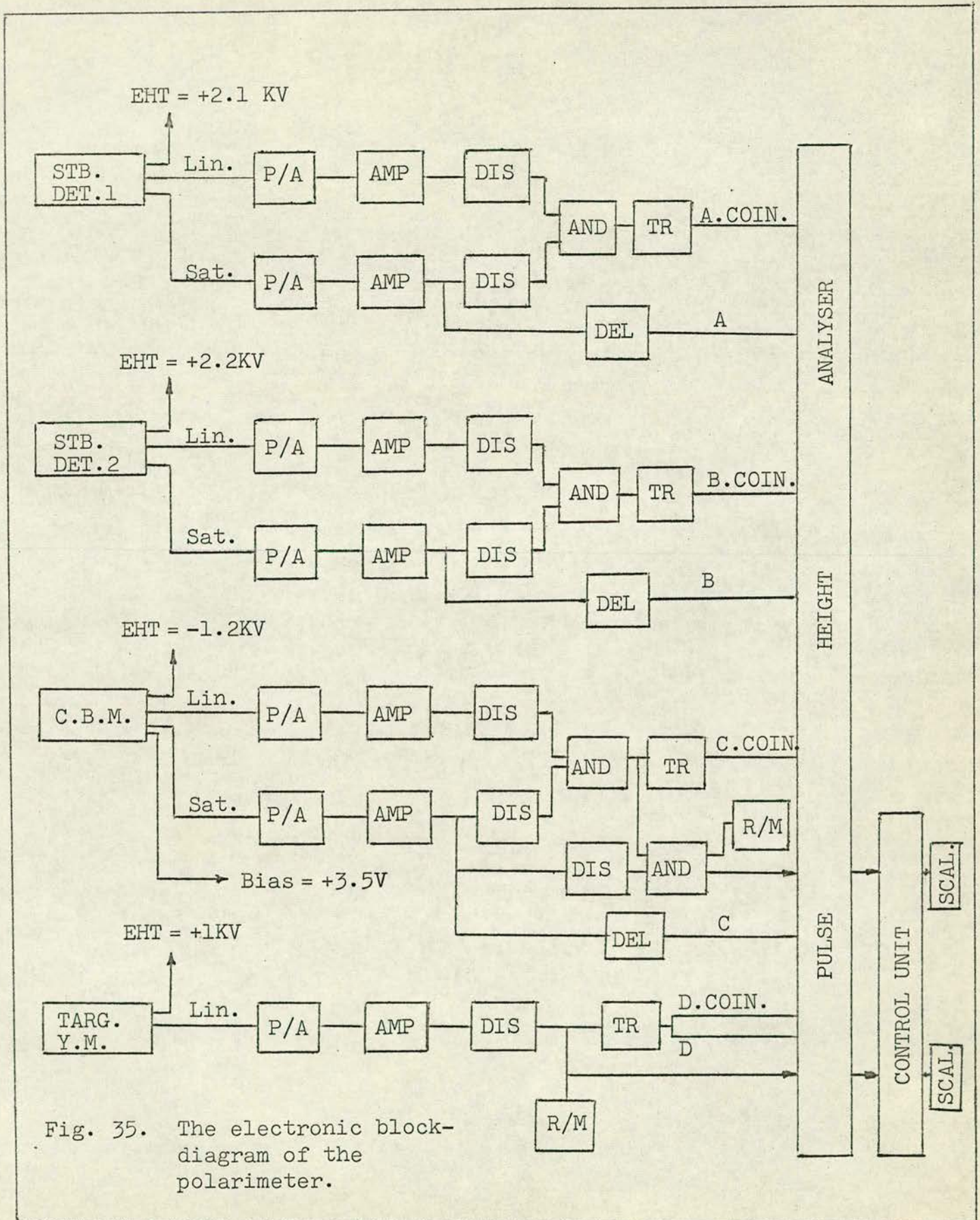The ratemeters in parallel to the CBM and TYM scalers are run

Fig. 35. The electronic block-
diagram of the
polarimeter.

in a continuous sampling mode to assist in the setting up and running of the accelerator.

Once all the electronics are connected, according to Fig. 35, the system is tested with neutrons, from the $D(d,n)^3He$ reaction, emitted from the TiD target. For such purpose each of the stilbene detectors was moved to the centre of the beam, while the other one was kept at a distance, and then both the gated and ungated spectra, taken during the same measuring time, were displayed on the corresponding section of the analyser's memory. Such spectra are represented in Fig. 36 for both the stilbene detectors, where it is remarkable that the pulse shape discrimination spectra, i.e. the gated and ungated spectra, have the same height of neutron peak which means that most of the γ-s are rejected without losing neutrons.

The CBM, being permanently positioned in line with the collimated beam, is similarly treated and similar gated and ungated spectra were obtained with the discriminator following the saturated output set at a level more than required to obtain gated spectrum of the same height as the ungated one; this is to cut more γ-s as the CBM being directly in the neutron beam, is detecting more neutrons than either of the two stilbene detectors, and is used for monitoring purposes.

3.3. Experimental Procedure

The experimental measurements were preceded by accurate align-ment of the apparatus; this was followed by measuring the beam profile.

Fig. 36. Gated and Ungated PSD spectra of the two stb. detectors

· Ungated spectrum
⅄ Gated spectrum
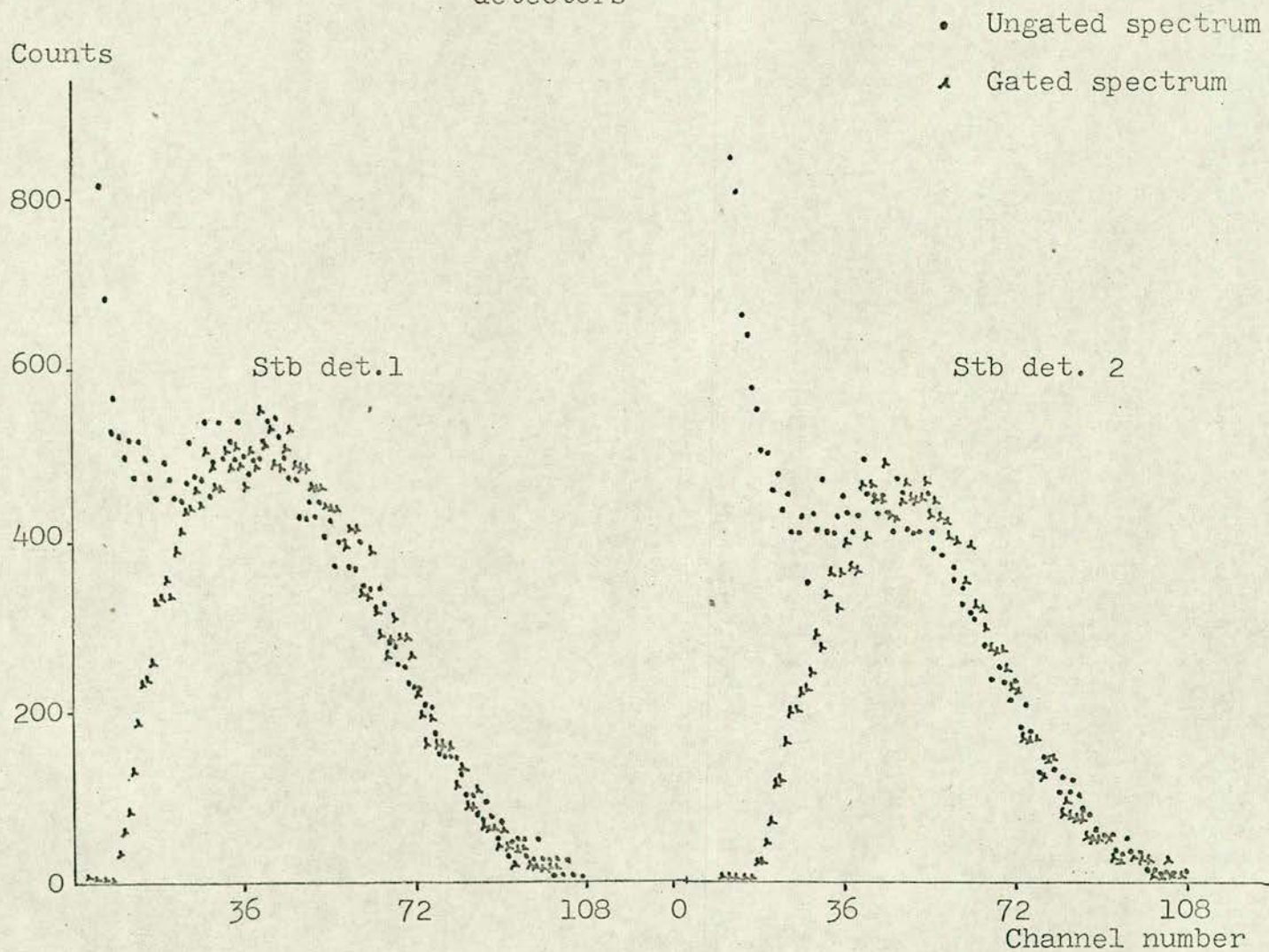
The alignment of the apparatus is carefully checked with a
telescope placed between the CBM and the two stilbene detectors
(Fig. 30).   The telescope was firstly focussed on the target, then
on the entrance and the exit of the collimator.   The special
design and position of the target system, made the focussing on the
target easier.

After the position of the target has been checked, the next
step is to focus the telescope on the scatterer and centre of the
rig, carrying the two side detectors;   the centre of the rig was
located by carefully fixing cross-wires, which were removed, as
well as the telescope, after the alignment of the apparatus was
checked.   The whole arrangement was inclined at an angle 15° to the
horizontal.

The beam profile measurement is important from several aspects.
First, of   all,   one has to be sure that the beam is well
collimated, hence the beam profile should be well defined.   With a
well defined beam profile both the smallest angle, at which the
measurements can be made and the angular resolution of the polari-
meter are determined.   Besides, the number of neutrons incident on
the scattering sample is determined from the beam profile;   the
number of incident neutrons is required for calculating the differ-
ential scattering cross-section.

The beam profile was measured by scanning the beam diametrically
by each of the two stilbene detectors in turn; the detector not scaning the beam was at
a distance about 10 cm from the centre of the beam, in order to
exclude scattering of neutrons, from it, to the one measuring the

beam profile.   The detector scanned across the beam was moved in 2.33 mm steps.   It was left in each position to measure the number of neutrons incident during 256 seconds.   At the end of each measurement the spectrum was typed out and the readings of both the CBM and TYM scalers were noted.

The intensity of neutrons incident on the stilbene detector was then found from the total number of counts in the neutron peak, after the γ-rays were subtracted, then normalized with respect to the number of counts registered by the TYM.   The TYM reading was used for normalization, instead of the CBM, as the latter was affected when the stilbene detector was in the neutron beam.

The normalized relative counting rate is then plotted, as a function of distance, for both the stilbene detectors.

The beam profile as measured by each of the two stilbene detectors, separately, is represented in Fig. 37, where the solid line represents the shape of the beam as expected from the geometry of the experiment.   The spread in the neutron beam and the full width at half maximum (FWHM), as found from the beam profile, are 13.5 mm and 13.1 mm respectively.   Such a spread in the neutron beam corresponds to an angle of 1.4° measured from the position of the scattering sample;   the FWHM (i.e. 1.3°) corresponds to angular resolution $\pm 0.65^\circ$.

Because of the spread in the neutron beam, i.e. 1.4°, the smallest angle chosen for measurement was 1.9°.
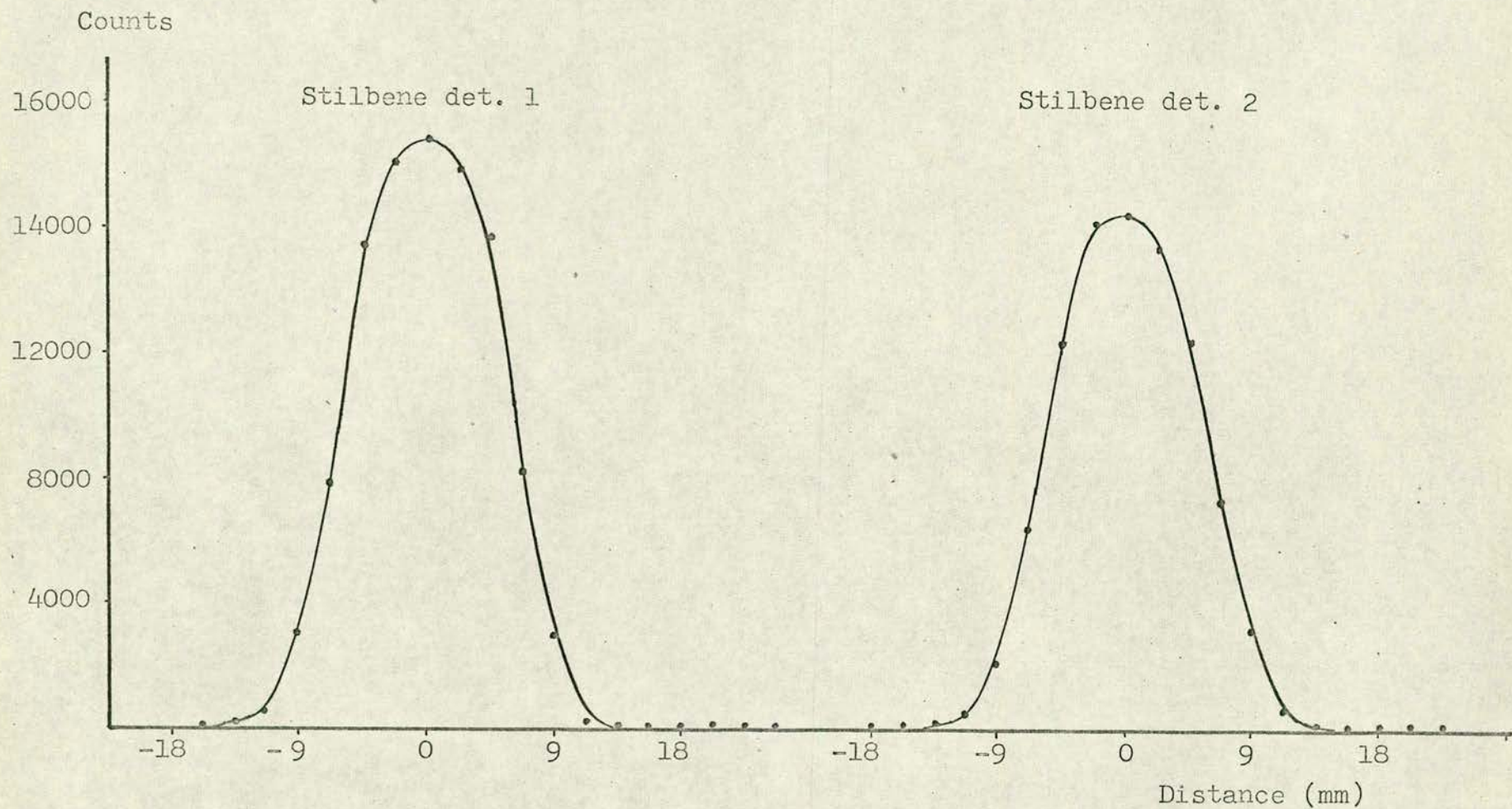
Fig. 37.   The beam profile as measured by each stilbene detector.
The solid curve represent the shape of the beam as
calculated from the geometry of the polarimeter.

3.3.1. Experimental measurements using scattering from lead

Measurements were carried out for neutrons scattered from a lead sample. This sample was a cylinder, 2.6 cm long and 1.2 cm diameter. The measurements were performed with both the stilbene detectors set, in the vertical plane, at five small angles, 1.9°, 2.2°, 3.4°, 6.3° and 11.6°.

Neutrons, incident on the Pb sample, were produced in the $D(d,n)^{3}He$ reaction induced with deuterons, accelerated in the Cockcroft-Walton accelerator up to an energy 820 KeV, bombarding a thick TiD target. The deuteron beam current, during the measurements, was ~ 40 µA.

The measurements, at a particular angle, were carried out first with the Pb sample in the way of the beam then without the sample. The measurement with the Pb sample out of the beam was required both for calculating the background and the total interaction cross-section. The two measurements were repeated in 2048 sec. intervals until the required statistical accuracy was achieved.

3.4. Treatment of the Experimental Data

The treatment of the experimental data usually started with determining from the cumulative scattering spectrum the number of neutrons scattered from the Pb sample at the angle of interest. This was followed by calculating the differential cross-sections, total cross-sections and finally the $D(d,n)^{3}He$ polarization. These steps, along with the corrections required, will be described in the following sections.

3.4.1. Determination of the number of neutrons scattered at a particular angle

The number of neutrons scattered from the Pb sample, at a particular angle, was determined from the cumulative scattering spectrum, i.e. the one obtained by adding up all the measured scattering spectra. As the measurements were in the reaction plane, the spectra detected by each of the two stilbene detectors were treated separately.

From the cumulative scattering spectrum the background spectrum was subtracted, i.e. the one resulting after adding up all spectra measured with the sample removed from the way of the beam, normalized to the same CBM reading.

It has been shown, in section 3.2, how the electronics is set up to reduce to a small proportion the number of gammas accepted (see Fig. 34). However some of the high energy gammas resulting from slowing down and radiative capture processes in the shielding material were not removed by this process.

The scattering spectrum obtained has therefore to be integrated from a particular channel where this high energy gamma contribution is negligible. In order to determine this particular channel, the scattering spectrum was overlapped with another two spectra, one of them a gamma spectrum, detected by the stilbene detector from a γ-source and the other one the neutron spectrum measured by the same detector at the centre of the neutron beam.

There was a need to check that the pulse shape discrimination output from the stilbene

detectors is energy independent, i.e. the position of the γ-peak will be the same for γ-rays of different energies. This was realised by observing, separately, spectra due to γ-rays emitted from ^{22}Na, ^{60}Co, ^{137}Cs and Th sources. Although these spectra are due to gammas of different energies, when they were detected by either stilbene detector, and then all normalised in intensity, it was found that they all agree both in shape and position of the peak. This was the case for both the two stilbene detectors. In Fig. 38 are represented such γ-spectra normalised to the ^{22}Na spectrum, for one of the stilbene detectors.

Thus the spectrum from the scattering measurement was over-lapped with both a ^{22}Na γ-spectrum and the neutron spectrum, measured at the centre of the beam. Both these spectra were normalised to the areas under the peaks of the scattering spectrum. Such a procedure was carried out for each stilbene detector and for all the five scattering angles. The channel number limits for the neutron peak were found to be the same, for a particular stilbene detector, at all these angles. The experimental points of the scattering spectrum fitted nicely to the overlapped spectra as shown in Fig. 39 for the two stilbene detectors at a scattering angle of 3.4°.

3.4.2. Calculation of the differential scattering cross-section

The differential scattering cross-section σ(Θ), into unit solid angle at scattering angle Θ, is given by the expression[159]:

$$\sigma(\Theta) = \frac{Nr^2}{N_o n} \qquad (3.4.1)$$

Fig. 38. γ-spectra emitted from different sources and detected by one of the side detectors.
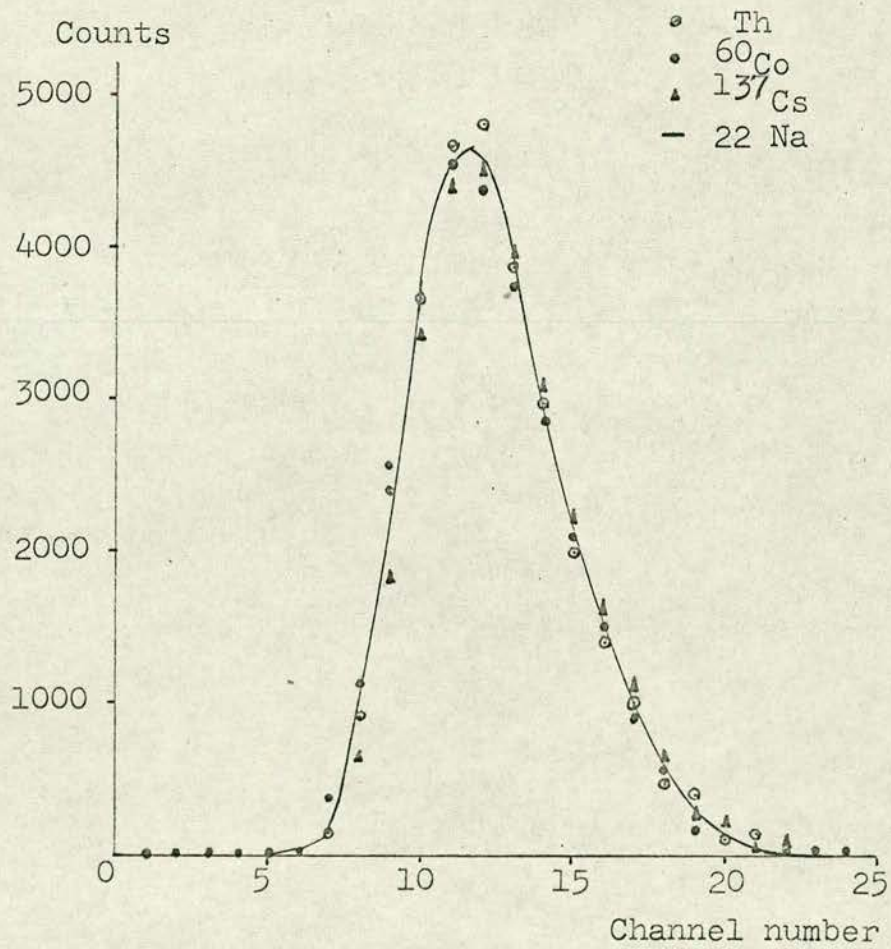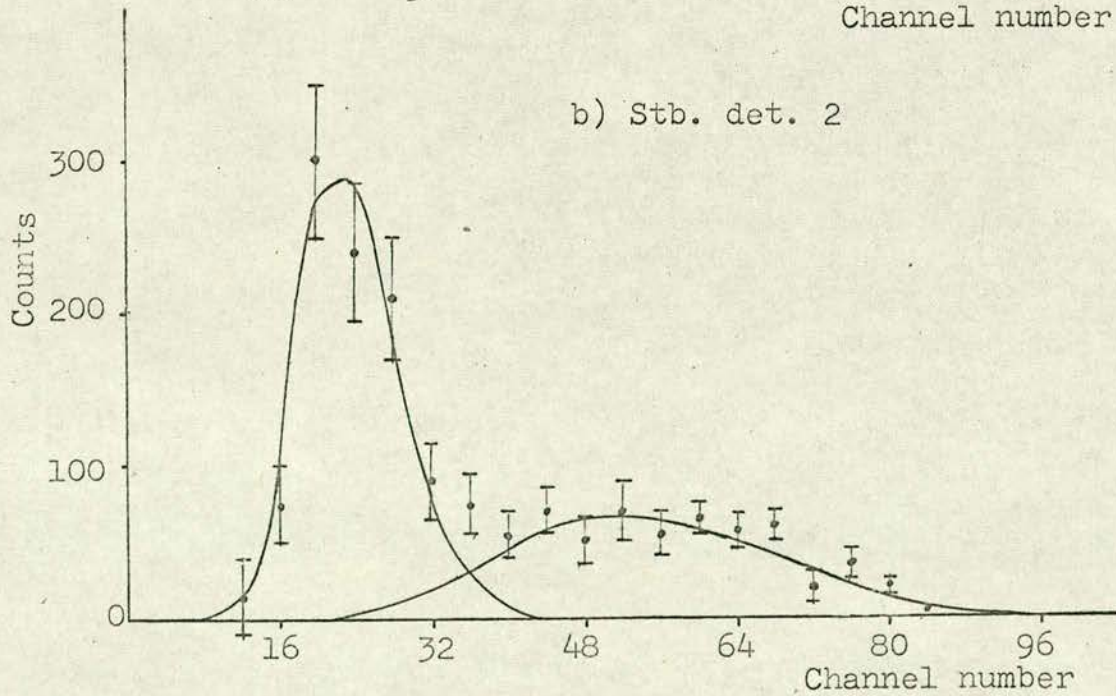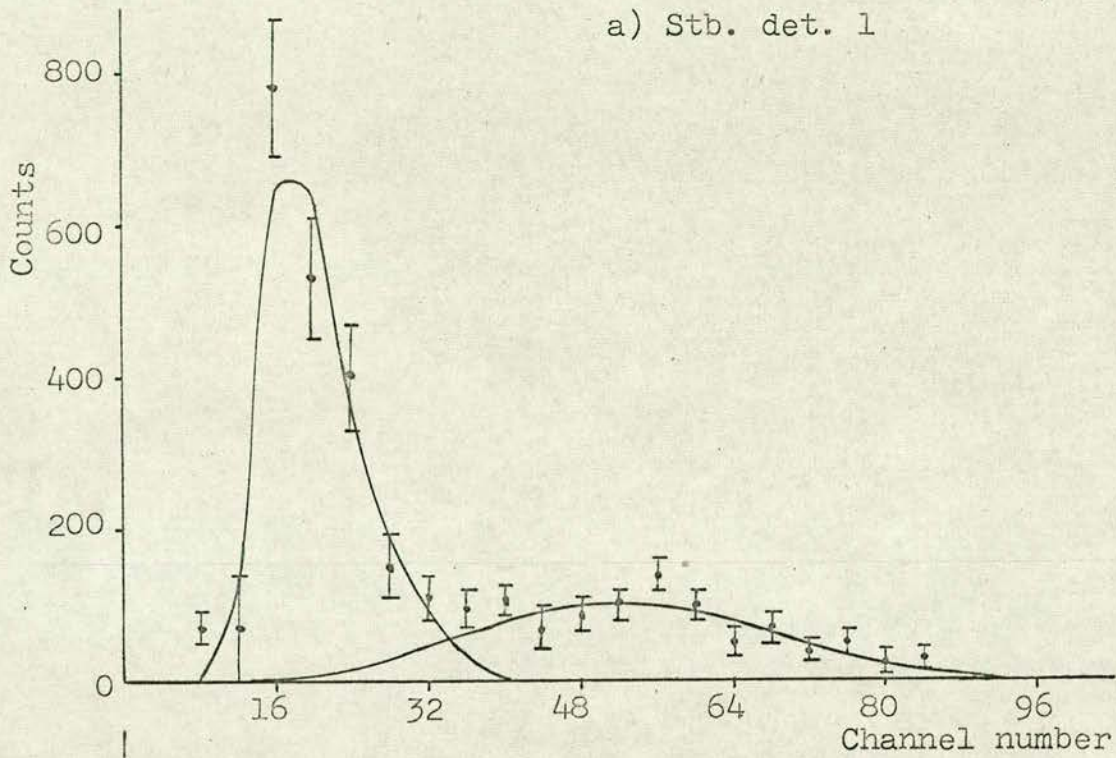
Fig. 39. The scattering spectra detected at 3.4° compared with spectra from sources (solid curves)

where N, N_o, r and n are the scattered neutron flux (neutrons/cm²
sec), incident neutron flux, distance between detector and
scatterer, and the number of nuclei in the scatterer respectively.

Expression (3.4.1) was used for calculating the differential
scattering cross-sections, for each of the two stilbene detectors
separately.   For such purpose the measured number of background
neutrons was subtracted from the measured number scattered by the
sample; both of them being normalised to the same CBM reading
before subtraction.   The ratio of background neutrons to scattered
neutrons, given in Table 3.1 at the five scattering angles, was
high and this is typical of small angle scattering experiments.

Table 3.1

Angle	Background to scattering ratio
1.9°	0.62
2.2°	0.58
3.4°	0.49
6.3°	0.42
11.6°	0.41

As the measurements were carried out in the reaction plane,
one of the two detectors should be measuring the 'right' cross-
section while the other one is measuring the one to the 'left'.   In
Fig. 40 the cross-sections obtained with both the 'right' and 'left'
detectors are represented.

Fig. 40. The experimental cross-sections as measured
both to 'right' and 'left'.

▨ - cross-sections measured with 'right' detector.

◻ - cross-sections measured with 'left' detector.

3.4.3. The effect of multiple scattering in the Pb sample used

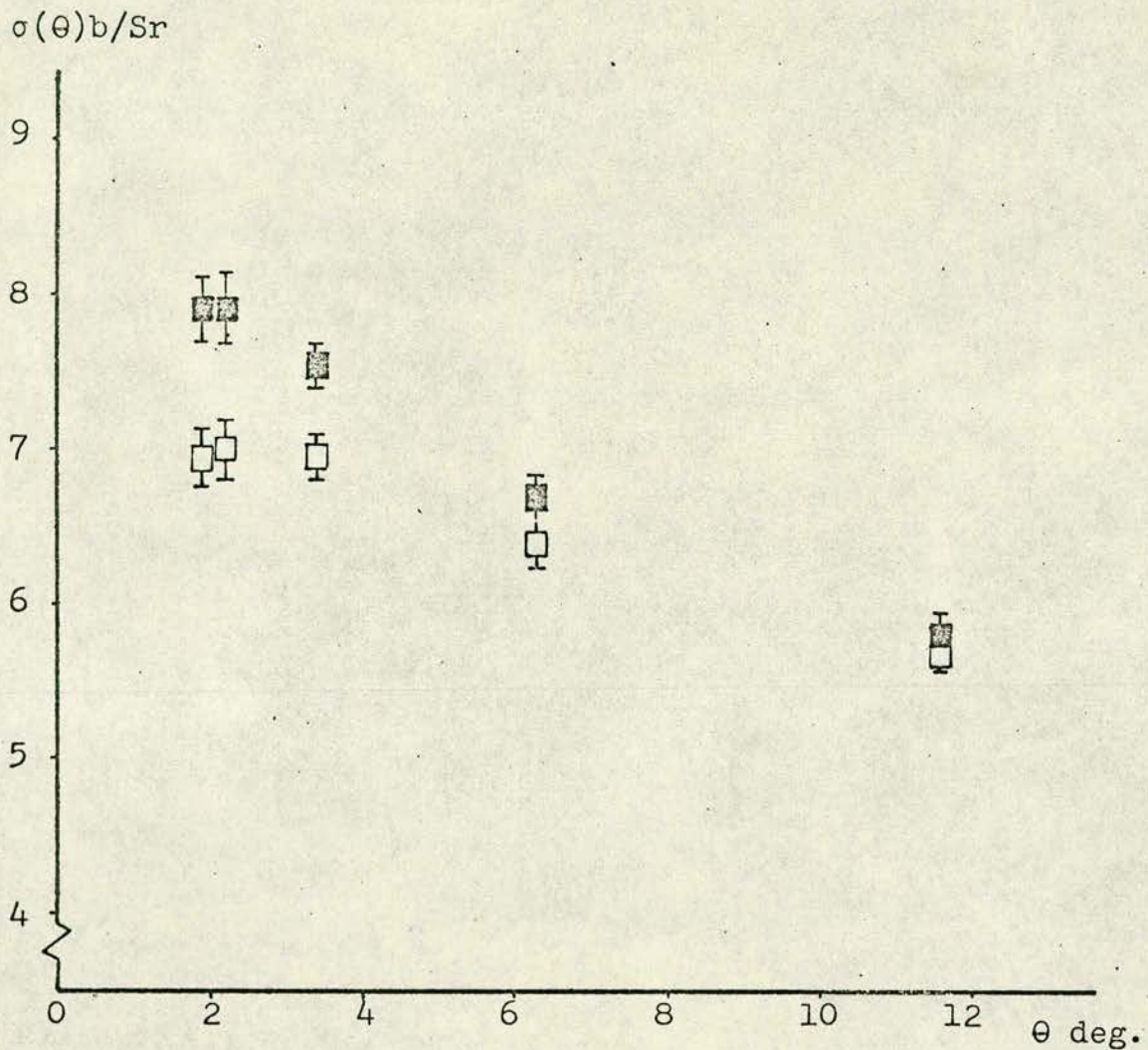In the ideal case, i.e. when a very thin scatterer is used, only single scattering occurs in the sample. Due to the thickness of the sample used, scattering processes of higher order, e.g. double and triple scattering, can take place, along with the single scattering process, before neutrons emerged from the sample towards the detector. The detected number of scattered neutrons, and consequently the measured cross-section, has to be corrected for such an effect.

This problem was approached differently by several authors. Some of them used an analytic procedure[76] to account for the effect, others calculated the effect using an approximate analytical method coupled with a Monte Carlo method in order to calculate the multidimensional integrals involved[160,161,162].

As a first step towards the evaluation of the effect for the scatterer used, the elementary scheme of scattering used by Dukarevich et al.[60] was applied according to which the neutron is scattered first through an angle θ_1 in a solid angle $d\omega_1$. The second scattering is in the solid angle $d\omega_0$ and a direction making an angle θ_2 with the direction of motion after the first scattering and an angle θ_0 with the initial direction. θ_2, θ_1 and θ_0 are related, in the case when the foregoing angles are $< 30°$, by the expression:

$$\theta_2^2 = \theta_1^2 + \theta_0^2 - 2\theta_1\theta_0 \cos \alpha \tag{3.4.2}$$

where α is the angle between the planes in which θ_1 and θ_0 lie.

Approximately the first maximum of the function given by expression (1.3.10), of section 1.3, for diffraction of neutrons by a 'black' nucleus, is given by the Gaussian function[60]:

$$\frac{d\,\sigma(\Theta)}{d\,\omega} = \frac{d\,\sigma(0)}{d\,\omega}\, e^{-k^2\Theta^2} \tag{3.4.3}$$

where $k = (R + \lambda)/2\,\lambda$

Following the formulae given in ref.[60] for the total number of neutrons which are doubly scattered in a solid angle $d\,\omega_0$, it is easy to deduce an approximate expression for the ratio of the total number of neutrons $d\,N_2$ which are doubly scattered, at angle Θ_0, to the total number of incident neutrons N_0. Such a ratio will be given by:

$$\frac{d\,N_2}{N_0} = d\,\omega_0\,\exp(-\sigma_t\,nd)\frac{(dn)^2}{2}\,[\frac{d\,\sigma(0)}{d\,\omega}]^2\,\frac{\pi}{2k^2}\,\exp(-\frac{3}{2}\,k^2\Theta_0^2) \tag{3.4.4}$$

where d is the scatterer's thickness, n is the number of nuclei per cm^3 and σ_t is the total cross-section. Both k and $\frac{d\,\sigma(0)}{d\,\omega}$ were determined from a plot of $\ln[d\,\sigma(\Theta)/d\,\omega]$ versus Θ_0^2. From the slope of the resulting straight line k was determined; extrapolation to the angle $\Theta_0 = 0$ yielded the uncorrected value of $d\,\sigma(0)/d\,\omega$.

The effect of double scattering in the Pb sample, calculated using this procedure, was found to be ~ 12% at a scattering angle $\Theta = 1.9^\circ$.

For accurate calculation of the effect of multiple scattering, in the Pb sample, the Monte Carlo code used by Kuchnir et al.[68] was applied. The code[163] calculates four fundamental scattering probabilities:

P = probability per unit solid angle that the neutron will be scattered in the direction of the detector after its first collision in the sample;

P_1 = probability per unit solid angle that the neutron will emerge from the sample in the direction of the detector after exactly one collision;

P_2 = probability per unit solid angle that the neutron will emerge from the sample in the direction of the detector after exactly two collisions;

P_3 = probability per unit solid angle that the neutron will emerge in the direction of the detector after exactly three collisions.

The ratio of the total number of scattered neutrons to the number of singly scattered ones is equal to[163]:

$$(P_1 + P_2 + P_3)/P \qquad (3.4.5)$$

As multidimensional integrals are involved in the expressions[163] used for evaluating P_2 and P_3 the code calculates them using a Monte Carlo method. The code traces a sufficient number of histories in order to determine P_2 and P_3 so that the errors on $(P_1 + P_2 + P_3)$ are comparable with those of the angular distribution measurements.

The effect of multiple scattering, calculated applying the code, for the Pb sample used amounted to 14.6% at a scattering angle of 1.9° decreasing to 11% at 11.6°.

3.4.4. Calculation of the $D(d,n)^3He$ neutron polarization

According to expression (1.1.2) of section 1.1 the product $P P_n$ will be given by:

$$P P_n = \frac{\sigma(\Theta,0) - \sigma(\Theta,\pi)}{\sigma(\Theta,0) + \sigma(\Theta,\pi)} \tag{3.4.6}$$

The denominator of expression (3.4.6) is in fact equal to $2\sigma(\Theta)$, where $\sigma(\Theta)$ is the differential cross-section for incident unpolarized neutrons. Accordingly the $D(d,n)^3He$ neutron polarization P_n will be given by:

$$P_n = \frac{\sigma(\Theta,0) - \sigma(\Theta,\pi)}{2 P \sigma(\Theta)} \tag{3.4.7}$$

According to expression (1.3.4) of section 1.3 the product $P \sigma(\Theta)$ is given by:

$$P \sigma(\Theta) = \frac{-k \sigma_t \gamma \cot \Theta/2}{2\pi} \tag{3.4.8}$$

Thus in order to calculate P_n it is required only to know the difference between the experimental cross-sections both to 'right' and 'left', i.e. the term $\sigma(\Theta,0) - \sigma(\Theta,\pi)$, and the total interaction cross-section. However one has to account for the spatial extension of both scatterer and detector and this is done by averaging the term $P \sigma(\Theta)$ over the geometry of both scatterer and detector.

For such a purpose a computer program, based on a modification of one developed by Monahan and Elwyn[164,165], was used. The code calculates the nominal values for both $\sigma_{sh}(\Theta)$, given by expression (1.3.3) of section 1.3, and $P \sigma(\Theta)$; these quantities are then averaged, by the same code, over the geometry of both scatterer and

detector.   The integrals over the finite dimensions of scatterer and detector, involved in this averaging process are evaluated analytically[165].

The effect of the finite geometry proved to be, for the present geometrical arrangement, significant at small angles. The averaged values differed from the nominal ones by 12.6% and 7.4% respectively for $\sigma_{sh}(\theta)$ and $P\ \sigma(\theta)$ at scattering angle 1.9°.   The difference, between the nominal and averaged values, decreased with increasing angle to become 1.4% and 0.8% respectively at a scattering angle of 6.3°.

The total cross-section σ_t was calculated using the CBM readings when the sample was in the way of the beam and with the sample removed, normalised to the same TYM reading.

The resulting value of the total cross-section is $\sigma_t = 7.5 \pm 0.5$ barns and this value was used in the abovementioned code to calculate the averaged values of both $\sigma_{sh}(\theta)$ and $P\ \sigma(\theta)$.

The value of P_n was calculated, applying this procedure, from the difference between 'right' and 'left' cross-sections at scattering angles 1.9°, 2.2° and 3.4° and the resulting values of $D(d,n)^3He$ polarization $P_n(\%)$ are -14.6 ± 4.7, -14.8 ± 5.6 and -15.0 ± 6.2 respectively.   These three values yielded an average value of $P_n = -14.8 \pm 3.2\%$.

As the TiD target thickness was about 840 KeV, this average value of P_n is related to a mean deuteron energy of 575 KeV.

3.5. D(d,n)^{3}He Polarization Measurements at Deuteron Energy 0.5 MeV

In this section D(d,n)^{3}He polarization measurements will be described, using the deuteron beam from the 0.5 MeV Van de Graaff accelerator mentioned in section 2.5.   These measurements were carried out in order to compare with those performed with the ^{4}He polarimeter at the same deuteron energy, and target thickness, described in section 2.5.

3.5.1. Experimental arrangement

The Mott-Schwinger polarimeter was set, for these measurements, with a geometrical arrangement different from that described in section 3.1.   The electronics is still basically the same as described in section 3.2.

According to this geometrical arrangement, represented in Fig. 41, neutrons emitted from the TiD target at 47° are collimated, by the same collimator described in section 3.1, and then scattered by the scatterer; the collimator face, in this arrangement, is at a distance ~ 30 cm from the target.   The scatterer is located nearly midway between the source and the rig carrying the stilbene detectors.   The stilbene detectors are located at a distance from the scatterer nearly twice what it was before.   Both the CBM and TYM are placed as in the previous arrangement.

The scatterer is held in a specially designed holder.   The holder carried samples of Cu, Pb and U of nearly the same diameter (14 mm) but of different lengths.   The lengths are 1.5, 2.54 and 2.5 cm respectively for Cu, Pb and U chosen on the basis of calculations
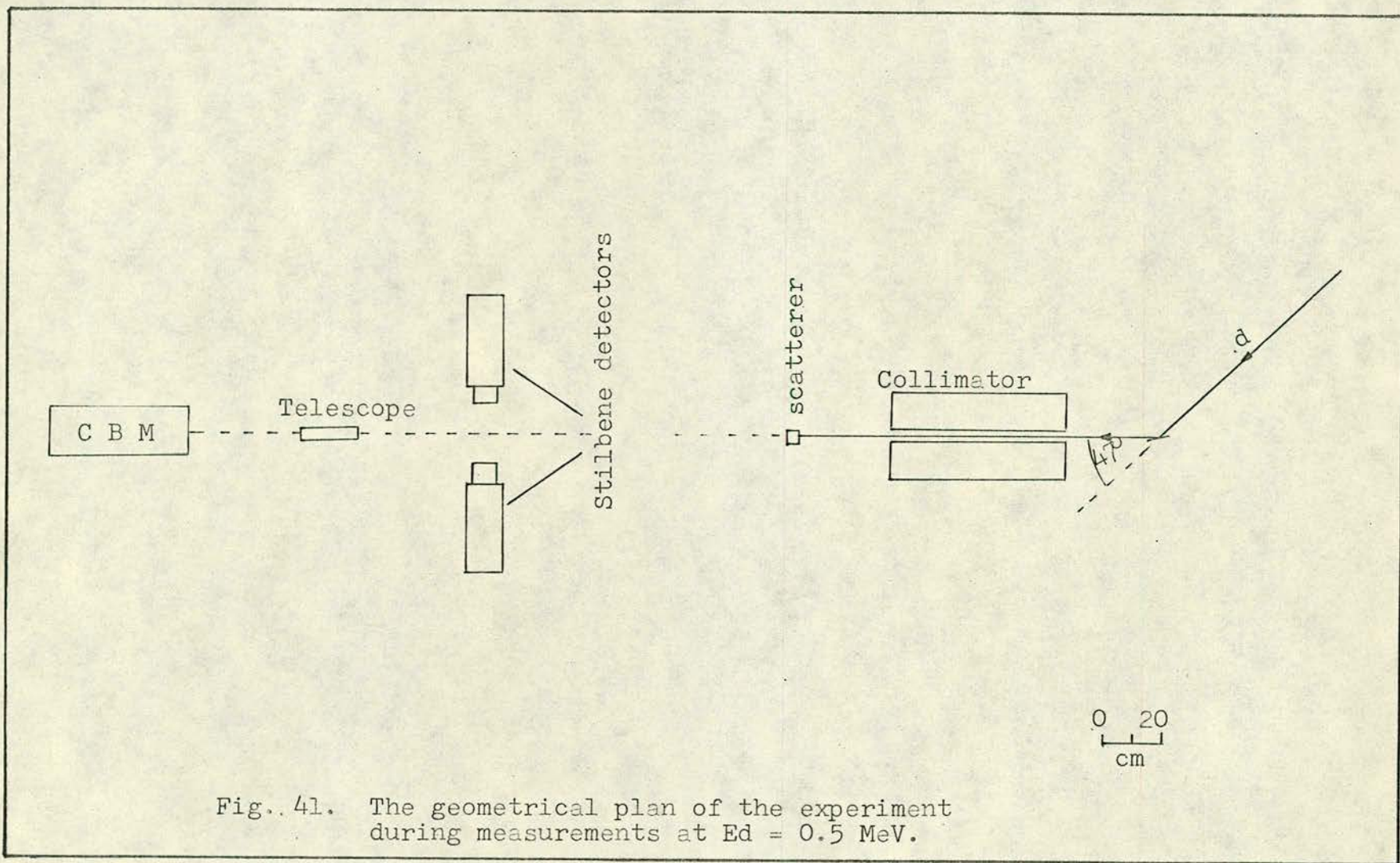
C B M

Telescope

Stilbene detectors

scatterer

Collimator

d

Fig. 41. The geometrical plan of the experiment during measurements at Ed = 0.5 MeV.

0   20
cm

carried out using the Monte Carlo code, mentioned in section 3.4.3, so that the multiple scattering of neutrons is nearly of the same order in the three samples. The effect of multiple scattering, according to these thicknesses, was $\leq$ 20% at the smallest scattering angle $\sim 1.6^{\circ}$.

Any of the three samples could be moved horizontally (Fig. 42a) either into the beam or out of it by a motor controlled from a panel (Fig. 42b).

The electronics of the polarimeter was connected and adjusted as described in Section 3.2. The racks of electronics, including the sample holder control panel, multichannel analyser and the Van de Graaff control panel are illustrated in Fig. 43.

3.5.2. The experimental measurements

The experimental measurements were carried out with neutrons emitted from a TiD target, of the same thickness as the one used during measurements with the ^{4}He polarimeter described in section 2.5, at a reaction angle of 47°, and the experimental procedure was the same as described in section 3.3.

The experimental measurements started, after the polarimeter was aligned, by measuring the beam profile. The beam profile, as measured separately by each of the two stilbene detectors, is represented in Fig. 44. From this beam profile, the spread in the beam is 17 mm which corresponds to an angle of 0.9° from the position of the scatterer. The average full width at half maximum corresponds to an angle of 0.95°; accordingly the angular resolution is $\sim \pm 0.5^{\circ}$. Thus the smallest angle chosen for this set of
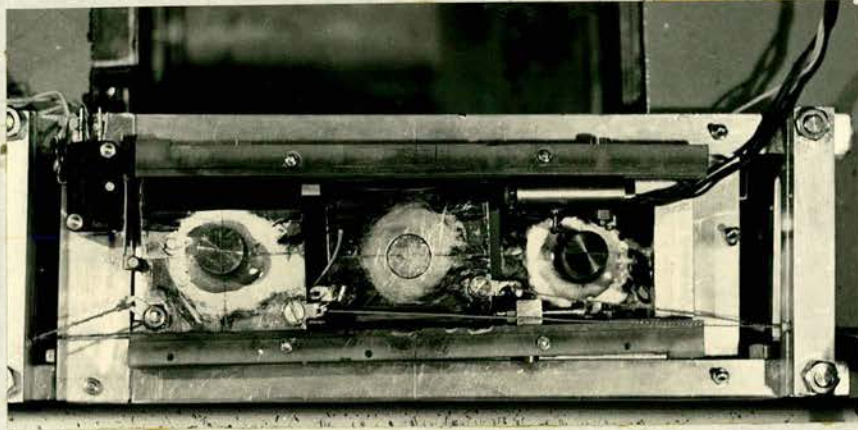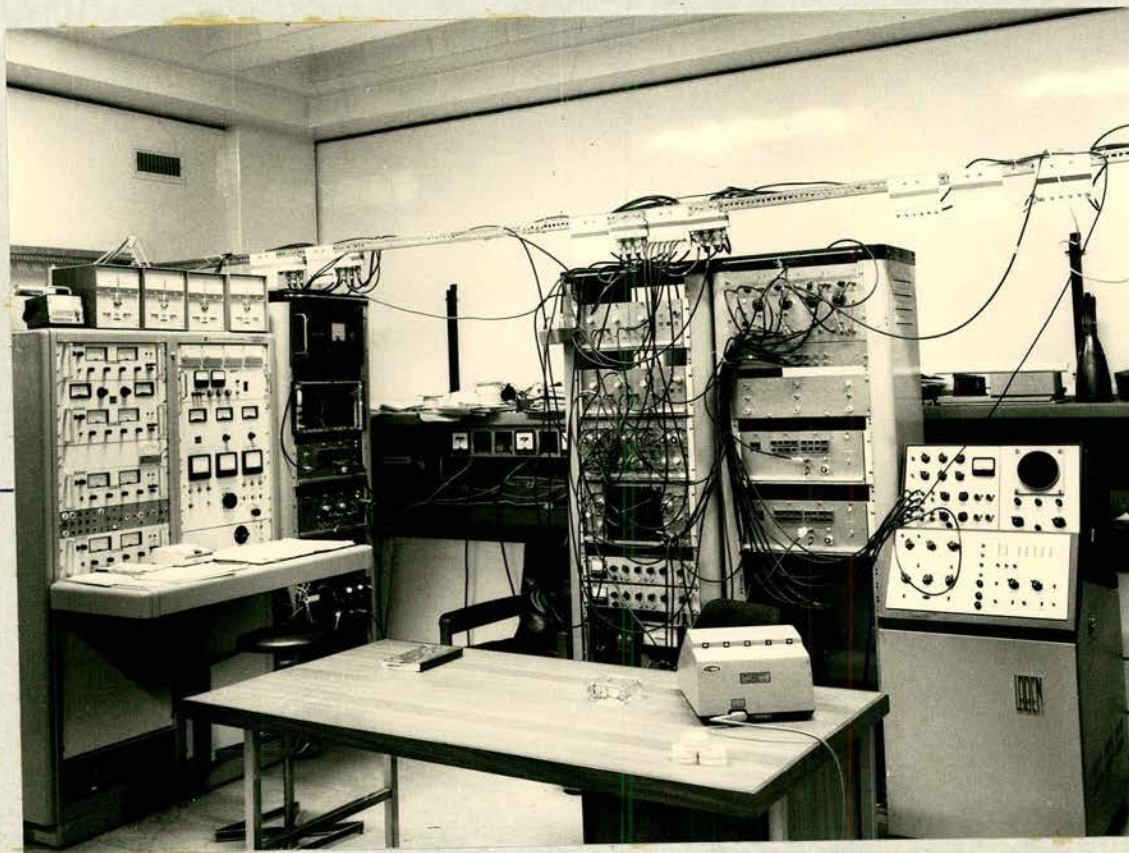
Fig. 42a. Photograph of the sample holder.

Fig. 42b. Photograph of the control panel
coupled to the sample holder.

The Van de
Graaff
control
panel

Electronics
of the
polarimeter

124

Fig. 43.   Photograph showing the racks of electronics,
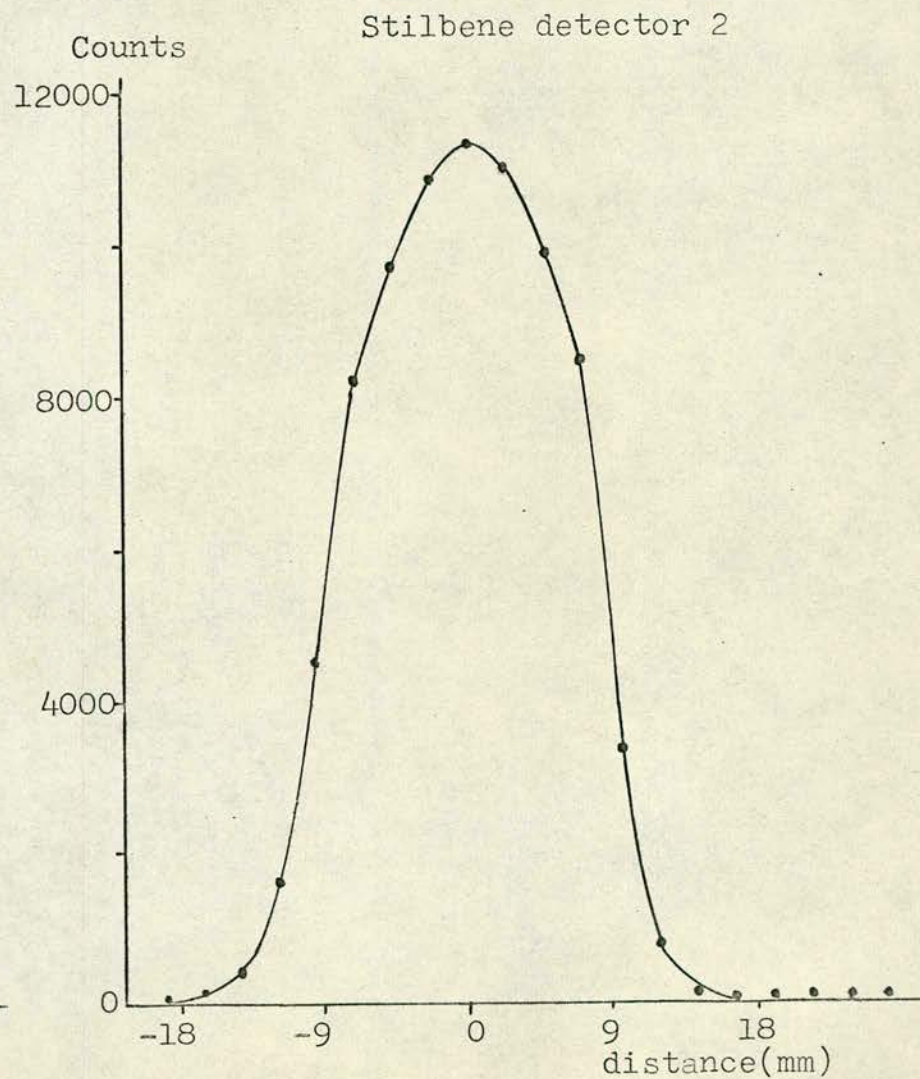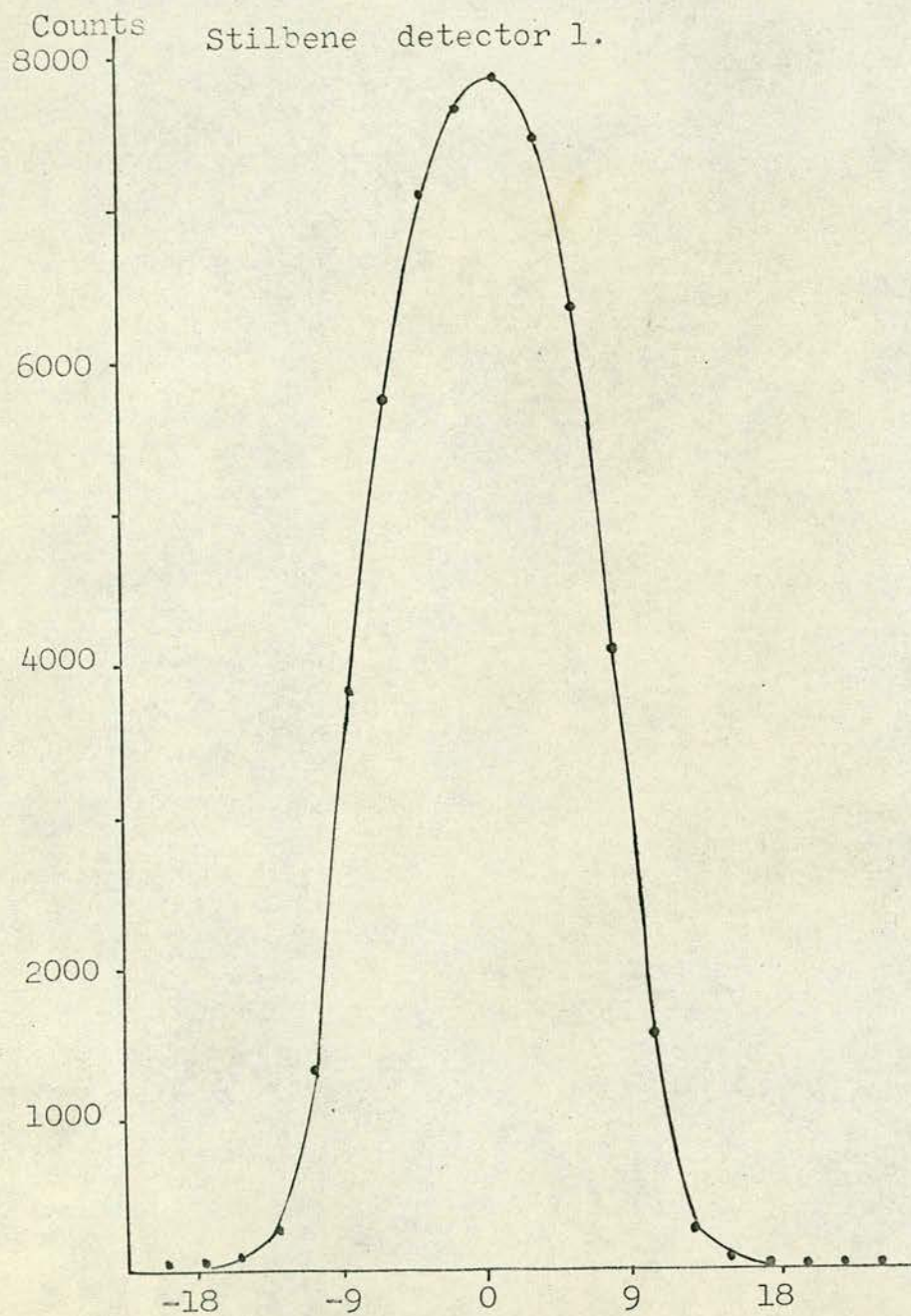multichannel analyser and the V.D.G. control panel.

Fig. 44. The beam profile as measured by each of the two stilbene detectors.

measurements was 1.6°.

The measurements were carried out with both the stilbene detectors in the reaction plane, for neutrons scattered from the sample, i.e. Pb or U, at angles 1.6°, 2.1°, 3.6°, 5° and 7.5°. For the Cu sample these angles were 1.65°, 2.2°, 3.7°, 5.2° and 7.7° respectively because the Cu sample was held at a distance from the stilbene detectors slightly less than that for both the Pb and U samples. The deuteron beam current was about 55 µA during the measurements.

The measurements, at a particular scattering angle, were carried out with each of the three scattering samples being in the way of the beam for 2048 seconds and one more measurement was usually carried out without any sample in the way of the beam as required for both determination of the background neutrons and the total cross-sections.

The ratio of the background neutrons to the recorded number of scattered neutrons was 0.7 for Cu at 1.65° and it decreased to 0.6 at 7.7°, for Pb it was 0.57 at 1.6° decreasing to 0.49 at 7.5°, for uranium it was 0.47 at 1.6° and decreased to 0.37 at 7.5°.

3.5.3. <u>Analysis of the experimental data and results</u>

The same procedure, described in section 3.4, was carried out for the analysis of the experimental data obtained. The resulting experimental cross-sections, both to 'right' and 'left' are represented in Fig. 45 for Cu, Pb and U.

The values of the total cross-sections σ_t, obtained from these measurements, are 3.39 ± 0.04, 7.46 ± 0.09 and 7.98 ± 0.10 respectively
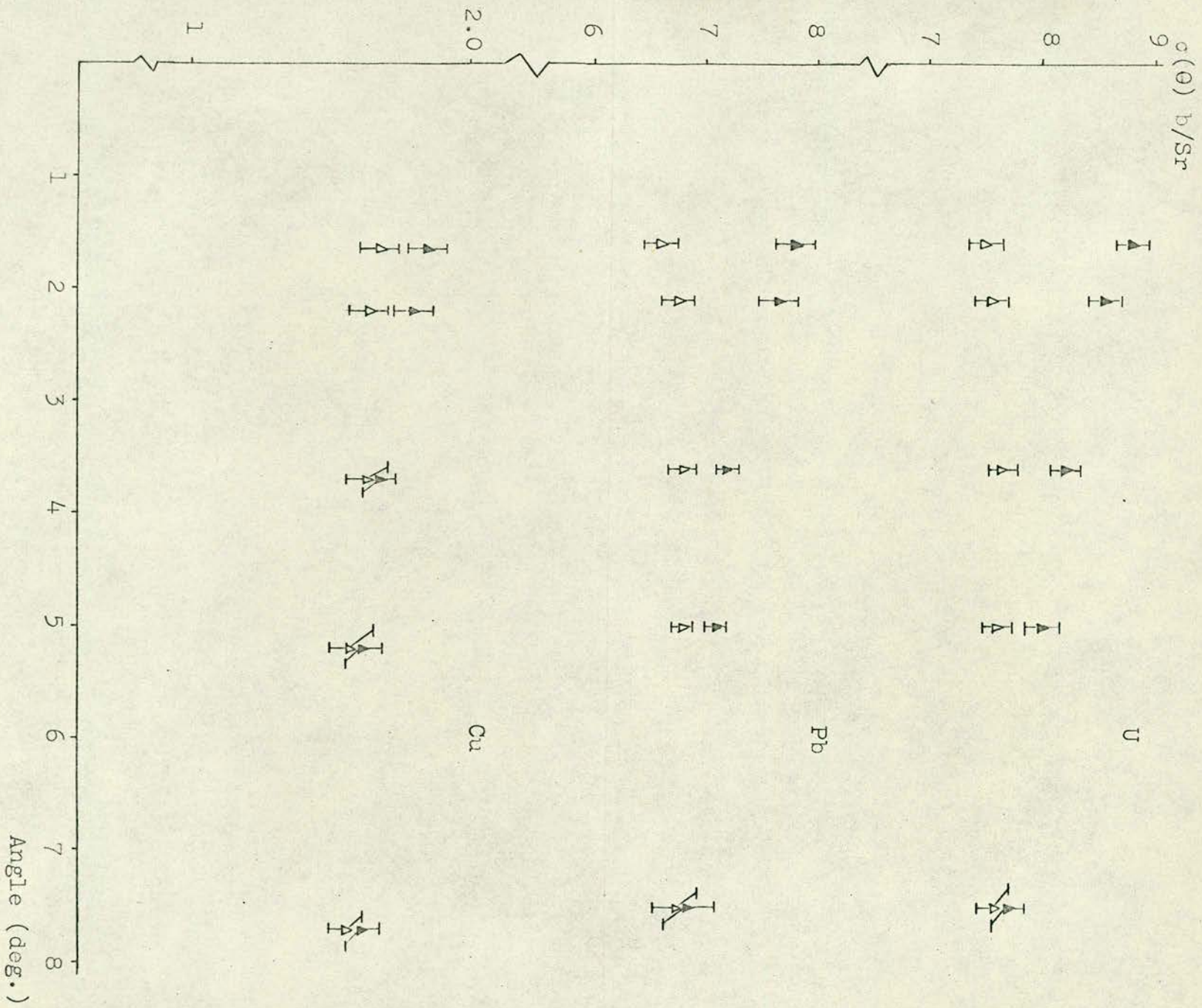
Fig. 45. The experimental differential cross-sections of Cu, Pb and U.

127

for Cu, Pb and U.

Calculations of both $\sigma_{sh}(\Theta)$ and $P \sigma(\Theta)$, i.e. the nominal and averaged values, as explained in section 3.4.4, did not result in a significant difference between the nominal values and averaged ones. The effect of the finite geometry, of both scatterer and detector, proved to be about 1% for both U and Pb at 1.6°, for Cu it was 0.6% at scattering angle 1.65° and the effect decreased to 0.2% for both Pb and U at 3.6° and for Cu it decreased to 0.2% at scattering angle 2.2°.

The resulting $D(d,n)^3He$ polarization was calculated, as explained in section 3.4.4, at scattering angles 1.6°, 2.1°, 3.6° and 5°, both for lead and uranium. For Cu it was calculated only at scattering angles 1.65° and 2.2°. The resulting values of $P_n(\%)$ are given in Table 3.2. It is noticeable that the statistical accuracy associated with the value of P_n decreases with increasing scattering angle due to the fact that the analysing power is poorer at large scattering angles. The resulting values of P_n are internally consistent within the limits of the associated errors. The values of P_n obtained with both Pb and U samples at scattering angles 1.6°, 2.1° and 3.6° yielded an average value of $D(d,n)^3He$ polarization $P_n(\%) = -13.7 \pm 1.5$.

Table 3.2. The values of P_n as calculated from the experimental cross-sections at different angles.

Scatterer	Angle	The resulting polarization P_n(%)
Cu	1.65°	-14.29 ± 8.77
	2.2°	-18.00 ± 11.47
Pb	1.6°	-14.95 ± 3.05
	2.1°	-13.95 ± 3.99
	3.6°	-12.99 ± 5.05
	5.0°	-13.19 ± 6.47
U	1.6°	-13.60 ± 2.20
	2.1°	-13.79 ± 2.85
	3.6°	-12.78 ± 4.44
	5.0°	-12.82 ± 6.60

CHAPTER FOUR

DISCUSSION OF THE RESULTS OBTAINED AND COMPARISON
BETWEEN THE TWO POLARIMETERS

CHAPTER FOUR

DISCUSSION OF THE RESULTS OBTAINED AND COMPARISON BETWEEN THE TWO POLARIMETERS

All the results obtained with both ^{4}He and Mott-Schwinger polarimeters will be discussed in this chapter and then the two polarimeters will be compared at the end of the chapter.

4.1. The D(d,n)^{3}He Polarizations

The D(d,n)^{3}He polarization values resulting from using both polarimeters, cover the deuteron energy range between 0.33 and 4.0 MeV. The values of P_n(%) obtained are represented in Fig. 46 along with values reported so far by other authors, for a laboratory angle $45^o \pm 5^o$ and mean deuteron energies $\leq$ 10 MeV. The values from references[90-92,99,104,105,113-115,121] are not represented in this figure for reasons discussed in section 1.4 but they were represented in Fig. 7.

The present value of P_n at 0.33 MeV, represented in Fig. 46, is the value obtained using scattering from helium (given in Table 2.4), and it is in good agreement with a value of P_n = -13.7 $\pm$ 1.5 (%) obtained with the Mott-Schwinger polarimeter which was reported in section (3.5.3). The value of P_n at a mean deuteron energy of 575 KeV (see Fig. 46) is the average value reported in section (3.4.4) and obtained with the Mott-Schwinger polarimeter. These two values of the D(d,n)^{3}He polarization (below 1 MeV) are consistent with other values previously published and represented in Fig. 46.
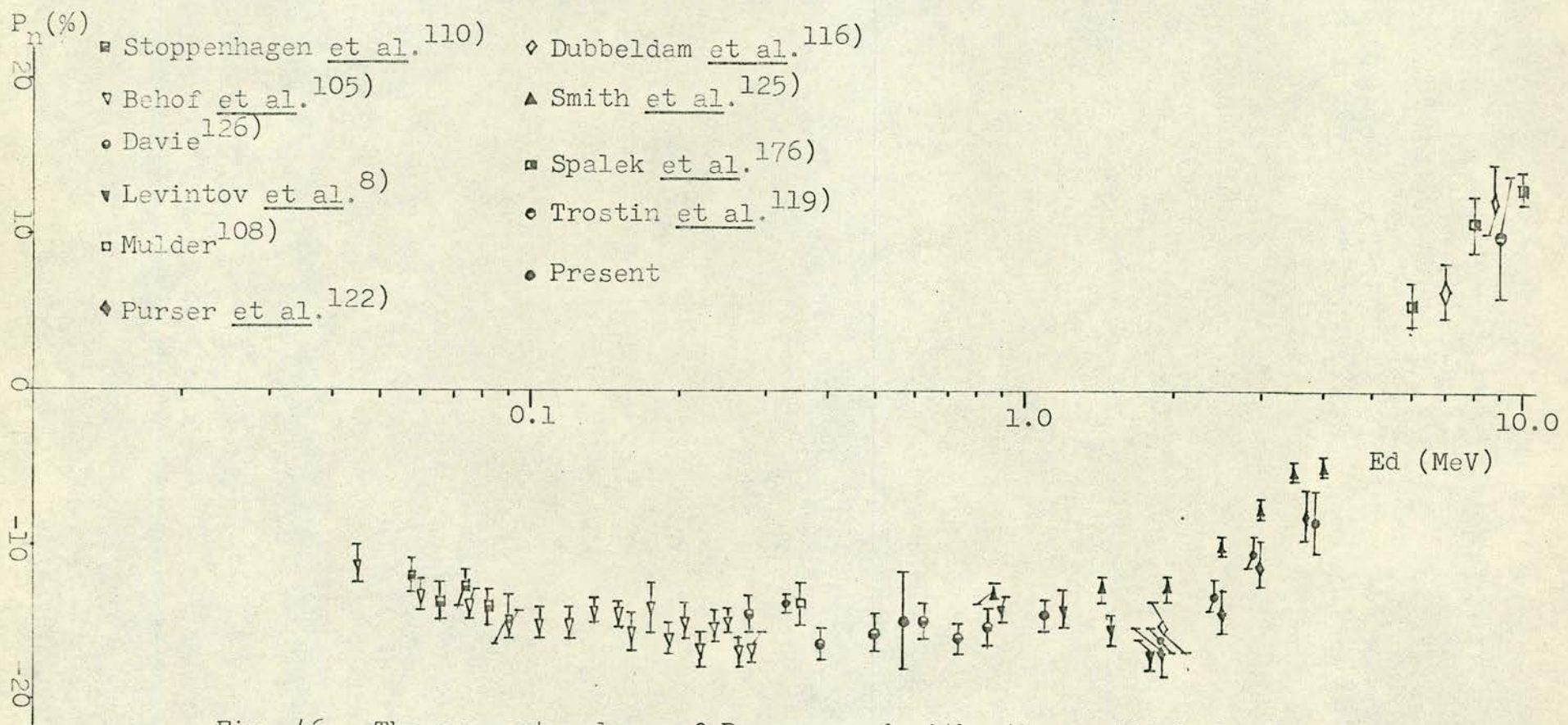
Fig. 46. The present values of P_n compared with other published values.

The present values of P_n (at deuteron energies > 1 MeV) are con-
sistent with other values, represented in Fig. 48, except those of
Smith and Thornton[129] in the energy range from 2.0-4.0 MeV.   Smith
and Thornton reported in their paper about unsubtracted background,
associated with their time of flight spectra;   they stated that such
background, similar to the one reported by the Walter group[22,23],
originate from scattering of neutrons in the material adjacent to the
helium scintillator[129].   The unsubtracted background observed by the
Walter group is due to the unpolarized 'tail' associated with the helium
recoil spectrum;   it is similar to the tails associated with all the
helium recoil spectra detected in the present measurements.   Such
tails were detected during measurements with both the helium polari-
meters used by Walter group[22,23,166,167] where account was taken of
them in all the data they published.   Smith and Thornton gave an
upper limit of 0.01 to the systematic error in the measured asymmetry
due to the background they observed, but they appear not to have
accounted for this in their published values[129].   The values of
P_n(%) reported by Smith and Thornton for deuteron energies between
2-4 MeV are lower than the present values, as well as the values
reported by Walter group[116,122], by about 2-3%.   On comparing the
polarization measurements for the $T(P,n)^3He$ and $^7Li(P,n)^7Be$ re-
actions reported by the Thornton group[168,169] and the Walter group[117,
170-172] it is found that the general trend of the values reported
by the first group is lower than the latter for both reactions (see
Table 4.1).

        In the discussion about the effect of the tail on the value of
the measured asymmetry and consequently the value of P_n, given in

Table 4.1. Comparison between values of P_n obtained by Thornton group and Walter group.

Reaction	Thornton Group[168,169]			Walter Group[117,170-172]		
	E_p(MeV)	$\theta_{Lab.}$	P_n	E_p(MeV)	$\theta_{Lab.}$	P_n
$T(P,n)^3He$	3.1	20°	0.122 ± 0.01	2.9	16°	0.147 ± 0.02
	3.1	35°	0.216 ± 0.008	3.1	33°	0.23 ± 0.02
				2.9	33°	0.26 ± 0.03
	3.9	20°	0.027 ± 0.007	4.0	16°	0.056 ± 0.020
	3.9	30°	0.060 ± 0.015	4.0	33°	0.081 ± 0.020
	3.9	50°	0.128 ± 0.015	4.0	50°	0.140 ± 0.020
	3.9	70°	0.127 ± 0.015	4.0	70°	0.155 ± 0.020
	5.0	50°	-0.002 ± 0.009	5.0	50°	0.062 ± 0.020
	5.0	70°	0.118 ± 0.011	5.0	70°	0.129 ± 0.020
$^7Li(P,n)^7Be$	3.0	45°	0.275 ± 0.005	2.99	50°	0.314 ± 0.018
	3.5	45°	0.314 ± 0.005	3.58	50°	0.384 ± 0.020
	4.0	50°	0.302 ± 0.010	3.98	50°	0.382 ± 0.016
	4.0	15°	0.170 ± 0.010	3.97	20°	0.191 ± 0.025
	4.0	30°	0.270 ± 0.007	3.97	30°	0.284 ± 0.025
	4.0	45°	0.313 ± 0.010	3.97	40°	0.330 ± 0.030
	4.5	15°	0.192 ± 0.005	4.70	20°	0.25 ± 0.025
	4.5	45°	0.231 ± 0.007	4.70	40°	0.242 ± 0.025

section 2.9, it was shown that neglecting the tail correction, for the case under consideration, would reduce the value of P_n by about 2%. So it is quite possible that the difference between the values of P_n (measured for the $D(d,n)^3He$ reaction) reported by Smith and Thornton[129] and the present values is due to scattering processes which produce the tail in the He recoil spectra not being separated from the desired neutron scattering by their time of flight system.

4.2. The Angular Distribution of P_n

The two angular distributions of the $D(d,n)^3He$ polarizations, measured at mean deuteron energies 1.1 and 2.44 MeV, reported in section 2.10 are represented in Fig. 47-48 and the present values of P_n are compared with other published values.

The present values of P_n(%) at 1.1 MeV are compared with those of Drigo et al.[125] (obtained at 1.09 MeV and laboratory angles 35° and 55°), Gorlov et al.[86] (obtained at 1.2 MeV and 37° lab.) and Levintov et al.[8] (obtained at 1.2 MeV and 49° lab.).

The agreement between the present values of P_n and these values is satisfactory (see Fig. 47) except for the point of Drigo et al.[125] at 55° lab.

The present values of P_n(%) at 2.44 MeV are compared with those of Purser et al.[122] (measured for deuteron energy 2.5 MeV and laboratory angles 35° and 40°) and with the angular distribution of Smith and Thornton[129] measured at 2.51 MeV. The agreement between the present values and the one of Purser et al.[122] at 40° is satisfactory (within the statistical accuracy). The present
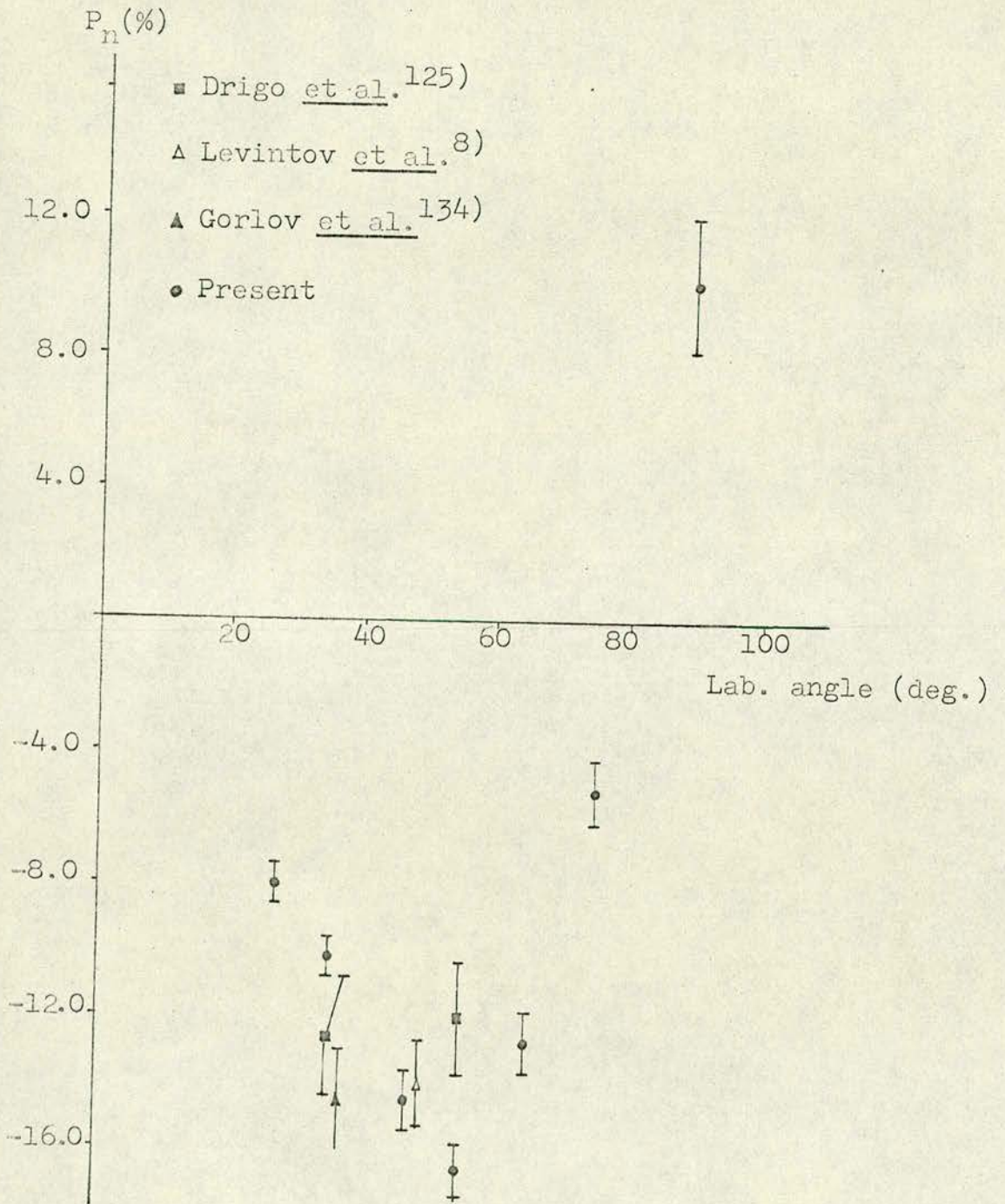
Fig. 47. Values of the present angular distribution of polarization at 1.1 MeV, compared with other published values.
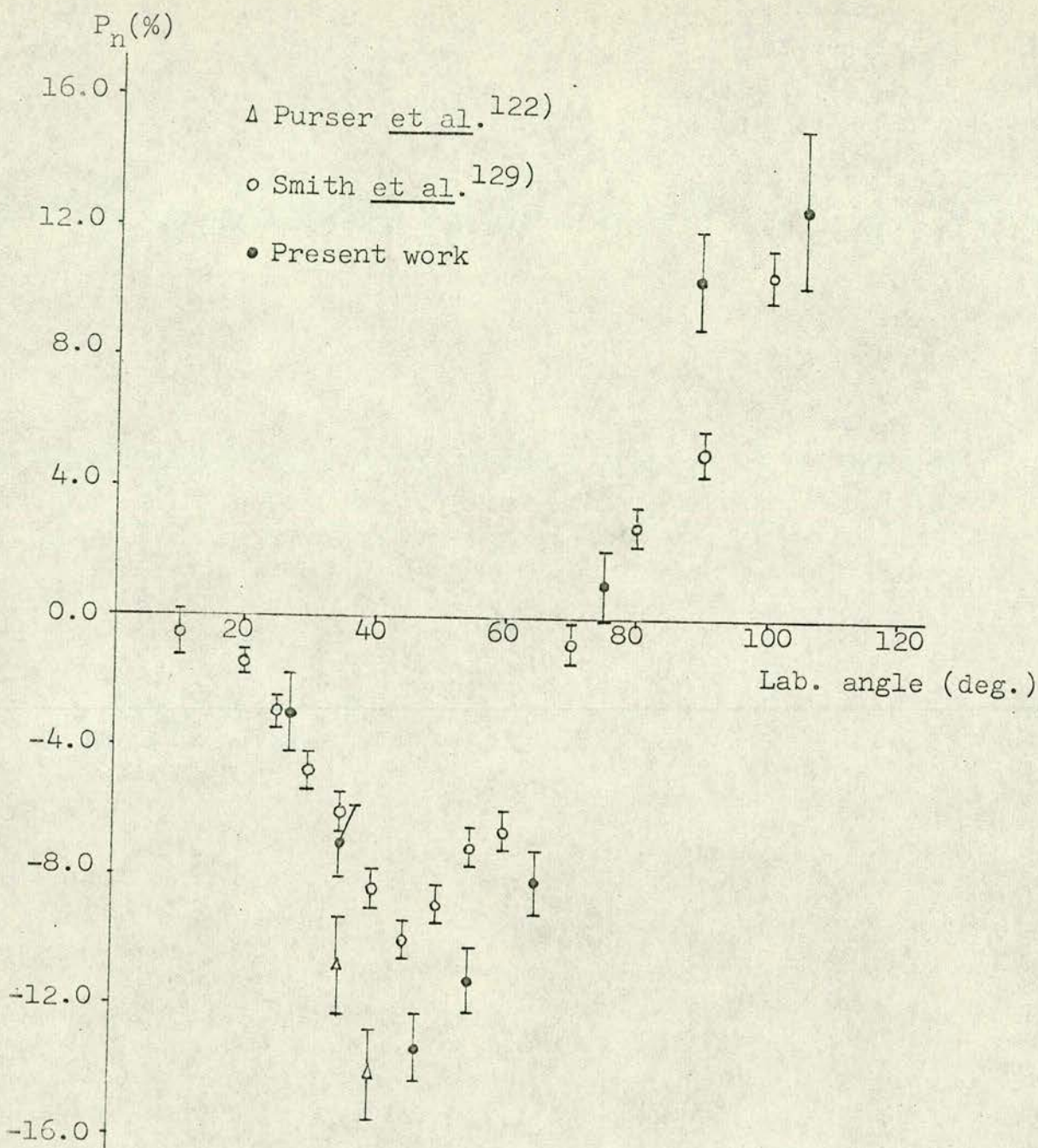
Fig. 48.   Values of the present angular distribution
of D(d,n)^{3}He polarization at 2.44 MeV,
compared with other published values.

distribution is similar to the one of Smith and Thornton[129] in both shape and zero point (see Fig. 48), but their values at reaction angles 45°, 50°, 55°, 60°, 90° are lower than the present ones possibly due to the reason given in section 4.1.

4.3. Least Square Fits to Present and Other Recently Reported Distributions

In general the angular dependence of the polarization P_n is of the form[4]:

$$P_n(Ed,\theta) = \frac{1}{\sigma(Ed,\theta)} \sum_{L=1}^{L_{max}} A_L(Ed) \, P_L^1 (\cos \theta) \qquad (4.3.1)$$

where $P_L^1 (\cos \theta)$ are the associated Legendre polynomials. Fierz[142] has shown that for the $D(d,n)^3He$ reaction this formula reduces to:

$$P_n(Ed,\theta) \, \sigma (Ed,\theta) = \pi = \sum_n A_n \sin 2n\theta \qquad (4.3.2)$$

π is usually called the differential polarization. Thus the expansion coefficients A_n can conveniently correlate data on the $D(d,n)^3He$ reaction.

A least squares fit, based on expression (4.3.2), was applied to the present two angular distributions of P_n. A two-term fit was first applied to the data and then a three-term one. The $D(d,n)^3He$ differential cross-sections, required for the least square fit, were obtained (by interpolation) from the values given in references[156,173]. From these fits it was found that the expansion coefficients A_3 (in the three-term fit) are insignificant (see

Table 4.2) and accordingly the present data can be fitted with enough degree of accuracy using the first two terms of the sin 2 n θ expansion. Thus the two angular distributions were compared with distributions calculated according to the expression:

$$P_n = (A_1 \sin 2\theta + A_2 \sin 4\theta)/\sigma(\theta) \quad (4.3.3.)$$

where coefficients A_1 and A_2 were those resulting from the two terms fit (given in Table 4.2). In Figs. 49-50 are shown the two distributions compared with those obtained from expression (4.3.3).

According to the analysis carried out by Fierz[142], for the D-D system, the differential polarization π should be representable by the first term of the expansion (4.3.2), for deuteron energies up to 2 MeV. For higher energies one would expect that higher terms should occur as higher partial waves are necessary to describe the differential cross-sections[174]. In order to contribute to the study about the dependency of the expansion coefficients A_n on the deuteron energy, the same code, applied for least square fits of the two distributions at 1.1 and 2.44 MeV, was applied to the recently published data of Smith and Thornton[129] and Spalek et al.[127]. In order to fit the data of Smith and Thornton the differential polarizations were calculated from their polarization values and $D(d,n)^3He$ differential cross-sections given by Brolley and Fowler[156], (for deuteron energies < 4 MeV) and Schulte[175] at 4.0 and 5.0 MeV; for fitting the data of Spalek et al. the values of differential polarizations they reported recently[176] were used. The resulting values of A_n, both from two and three-term fits, are
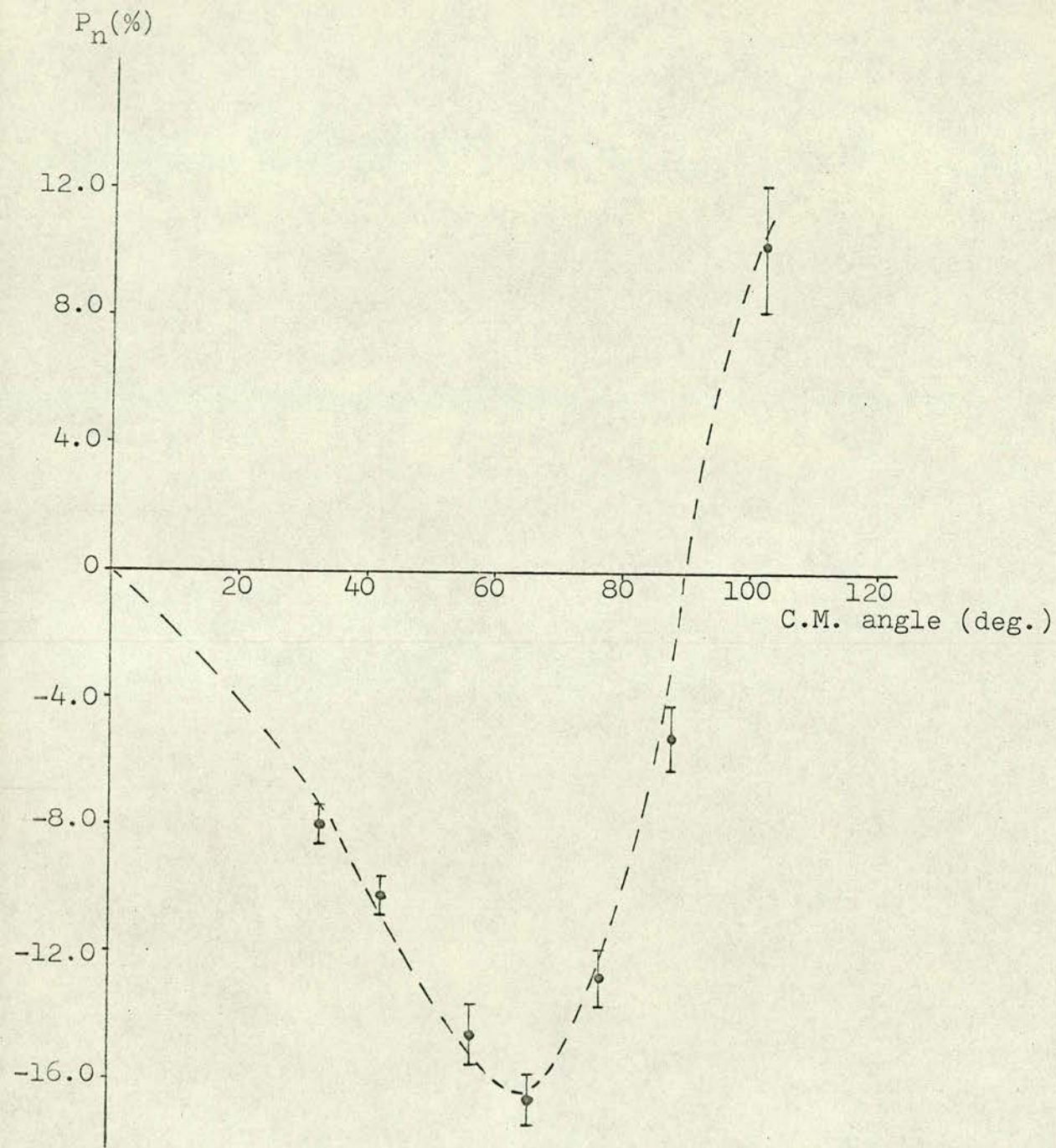
Fig. 49. The angular distribution of P_n at 1.1 MeV compared with the one obtained from two term fit (dashed curve).
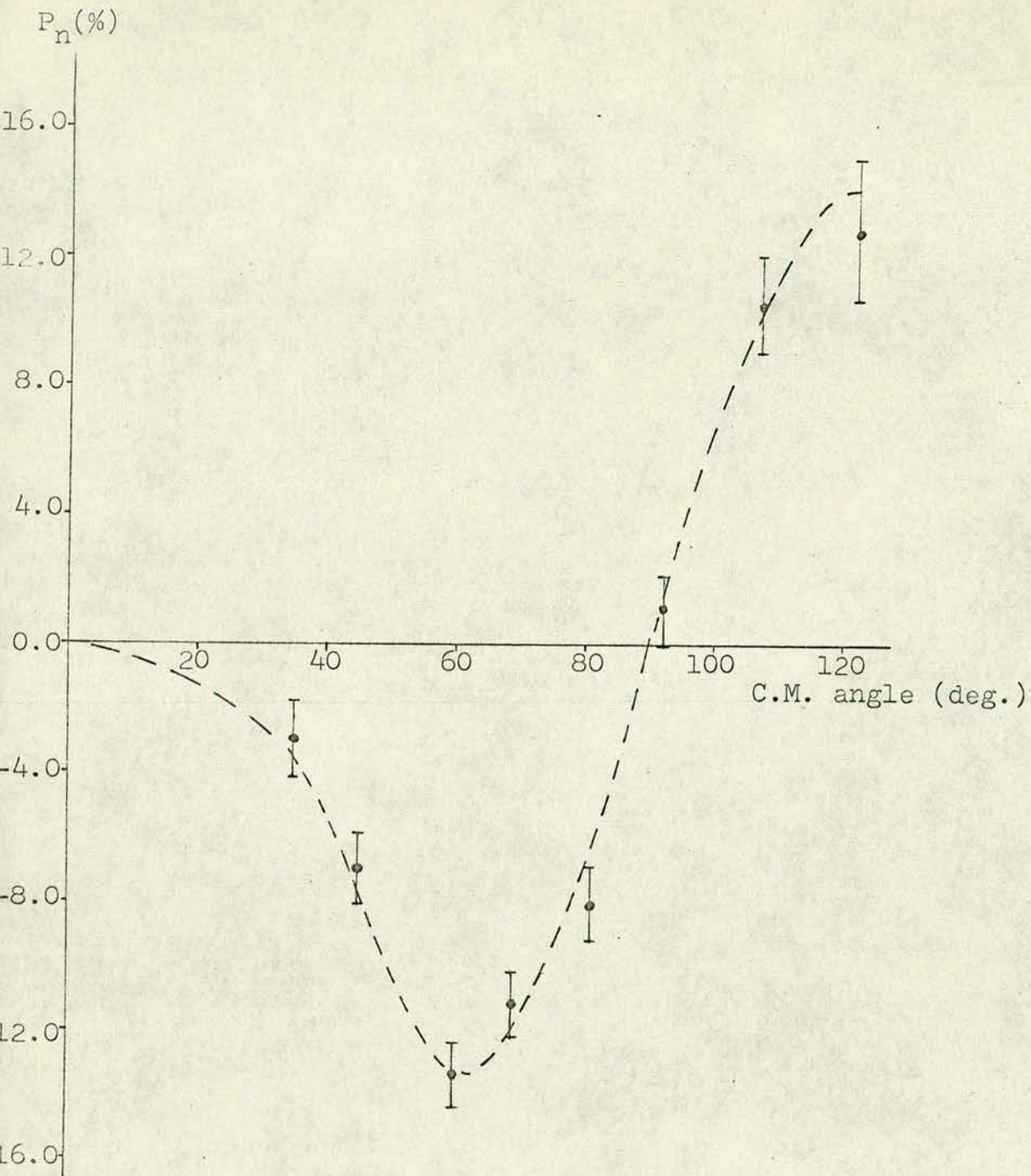
Fig. 50. The angular distribution of P_n at 2.44 MeV compared with the one obtained from two term fit (dashed curve).

represented in Table 4.2 along with all the previously published
ones for deuteron energies $\leq$ 10 MeV.   Except for the measurements
at 0.375 MeV and 3 MeV - ref.[129], no terms of order higher than
sin 4 Θ, in expansion (4.3.2), are clearly present in any of the
angular distributions available in this energy range (see Table 4.2).

The values of A_n, obtained from two term fits, as a function
of deuteron energy are represented in Figs.51-52 respectively for
A_1 and A_2.   The values of A_1 seem to fit nicely with the trend
represented by the dashed curve (see Fig. 51).

The values of A_2 seem to be more significant at deuteron
energies $\geq$ 2 MeV: it appears that the expansion coefficients A_n
(given in Table 4.2) obtained from two terms fits may be used to
calculate the differential polarization, required for the use of
the $D(d,n)^3He$ reaction as a source of polarized neutrons at un-
measured angles and deuteron energies.

4.4.   The Differential Cross-sections of Cu, Pb and U at Small Angles

The differential cross-sections for unpolarized neutrons were
obtained by averaging the two cross-section values, i.e. to the
'right' and to the 'left', at each of the scattering angles. These
cross-sections were then corrected for multiple scattering (using
the Monte Carlo code described in Section 3.4.3), for the finite
angular spread due to the finite dimensions of the scatterer and the
detector (using the code described in section 3.4.3) and for
inelastic scattering.   The inelastic scattering contribution in
the resulting cross-sections was evaluated both from published

Table 4.2:   Coefficients of the expansion $P_n(\Theta)\sigma(\Theta) = \sum_n A_n \sin 2n\Theta$

Ed (MeV)	Two term fit		Three term fit			Ref.
	A_1	A_2	A_1	A_2	A_3	
0.375	−0.627±0.016	+0.037±0.014	−0.627±0.014	+0.023±0.013	−0.036±0.013	105
0.870	−1.008±0.027	+0.051±0.027	−1.009±0.007	+0.066±0.006	+0.007±0.007	129
1.090	−1.180±0.150	−0.230±0.140				125
1.100	−1.069±0.037	+0.110±0.075	−1.125±0.043	+0.086±0.073	−0.067±0.066	present
1.430	−1.004±0.030	−0.045±0.028	−0.979±0.016	+0.008±0.016	+0.055±0.016	129
1.900	−0.820±0.140	+0.180±0.150	−0.810±0.120	+0.180±0.130	+0.190±0.120	116
1.900	−0.820±0.060	+0.250±0.060	−0.780±0.070	+0.300±0.080	+0.060±0.070	122
1.960	−0.794±0.030	+0.051±0.030	−0.825±0.035	+0.019±0.041	−0.046±0.032	129
2.120	−0.870±0.070	−0.100±0.09				125
2.440	−0.604±0.055	+0.205±0.051	−0.564±0.054	+0.187±0.069	−0.093±0.072	present
2.500	−0.740±0.090	+0.180±0.280				122
2.510	−0.457±0.019	+0.082±0.018	−0.461±0.010	+0.086±0.010	−0.001±0.001	129
3.000	−0.470±0.080	+0.030±0.120	−0.400±0.100	+0.120±0.140	+0.120±0.110	116
3.000	−0.410±0.050	+0.210±0.050	−0.380±0.060	+0.230±0.070	+0.040±0.060	122
3.000	−0.352±0.025	+0.103±0.023	−0.404±0.030	+0.024±0.034	−0.079±0.026	129
3.140	−0.520±0.070	+0.090±0.090				125

(Contd.

Table 4.2. (Contd.)

Ed (MeV)	Two term fit		Three term fit			Ref.
	A_1	A_2	A_1	A_2	A_3	
3.500	−0.192±0.020	+0.110±0.021	−0.197±0.029	+0.090±0.034	−0.013±0.024	129
3.700	−0.180±0.040	+0.190±0.040	−0.180±0.060	+0.180±0.070	−0.050±0.060	116
3.700	−0.150±0.060	+0.190±0.070	−0.070±0.090	+0.270±0.100	+0.080±0.070	122
4.000	−0.131±0.040	+0.086±0.043	−0.076±0.062	+0.155±0.075	+0.056±0.050	129
5.000	+0.234±0.196	+0.012±0.278	+0.409±0.196	−0.190±1.060	+0.116±0.595	129
6.000	+0.419±0.031	+0.113±0.037	+0.412±0.037	+0.105±0.044	−0.014±0.041	176
7.000	+0.640±0.080	+0.160±0.090	+0.680±0.080	+0.220±0.100	+0.090±0.080	116
8.000	+0.724±0.030	+0.239±0.044	+0.675±0.040	+0.197±0.049	−0.083±0.046	176
8.900	+1.120±0.130	+0.260±0.100	+1.120±0.130	+0.160±0.170	−0.130±0.170	116
10.000	+0.841±0.028	+0.107±0.033	+0.845±0.039	+0.112±0.049	+0.007±0.042	176
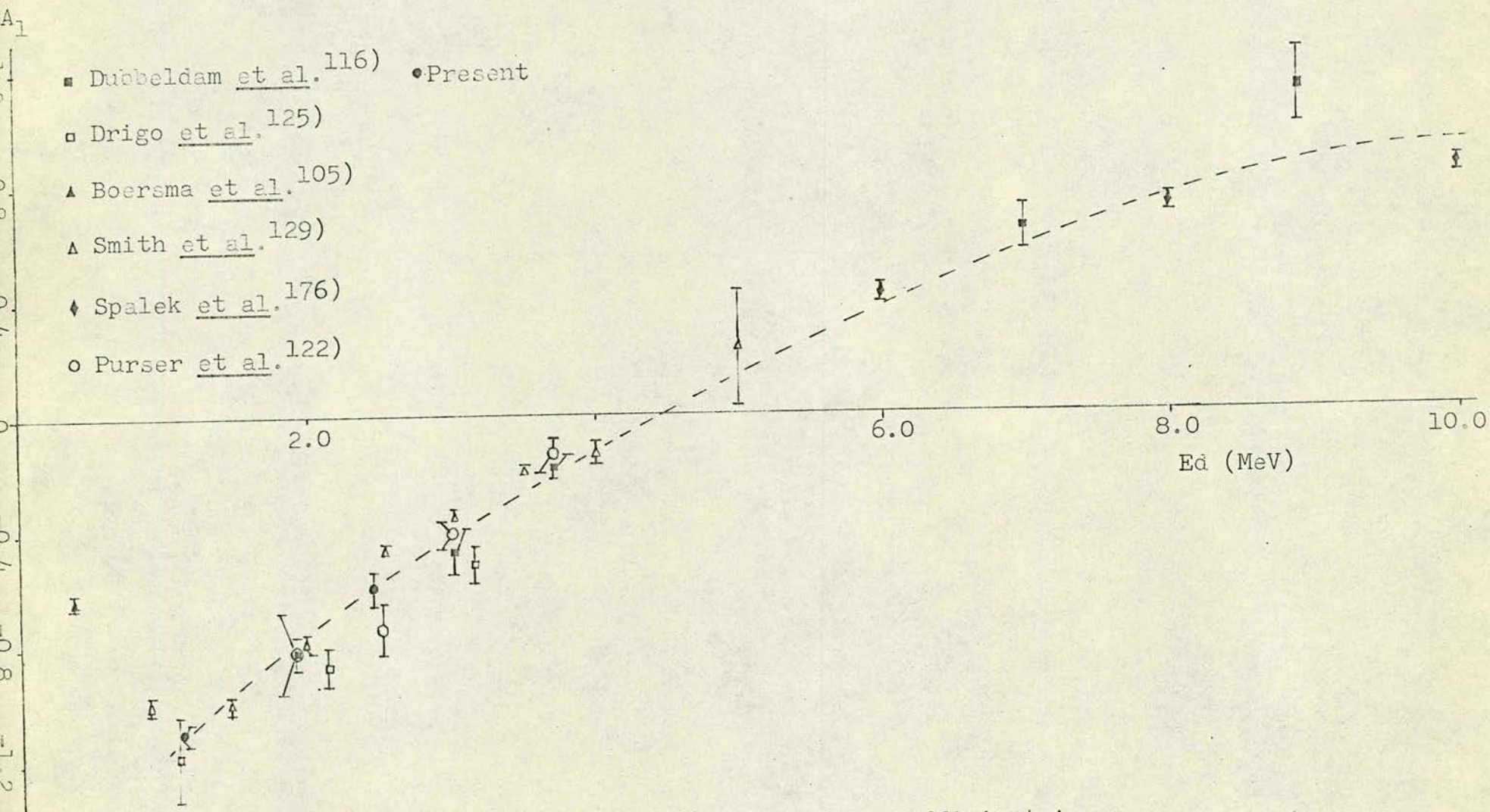
Fig. 51. The values of the expansion coefficient A_1 as function of deuteron energy.

- Dubbeldam et al. [116] • Present
- Drigo et al. [125]
- Boersma et al. [105]
- Smith et al. [129]
- Spalek et al. [176]
- Purser et al. [122]

A_1

Ed (MeV)

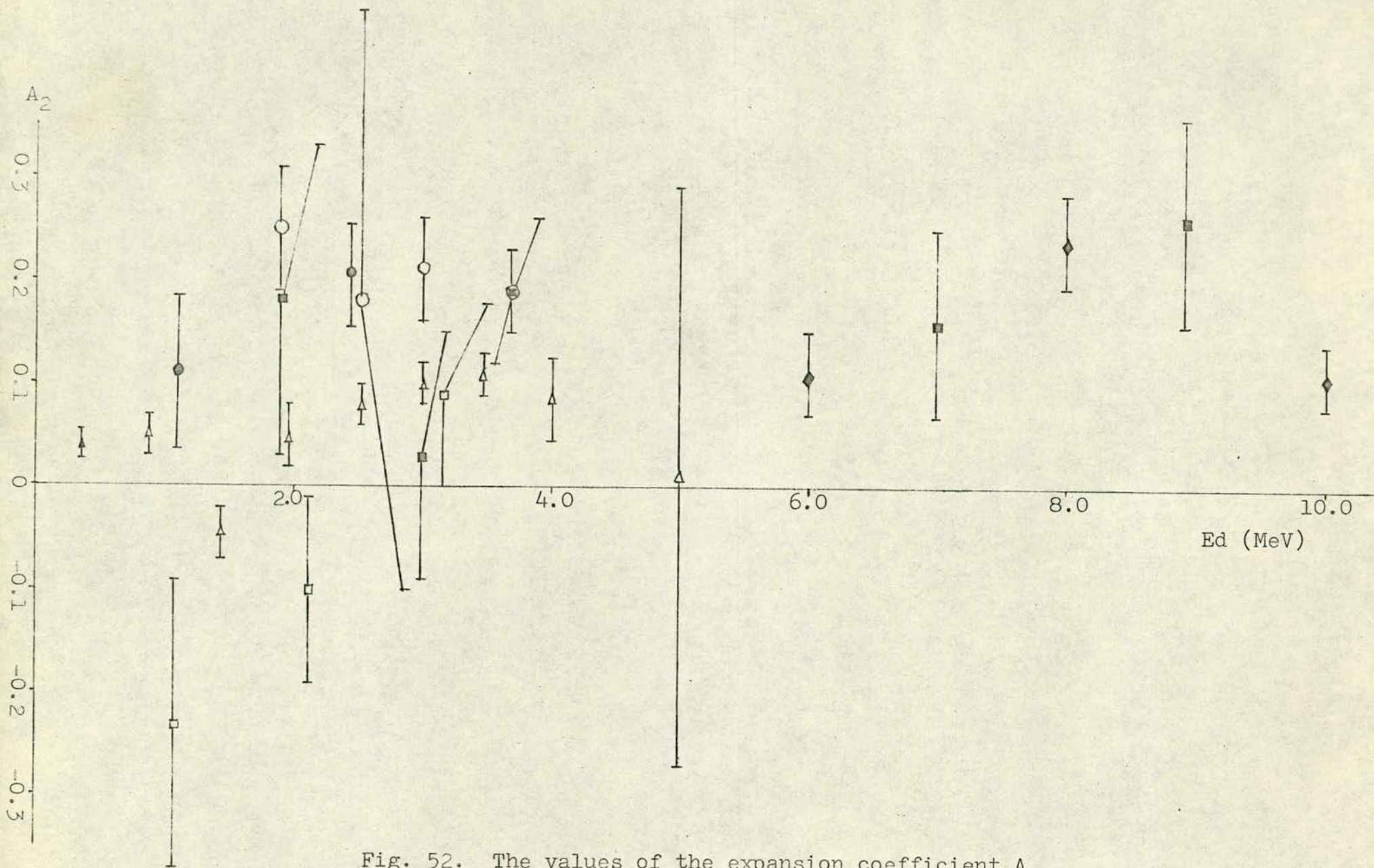2.0   6.0   8.0   10.0

144

Fig. 52. The values of the expansion coefficient A_2
as function of deuteron energy.

data[84,177,178] and using a computer code developed by Wilmore[179]; using data for Cu, Pb and U taken from Nuclear Data Sheets[180]. The inelastic contributions, as evaluated both ways, proved to be small (about 0.1 barn for Cu and 0.3 barn for both lead and uranium).

Further, the calculated Mott-Schwinger contribution to the differential cross-section for unpolarized neutrons was subtracted to give the sets of points, shown in Figs. 53-54, which should represent the differential cross-sections due only to nuclear inter-action. In Fig. 53 are represented the points resulting from measurements with Pb, described in section 3.3.1, where the neutrons (at mean deuteron energy 575 KeV and reaction angle 46°) were of energy 3.3 MeV while in Fig. 54 are represented the points resulting from measurements described in section 3.5.2, where neutrons were incident on the samples with energy 3.0 MeV. All the resulting cross-sections are compared with the solid curves which are based on optical model calculations, for scattering angles ranging from 1° - 10°, carried out using the same code used before by Wilmore[181] and normalised to the experimental points by factors 1.06, 1.06, 1.09 and 1.08 respectively for Pb at 3.3 MeV and Cu, Pb and U at 3.0 MeV.

It is noticeable that satisfactory agreement exists between the experimental cross-sections and the theoretical ones for all the three elements. The anomalous scattering of neutrons by uranium, mentioned in ref.[58-60,62,65,66,71], is not observed in the present measurements. This anomalous behaviour of the uranium
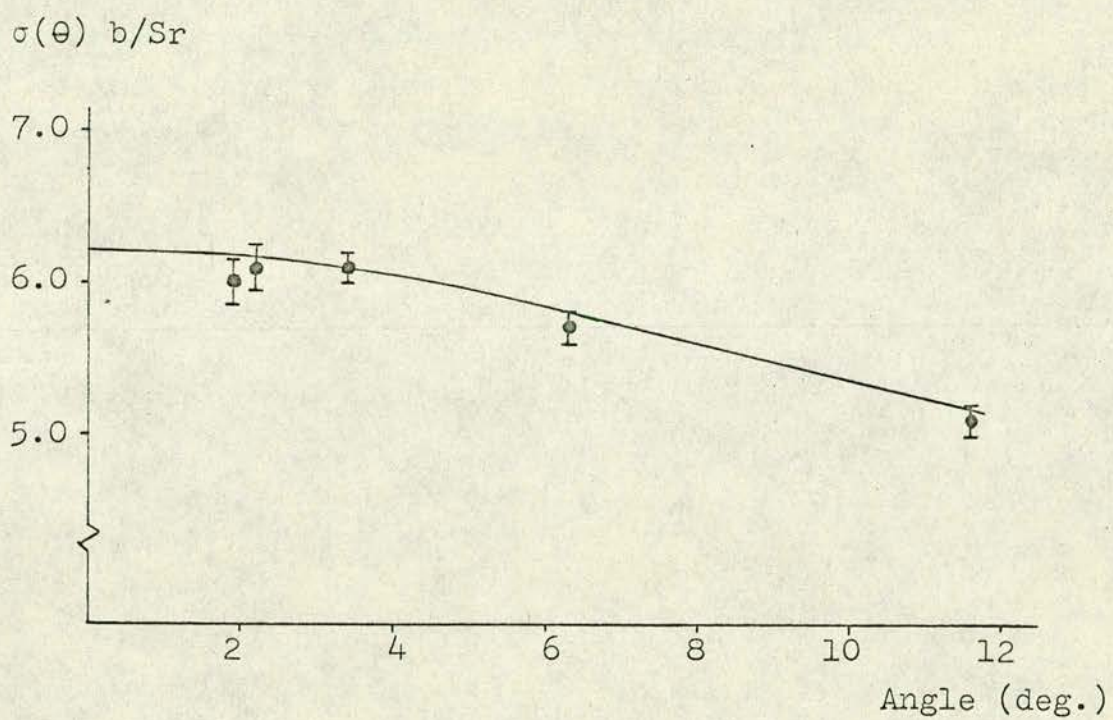
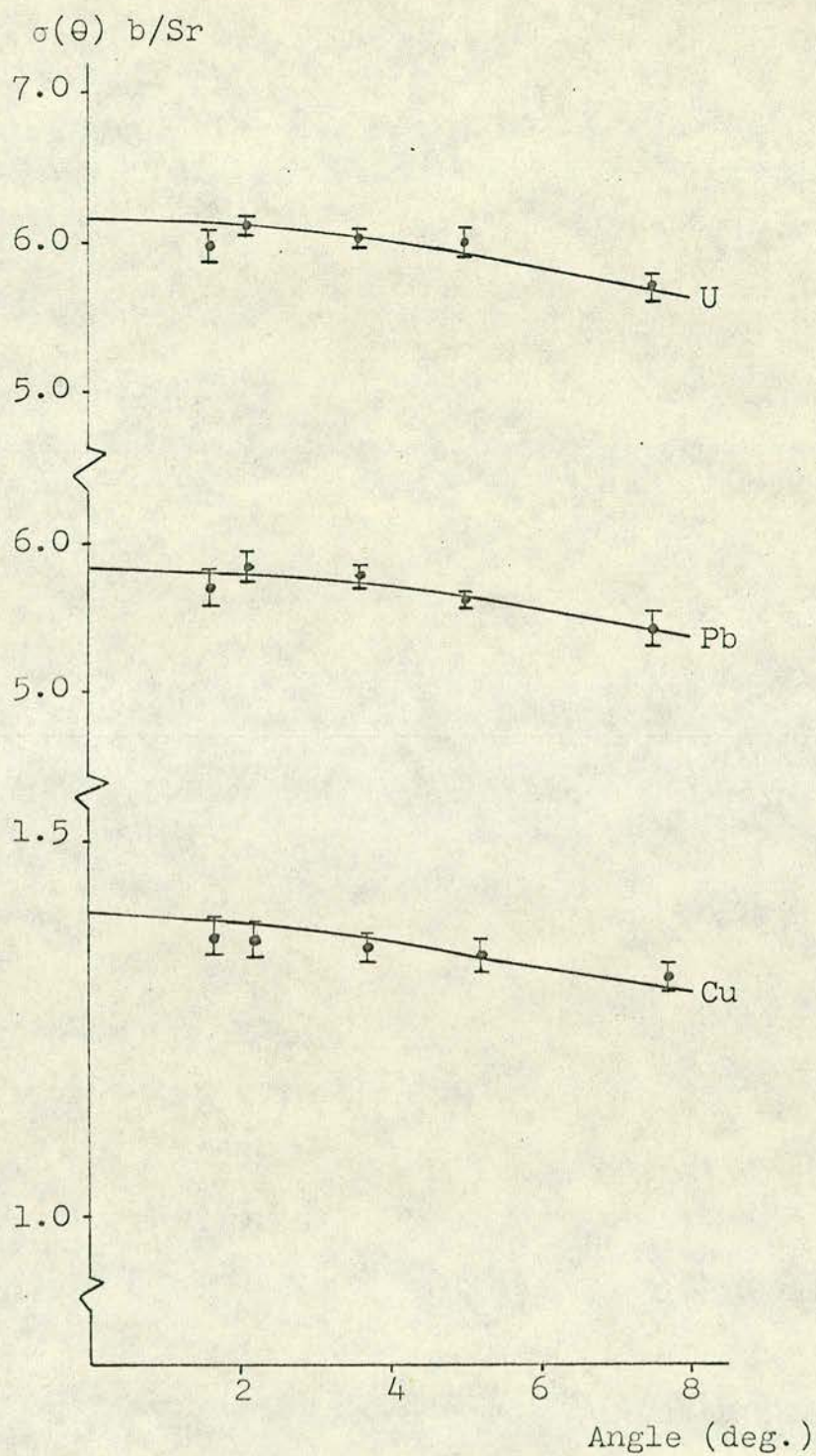Fig. 53. The differential cross-section of Pb
          at 3.3 MeV.

Fig. 54. The differential cross-sections
for Cu, Pb and U at 3.0 MeV.

scattering cross-sections was discussed in detail in section 1.3.3, where it was related to the model used for describing the nuclear cross-section; the present measurements support such a conclusion. It appears that the nuclear scattering contribution with the Mott-Schwinger one added to it are enough to account for the measured cross-sections at the small angles considered.

4.5. Comparison of the Two Polarimeters

The obvious disadvantage of the Mott-Schwinger scattering polarimeter is the low counting rate due to the fine collimation of the neutron beam and to the definition of a small scattering angle.

The efficiency of polarization determination should, in an ideal system with no background, depend on the solid angle (ω_1) subtended by the scatterer at the neutron source, the solid angle (ω_2) subtended by a side detector at the scatterer, the thickness of scatterer (t), the number of scattering nuclei per unit volume (n), the differential scattering cross-section (σ) and the square of the analyzing power for the scattering process (P).

Thus a figure of merit for comparing polarimeters, $P^2 \sigma n t \omega_1 \omega_2$, may be formed. This figure of merit is used in Table 4.3 to compare the Mott-Schwinger polarimeter, with the geometry described in Section 3.1, with the n-^{4}He scattering polarimeter, described in Section 2.2.

For the purpose of comparison in Table 4.3 it is assumed that the liquid scintillator neutron detectors in the He polarimeter

and the stilbene neutron detectors in the Mott-Schwinger system
have the same detection efficiency.

Thus it would seem that the Mott-Schwinger polarimeter should
take 50 times as long to obtain a polarization value with the
same statistical accuracy as the ^{4}He polarimeter.   Because the
background counting rate was significant, the measurements reported
in this thesis using the Mott Schwinger polarimeter involved equal
counting times with and without scattering sample, so doubling the
time taken for the Mott-Schwinger measurement and making the ratio
of figures of merit ~ 1:100 in reasonable agreement with an experi-
mentally determined ratio ~ 1:120 (10 min with the He polarimeter,
~ 20 hours with the Mott-Schwinger polarimeter at 2° scattering angle
for statistical accuracy of polarization measurement ~ 5%).
However, the geometry of the present Mott-Schwinger polarimeter
was chosen to make possible the tests of agreement between observed
behaviour and the Schwinger theory.   Once this agreement is accepted
a larger spread in scattering angle would not be objectionable, say
to collect all the polarization information in the angular range
from 1.7° to 3.7° in one measurement.   If this were done by moving
the stilbene detectors closer to the scattering sample ω_2 could be
increased tenfold; if it were achieved by dividing the angular
spread equally between the spread in angle of incidence of neutrons
on the scattering sample (by shortening the sample to target
distance) and some movement of the stilbene detectors towards the
scattering sample a factor of about 40 improvement in $\omega_1 \omega_2$ could
result.

Table 4.3. Comparison of efficiency of Mott-Schwinger and ^{4}He scattering fast neutron polarimeters, ignoring background effects, for neutrons $\sim$ 3 MeV.

	Mott-Schwinger (Pb sample)	^{4}He
Solid angle subtended by scatterer at target, ω_1	9×10^{-5} sr	3×10^{-3} sr
Solid angle subtended by side detector at scattering sample, ω_2	3×10^{-4} sr	5×10^{-2} sr
Number of scattering nuclei per cm^3, n	$4 \times 10^{-2} N_0$	$3 \times 10^{-3} N_0$
Scatterer thickness t	2.6 cm	5 cm
Differential scattering cross-section, $\sigma(\theta)$	6 b/sr at 2°	8×10^{-2} b/sr at 120°
Analysing power, $P(\theta)$	0.5 at 2°	$\sim$ 1 at 120°
Figure of merit for efficiency of polarization determination, $P^2(\theta)\sigma(\theta)nt\omega_1\omega_2$	$4 \times 10^{-9} N_0$	$2 \times 10^{-7} N_0$
Ratio of figures of merit	1 :	50

Thus a Mott-Schwinger scattering polarimeter could be made comparable in efficiency with the helium polarimeter and it is worthwhile to discuss whether any advantages are offered by the Mott-Schwinger system.

The analysing power is determined (eqn. (3.4.8) of section 3.4.4) from σ_t, the experimentally measured total cross-section. It is easy to obtain σ_t with substantially better statistical accuracy than attaches to the difference in differential cross-sections, $\sigma(\Theta,0) - \sigma(\Theta,\pi)$ of eqn. (3.4.7), which determines the polarization. Further, if σ_t is determined from measurements with the collimated beam monitor on the same scattering sample during the measurements to determine $\sigma(\Theta,0)$ and $\sigma(\Theta,\pi)$ then the dimensions and density of sample which enter the calculation of σ_t also enter the calculation of $\sigma(\Theta,0)$ and $\sigma(\Theta,\pi)$, and these factors cancel out in the determination of polarization from eqn. (3.4.7) and so can introduce no error.

In the Mott-Schwinger case the determination of polarization from eqn. (3.4.7) means that the neutron polarization is just proportional to $(N_R - N_L)$ where N_R and N_L are normalised numbers of counts recorded in the right hand and left hand stilbene detectors respectively and it does not matter if there is an equal background contribution to both N_R and N_L due for example to general scattered neutron background in the shielded area or to inelastically scattered neutrons. Working with the n-^{4}He scattering polarimeter on the other hand the polarization is determined from the scattering asymmetry, that is from an expression of the form $(N_R - N_L)/(N_R + N_L)$,

and equal background contribution to N_R and to N_L would give a false asymmetry and so false value of polarization. Equal background contributions to N_R and N_L are found with the He scattering, probably due to neutrons scattered by unintended paths between the helium gas scintillator and the side detectors, resulting in the low energy 'tail' of section 2.7.2. Such tails were also observed by different workers in this field[23,24,94,129,166-169, 182,183)] and it seems that they are associated with this type of polarimeter. Correction for such a tail was discussed in sections 2.7.2. and 2.9. and is usually subject to the judgement of the experimenter and so may introduce a small systematic error in the polarization values deduced.

It is concluded that a polarimeter for fast neutrons employing Mott-Schwinger scattering could contribute much more to polarization studies than has generally been realized.

Some of the measurements, reported in this thesis, were reported on two occasions. Part of the $D(d,n)^3He$ polarization measurements using the helium polarimeter, namely preliminary results of measurements at incident deuteron energies 2.0, 2.5, 3.0, 4.0 MeV and reaction angle 47° and the angular distribution of polarization at 1.2 MeV, were reported in ref.[184] Part of the results of measurements with the Mott-Schwinger polarimeter, namely measurements with Pb sample described in section 3.3.1 were reported in ref.[185]

References

1) Konopinski, E.J. and Teller, E., Phys. Rev. 73 (1948) 822.

2) Wolfenstein, L., Phys. Rev. 75 (1949) 342.

3) Alekseev, N.V., Arifkhanov, Vlasov, N.A., Davydov, V.V. and
   Samoilov, L.N., Usp. Fiz. Nauk. 83 (1964) 741;
   Soviet Phys. Usp. 7(1965) 619.

4) Haeberli, W., Fast Neutron Physics 2 (Interscience, New York,
   1963) Ch. VG.

5) Bishop, G.R., Preston, A., Westhead, J.M. and Halban, H.H.,
   Nature (London), 170 (1952) 113.

6) Ricamo, R., Helv. Phys. Acta, 26 (1953) 423.

7) Ricamo, R., Nuovo Cimento, 10 (1953) 1607.

8) Levintov, I.I., Miller, A.V., Tarumov, E.Z. and Shamshev, V.N.,
   Nucl. Phys. 3 (1957) 221; Nucl. Phys. 3 (1957) 237.

9) Willard, H.B., Biedenharn, L.C., Huber, P. and Baumgartner, E.,
   Fast Neutron Physics 2 (Interscience, New York,
   1963) Ch. V.E.

10) Hodgson, P.E., Advances in Physics 7 (1958) 1.

11) Burke, P.A., Nucl. Forces and the Few Nucleon Problem, VII,
    Pergamon Press 1960.

12) Bloch, F., Phys. Rev. 58 (1940) 829.

13) Schwinger, J., Phys. Rev. 69 (1946) 681.

14) Lepore, J.V., Phys. Rev. 79 (1950) 137.

15) Baumgartner, E. and Huber, P., Helv. Phys. Acta 26 (1953) 545.

16) Critchfield, C.L. and Dodder, D.C., Phys. Rev. 76 (1949) 602.

17) Dodder, D.C. and Gammel, J.L., Phys. Rev. 88 (1952) 520.

18) Seagrave, J.D., Phys. Rev. 92 (1953) 1222.

19) Gammel, J.L. and Thaler, R.M., Phys. Rev. 109 (1958) 2041.

20) Austin, S.M., Barschall, H.H. and Shamu, R.E., Phys. Rev.
    126 (1962) 1532.

21) Hoop, B. and Barschall, H.H., Nucl. Phys. 83 (1966) 65.

22) Weitkamp, W.G. and Haeberli, W., Nucl. Phys. 83 (1966) 46.

23) Sawers, J.R., Morgan, G.L., Schaller, L.A. and Walter, R.L.,
     Phys. Rev. 168 (1968) 1102.

24) Morgan, G.L. and Walter, R.L., Phys. Rev. 168 (1968) 1114.

25) Satchler, G.R., Owen, L.W., Elwyn, A.J., Morgan, G.L. and
     Walter, R.L., Nucl. Phys. A112 (1968) 1.

26) Arndt, R.A. and Roper, L.D., Phys. Rev. C1 (1970) 903.

27) Adair, R.K., Phys. Rev. 86 (1952) 155.

28) Demanins, F., Pisent,G., Poiani, G. and Villi C., Phys. Rev.
     125 (1962) 318.

29) White, R.E. and Farley, F.J.M., Nucl. Phys. 3 (1951) 476.

30) Stammbach, Th. and Walter, R.L., Nucl. Phys. A180 (1972) 225.

31) Broste, W.B., Simmons, J.E. and G.S. Mutchler, Bull. Am. Phys.
     Soc. 14 (1969) 1320.

32) Niiler, A., Drosg, M., Hopkins, G.C. and Seagrave, J.D.,
     Proc. of the Third Int. Symp. on Pol. Phenomena,
     Madison 1970, P. 559.

33) Schwandt, P., Clegg, T.B. and Haeberli, W., Nucl. Phys.
     A163 (1971) 432.

34) Adair, R.K., Darden, S.E. and Fields, R.E., Phys. Rev. 96
     (1954) 503.

35) Remund, A.E., Helv. Phys. Acta, 29 (1956) 545.

36) Olness, R.J., Seth, K.K. and Lewis, H.W., Nucl. Phys.
     52 (1964) 529.

37) Ferguson, A.T.G., White, R.E. and Wilmore, D., Nucl. Phys.
     76 (1966) 369.

38) Gorlov, G.V., Lebedeva, N.S. and Morozov, V.M., Doklady Akad.
     Nauk. 158 (1964) 574; Sov. Phys. Doklady 9 (1965)
     806.

39) Gorlov, G.V., Lebedeva, N.S. and Morozov, V.M., Jaderna Fiz.
     5 (1967) 910; Sov. J. Nucl. Phys. 6 (1968) 663.

40) Mahajan, A.S., Nucl. Phys. A95 (1967) 193.

41) Morozov, V.M., Gorlov, G.V., Zubov, Yu G. and Lebedeva, N.S.,
        ZhETF Pisma. Red. 12 (1970) 181; Sov. Phys. JETP
        Letters 12 (1970) 125.

42) Galloway, R.B., Proc. Roy. Soc. (Edinburgh) A70 (1972)

43) Hodgson, P.E., The Optical Model of Elastic Scattering,
        Oxford, 1963.

44) Wilmore, D. and Hodgson, P.E., Nucl. Phys. 55 (1964) 673.

45) Schwinger, J., Phys. Rev. 73 (1948) 407.

46) Mott, N.F., Proc. Roy. Soc. (London) 124 (1929) 425.

47) Sample, J.T., Can. J. of Phys. 34 (1956) 36.

48) Fox, R., Nucl. Phys. 43 (1963) 110.

49) Wilmore, D.S. and Hodgson, P.E., Int. Conf. Study Nucl. Struct.
        with Neutrons, Antwerpen, July 1965.

50) Alexandrov, Yu. A. and Bondarenko, I.I., J. Exp. Teor. Fiz.
        31 (1956) 726; Sov. Phys. JETP 4 (1957) 612.

51) Koprov, V.M., J. Exp. Teor. Fiz. 38 (1960) 639; Sov. Phys.
        JETP 2 (1960) 459.

52) Redmond, R.F., Phys. Rev. 140 (1965) B1267.

53) Weisskopf, W. and Feshbach, H., Phys. Rev. 114 (1959) 827.

54) Gorlov, G.V., Lebedeva, N.S. and Morozov, V.M., Izv. Akad.
        Nauk SSSR 34 (1970) 138.

55) Davydov, A.S., Teoriya Atomnogo Yadra (Theory of the Atomic
        Nucleus), Fizmatgiz, Moscow, 1958.

56) Anikin, G.V. and Kotukhov, I.I., Jad. Fiz. 12 (1970) 1121;
        Sov. J. Nucl. Phys. 12 (1971) 614.

57) Fossan, D.B. and Walt, M., Phys. Rev. Letters 12 (1964) 672.

58) Alexandrov, Yu. A., USSR Conf. on Nucl. Reac. at Low and
        Medium Energies, Moscow, Nov. 1957.

59) Alexandrov, Yu.A., Anikin, G.V. and Soldatov, A.S., J. Exp.
        Teor. Fiz. 40 (1961) 1878; Sov. Phys. JETP 13
        (1961) 1319.

60) Dukarevich, Yu.V. and Dyumin, A.N.,   J. Exp. Teor. Fiz.
          44 (1963) 130; Sov. Phys. JETP 17 (1963) 89.

61) Monahan, J. and Elwyn, A., Phys. Rev. 136 (1964) B1678

62) Elwyn, A.J., Monahan, J.E., Lane, R.O., Langsdorf, A. and
          Mooring, F.P., Phys. Rev. 142 (1966) 758.

63) Hogan, W.S. and Seyler, R.G., Phys. Rev. 177 (1969) 1706.

64) Walt, M. and Fossan, D.B., Phys. Rev. 137 (1965) 629.

65) Alexandrov, Yu.A. and Samosvat, G.S.,   Priprint Joint Inst.
          for Nucl. Res., Dubna 1965, JINR-P-2495.

66) Anikin, G.V., Alexandrov, Yu.A. and Soldatov, A.S., Int. Conf.
          Study of Nucl. Struc. with Neutrons, Antwerpen,
          July 1965.

67) Gorlov, G.V., Lebedeva, N.S. and Morozov, V.M., Jad. Fiz.
          8 (1968) 1086; Sov. J. Nucl. Phys. 8 (1969) 630.

68) Kuchnir, F.T., Elwyn, A.J., Monahan, J.E., Langsdorf, A.
          and Mooring, F.P., Phys. Rev. 176 (1968) 1405.

69) Adam, A., Deak, F., Jeki, L., Kiss, A., Kovessy, Z., Palla, G.
          and Hrasko, P., Jad. Fiz. 8 (1968) 439; Sov. J. Nucl.
          Phys. 8 (1969) 255.

70) Palla, G., Phys. Letters. 35B(1971) 477.

71) Alexandrov, Yu. A., J. Exp. Teor. Fiz. 33 (1957) 294; Sov.
          Phys. JETP 6 (1958) 228.

72) Lebedeva, N.S. and Morozov, V.M., Atomnaya Energiya 28 (1970)
          310.

73) Barashenkov, V.S. and Kaiser, H., Fortshr. Phys. 10 (1962) 33.

74) Moroz, L.G. and Tretjakov, V.N., Dokl. Acad. Nauk. BSSR 8
          (1964) 9.

75) Thaler, R.M., Phys. Rev. 114 (1959) 827.

76) Langsdorf, A., Lane, R.O. and Monahan, J.E., Phys. Rev.
          107 (1957) 1077.

77) Breit, G. and Rustgi, M.L., Phys. Rev. 114 (1959) 830.

78) Barashenkov, V.S., Proc. Int. Conf. Nucl. Struct., Stanford
          University, 1963.

79) Longley, H.J., Little, R.N. and Slye, J.M., Phys. Rev.
86 (1952) 419.

80) Sample, J.T., Neilson, G.C. and Warren, J.B., Can. J. Phys.
33 (1955) 350.

81) Voss, R.G.P. and Wilson, R., Phil. Mag. 1 (1956) 175.

82) Hillman, P., Stafford, G.H. and Whitehead, Nuovo Cimento.
4 (1956) 67.

83) Baz, A.I., Sov. Phys. JETP 31 (1956) 159.

84) Rhein, W.J., Phys. Rev. 98 (1955) 1300.

85) Gorlov, G.V., Lebedeva, N.S. and Morozov, V.M., Dokl. Akad.
Nauk SSSR 174 (1967) 60; Sov. Phys. DOKLADY
12 (1967) 451.

86) Gorlov, G.V., Lebedeva, N.S. and Morozov, V.M., Jad. Fiz.
4 (1966) 519; Sov. J. of Nucl. Phys. 4 (1967) 369.

87) Gorlov, A.V., Lebedeva, N.S. and Morozov, V.M., ZhETF Pisma
5 (1967) 131; Sov. Phys. JETP Letters 5 (1967) 106.

88) Elwyn, A.J., Lane, R.O., Langsdorf, A. and Monahan, J.E.,
Phys. Rev. 133 (1964) B80.

89) Huber, P. and Baumgartner, E., Helv. Phys. Acta. 26 (1953)
420.

90) Meier, R.W., Scherrer, P. and Trumpy, Helv. Phys. Acta.
27 (1954) 577.

91) McCormac, B.M., Steuer, M.F., Bond, C.D. and Hereford, F.L.,
Phys. Rev. 104 (1956) 718.

92) Pasma, P.J., Nucl. Phys. 6 (1958) 141.

93) Babenko, N.P. and Konstantinov, I.O., Pribory i Tekhn. Eksperim.
10 (1964) 291.

94) Davie, H. and Galloway, R.B., Nucl. Inst. and Meth. 92 (1971)
547.

95) Simmons, J.E. and Perkins, R.B., Rev. Sci. Inst. 32 (1961) 1173.

96) Robertson, L.P., Hanna, R.C., Ramavataram, K., Devins, D.W.,
Hodges, T.A., Moroz, Z.J., Hoey, S.J. and Plummer, D.J.,
Nucl. Phys. A134 (1969) 545.

97) Birchall, J., Kenny, M.J., McKee, J.S.C. and Reece, B.L.,
Nucl. Inst. and Meth. 65 (1968) 117.

98) Kane, J.R., Siegel, R.T. and Suzuki, A., Rev. Sci. Inst.
34 (1963) 817.

99) Baicker, J.A. and Jones, K.W., Nucl. Phys. 17 (1960) 424.

100) Stinson, A.M., Tang, S.M. and Sample, J.T., Nucl. Inst. &
Meth. 62 (1968) 13.

101) Miller, T.G., Gibson, F.P. and Morrison, G.W., Nucl. Inst. &
Meth. 80 (1970) 325.

102) Martin, J.C., Broste, W.B. and Simmons, J.E., Proc. of the
Third Int. Symp. on Pol. Phen. in Nucl. React.,
Madison 1970, P. 877.

103) Ot-Stavnov, P.S., J. Exp. Teor. Fiz. 37 (1959) 1815; Sov.
Phys. JETP 10 (1960) 1281.

104) Steuer, M.F., Bucher, W.P. and Hereford, F.L., Compt. Rend.
Congres. Intern. Phys. Nucl. (Dunod, Paris, 1959)
P. 545.

105) Boersma, H.J., Jonker, C.C., Nijenhuis, J.G. and Van Hall, P.J.,
Nucl. Phys. 46 (1963) 660.

106) Rogers, J.T. and Bond, C.D., Nucl. Phys. 53 (1964) 297.

107) Hansgen, H., Pose, H., Schirmer, G. and Seeliger, D.,
Nucl. Phys. 73 (1965) 417.

108) Mulder, J.P.G., Phys. Letters 23 (1966) 589.

109) Behof, A.F., May, T.H. and McGarry, W.I., Nucl. Phys. A108
(1968) 250.

110) Stoppenhagen, W.G. and Finlay, R.W., Bull. Am. Phys. Soc.
13 (1968) 873; Private Communication.

111) Thomas, K. and Hofmann, Zeit für Phys. 217 (1968) 128.

112) Prade, H. and Csikai, J., Nucl. Phys. A123 (1969) 365.

113) Roding, P. and Scholermann, H., Nucl. Phys. A125 (1969) 585.

114) Daehnick, W.W., Phys. Rev. 115 (1959) 1008.

115) Avignon, P., Deschamps, Y. and Rosier, L., J. Phys. Radium.
22 (1961) 563.

116) Dubbeldam, P.S. and Walter, R.L., Nucl. Phys. 28 (1961) 414.

117) May, T.H., Walter, R.L. and Barschall, H.H., Nucl. Phys. 45 (1963) 17.

118) Niewodniczanski, H., Szmider, J. and Szymakowski, J., J. Phys. 24 (1963) 871.

119) Trostin, I.S. and Smotryaev, V.A., J. Exp. Teor. Fiz. 44 (1963) 1160; Sov. Phys. JETP 17 (1963) 784.

120) Babenko, N.P., Konstantinov, I.O., Moskalev, A.P. and Nemilov, Yu.A., J. Exp. Teor. Fiz. 47 (1964) 767; Sov. Phys. JETP 20 (1965) 512.

121) Bondarenko, I.I. and Ot-Stavnov, P.S., J. Exp. Teor. Fiz. 47 (1964) 97; Sov. Phys. JETP 20 (1965) 67.

122) Purser, F.O., Sawers, J.R. and Walter, R.L., Phys. Rev. 140 (1965) B870.

123) Miller, T.G., Nucl. Inst. & Meth. 40 (1966) 93; Bull. Am. Soc. 9 (1964) 153.

124) Lam, S.T., Gedeke, D.A., Stinson, G.M., Tang, S.M. and Sample, J.T., Nucl. Inst. & Meth. 62 (1968) 1.

125) Drigo, L., Manduchi, C., Moschini, A., Russo Manduchi, M.T., Tornielli, G., and Zannoni, G., Nuovo Cimento Letters. 1 (1969) 237.

126) Davie, H., Ph.D. Thesis, Edinburgh University, 1972.

127) Spalek, G., Hardekopf, R.A., Taylor, J., Stammbach, Th. and Walter, R.L., Proc. Third Int. Symp. Pol. Phenom. in Nucl. React., Madison 70, P. 462.

128) Gorlov, G.V., Proc. Third Int. Symp. Pol. Phenom. in Nucl. React., Madison 70, P. 633.

129) Smith, J.R. and Thornton, S.T., Can. J. Phys. 50 (1972) 783.

130) Meyerhof, W.E. and Tombrello, T.A., Nucl. Phys. A109 (1968) 1.

131) Galloway, R.B., Nucl. Inst. & Meth. 92 (1971) 537.

132) Walter, R.L., Proc. Third Int. ymp. Pol. Phenomena in Nucl. React., Madison 70.

133) Kane, P.P., Nucl. Phys. 10 (1959) 429.

134) Gorlov, G.V., Lebedeva, N.S. and Morozov, V.M., Yad. Fiz. 8 (1968) 1086; Sov. J. of Nucl. Phys. 8 (1969) 630.

135) Fick, D. and Franz, H.W., Phys. Letters 27B (1968) 541.

136) Fick, D., Z. Physik 22 (1969) 451.

137) Ad'yasevich, B.P., Antonenko, V.G., and Fomenko, D.E., Yad. Fiz. 11 (1970) 732; Sov. J. of Nucl. Phys. 11 (1970) 411.

138) Blin-Stoyle, Proc. of the Phys. Soc. (London) 64 (1951) 700.

139) Blin-Stoyle, Proc. of the Phys. Soc. (London) 65 (1952) 949.

140) Cini, M., Nuovo Cimento 8 (1951) 1007.

141) Rook, J.R. and Goldfarb, L.J.B., Nucl. Phys. 27 (1961) 79.

142) Fierz, M., Helv. Phys. Acta. 25 (1952) 629.

143) Boersma, H.J., Nucl. Phys. A135 (1969) 609.

144) Hansgen, H. and Nitzsche, M., Nucl. Phys. A165 (1971) 401.

145) Rethmeier, J. and Van Der Meulen, D.R., Nucl. Inst. & Meth. 24 (1963) 349.

146) Morgan, M.I.L., Conf. on Accel. Targets Designed for the Production of Neutrons, Grenoble 1965, Euratom Rep., EUR 2641, PP. 239-263.

147) Smith, D.L.E., UKAEA Rep., AWRE O - 52167.

148) Shamu, R.E., Nucl. Inst. & Meth. 14 (1961) 297.

149) Tellex, P.A. and Waldron, J.R., J. Opt. Soc. Am. 451 (1955) 19.

150) Jenkin, J.G., and Shamu, Nucl. Inst. & Meth. 34 (1965) 116.

151) Roush, M.L., Wilson, M.A. and Hornyak, W.F., Nucl. Inst. & Meth. 34 (1965) 116.

152) Owen, R.B., Nucleonics 17 (1959) 92.

153) Whaling, W., Handbuch der Physik, Vol. XXXIV, Springer-Verlag, Berlin, 1958, P. 193.

154) Coon, J.H., Fast Neutron Physics, Interscience, New York, 1960, Ch. IV. D.

155) I.B.M. Manual C20-8011, Random Number Generation and Testing.

156) Brolley, J.E. and Fowler, J.L. Fast Neutron Physics 1
     (Interscience, New York, 1960) Ch. IC.

157) Masood Ali K, Galloway, R.B. and Vass, D.G., Nucl. Inst. &
     Methods 92 (1971) 553.

158) Masood Ali K, M.Sc. Thesis, Edinburgh University, 1970.

159) Walt, M., Fast Neutron Physics II (Interscience, New York,
     1960) Ch. VB.

160) Amster, H., Leshan, E.J., Walt, M., Fast Neutron Physics,
     Part I (Interscience, New York 1960).

161) Lane, R.O., Langsdorf, A.S., Monahan, J.E. and Elwyn, A.J.,
     Annals of Physics 12 (1961) 135.

162) Holmqvist, B., Gustavsson, B. and Wiedling, T., Arkiv För
     Fysik 34 (1967) 481.

163) Lane, R.O. and Miller, W.F., Nucl. Inst. & Meth. 16 (1962) 1.

164) Monahan, J.E. and Elwyn, A.J., Nucl. Inst. & Meth. 14 (1961)
     348.

165) Monahan, J.E. and Elwyn, A.J., Argonne National Lab., Rep.
     ANL 6420 Sept. 1961.

166) Sawers, J.R., Purser, F.O. and Walter, R.L., Phys. Rev.
     141 (1966) 825.

167) Taylor, J., Spalek, A., Stammbach, Th. and Walter, R.L.
     Phys. Rev. C1 (1970) 803.

168) Smith, J.R. and Thornton, S.T., Nucl. Phys. A186 (1972) 161.

169) Thornton, S.T., Morris, C.L., Smith, J.R. and Fogel, R.P.,
     Nucl. Phys. A169 (1971) 131.

170) Walter, R.L., Benenson, W., Dubbeldam, P.S. and May, T.H.,
     Nucl. Phys. 30 (1962) 292.

171) Benenson, W., May, T.H. and Walter, R.L., Nucl. Phys. 32
     (1962) 510.

172) Andress, W.D., Purser, F.O., Sawers, J.R. and Walter, R.L.,
     Nucl. Phys. 70 (1965) 313.

173) Volkov, V.V., Vorotnikov, P.E., Koltipin, E.A., Sidrov, N.E.
     and Jankov, G.B., Atomnaya Energia, Supplementum 5,
     Atomizdat Moscow 1957.

174) Goldberg, M.D. and Le Blanc, J.M., Phys. Rev. 119 (1960) 1992.

175) Schulte, R.L., Cosack, M., Obst, A.W. and Weil, J.L., Nucl. Phys. A192 (1972) 609.

176) Spalek, G., Hardekopb, R.A., Taylor, J., Stammbach, Th. and Walter, R.L., Nucl. Phys. A191 (1972) 449.

177) Cranberg, L., Oliphant, T.A., Levin, J. and Zafaratos, C.D., Phys. Rev. 159 (1967) 969.

178) Fetisov, N.E., Atomnaya Energia 3,3 (1957) 211.

179) Wilmore, D., AERE-R5053, Harwell 1966.

180) Nucl. Data Sheets B Vol. 2, No. 3, 1967.

    "   "   "   Vol. 2, No. 6, 1968.

    "   "   "   Vol. 4, No. 6, 1970.
    "
    "   "   "   Vol. 5, No. 3, 1971.

    "   "   "   Vol. 7, No. 2, 1972.

181) Wilmore, D., AERE-R4649, Harwell, 1964.

182) Meier, M.M., Schaller, L.A. and Walter, R.L., Phys. Rev. 150 (1966) 821.

183) Mutchler, G.S., Broste, W.B. and Simmons, J.E., Phys. Rev. C3 (1971) 1031.

184) Galloway, R.B., Davie, H., Maayouf, R.M.A. and Vass, D.G., Conf. on Nucl. Struc. Studies with Neutrons, Budapest, July 31 - Aug. 5, 1972.

185) Galloway, R.B. and Maayouf, R.M.A., Nucl. Inst. & Meth. (In print).

ACKNOWLEDGEMENTS

ABSTRACT OF THESIS

Name of Candidate .... Refaat Mahmoud Ali Maayouf

Address .... Physics Dept., J.C.M.B., Kings Buildings, Edinburgh.

Degree .... Ph.D. .... *Date* .... October 1972

Title of Thesis .... FAST NEUTRON POLARIZATION STUDIES.

The present situation regarding polarization of neutrons from the $D(d,n)^3He$ reaction for deuteron energies $\leq$ 10 MeV is surveyed along with the experimental arrangements used to obtain the data. Out of the techniques used before for measuring the $D(d,n)^3He$ polarization, two main techniques, used for the measurements reported in this thesis, are emphasized. One of them is by scattering from helium which is discussed along with calculations performed in order to test the degree of agreement between the phase-shifts available for determining the ^4He analysing powers. The other is by using Mott-Schwinger scattering from heavy nuclei at small angles. This one is discussed in detail and the differential scattering cross-sections at small angles measured to date along with the models used to describe them are surveyed.

Measurements of the $D(d,n)^3He$ polarization using both types of polarimeter are described. First, two sets of measurements with the ^4He polarimeter are described. One of them was carried out at an incident deuteron energy of 0.5 MeV; the other one was performed at deuteron energies between 1 and 5 MeV. This is followed by a description of the Mott-Schwinger polarimeter along with two sets of measurements. The first of them was carried out with deuterons incident with energy 0.82 MeV and the polarization of neutrons emitted at 46° was detected using scattering from lead. The other one was mainly for comparison with the measurement carried out at 0.5 MeV with the helium polarimeter and employed scattering from Cu, Pb and U samples.

All the results obtained with both polarimeters are discussed at the end of the thesis. The resulting $D(d,n)^3He$ polarizations at reaction laboratory angle 45 ± 5° are compared with values reported in the literature for the mean deuteron energy range $\leq$ 10 MeV. Two angular distributions of the reaction polarization reported in this thesis are also compared with published values. The measurements with the Mott-Schwinger polarimeter also resulted in differential scattering cross-sections of Cu, Pb and U at small angles which are compared with cross-sections based on optical model calculations. Finally both polarimeters are compared and the possibility of improving the efficiency of the Mott-Schwinger polarimeter is discussed.

Use other side if necessary.